博　士　論　文

Structural Study of Self-Assembled Aggregates Formed by Ionic Oligomeric Surfactants

（多鎖型界面活性剤が形成する自己組織化会合体の構造特性）

平成 26 年 12 月　博士（理学）申請

東京大学大学院理学系研究科

化学専攻

草野　巧巳

Abstract

In this theses, the structure of oligomeric surfactant aggregates was investigated for the purpose to elucidate the unique property of oligomeric surfactants.

Oligomeric surfactants are surfactants with multiple hydrophobic groups and multiple hydrophilic groups in a molecule. Normal surfactant is a monomeric surfactant that has only one hydrophilic head group and one hydrophobic carbonchain. Oligomeric surfactants show higher efficiency for lowering surface tension and lower critical micelle concentration (CMC). Additionally, it is reported by many researchers that they can form various aggregates without any additives in an aqueous solution due to their higher hydrophobic interaction. However, there are few studies about the aggregation behavior of oligomeric surfactants because they are difficult to synthesize. Investigations of the aggregation structure of oligomeric surfactants are important for enabling their application.

In this thesis, novel star-type trimeric surfactants of quaternary ammonium bromide ($3C_n$trisQ), which comprised three hydrocarbon chains and three hydrophilic groups connected by three ethylene spacer chains and a nitrogen atom, were investigated because they are easier to synthesize than previous ones. The $3C_n$trisQ molecule exhibited unique physicochemical properties, including lower CMC and a higher efficiency for lowering surface tension when compared with monomeric and gemini surfactants. Using SANS, rheology measurements, and cryo-TEM, the aggregates formed by $3C_{12}$trisQ were characterized in an aqueous solution and found sphere-to-rod transition and growth of wormlike micelles without any salts. It is elucidated that $3C_{12}$trisQ formed longer wormlike micelles due to higher end-cap energy than gemini surfactants. Furthermore $3C_{12}$trisQ could form various aggregates by adding sodium salicylate as salts.

Next, water-in-ionic liquid (IL) type reverse micelles (RMs) were successfully prepared in the absence of organic solvent by using oligomeric surfactants. Incorporation of organic solvents as one component in the system leads to a limitation of unique and novel properties originated from ILs. Therefore, organic-solvent-free system is important. RMs were successfully formed without organic solvent by using gemini surfactant (AOT) and star-type trimeric surfactant ($3C_{12}$trisQ).

The use of $3C_n$trisQ is highly promising for fundamental studies and applications of surfactants.

Contents

Chapter 1 General Introduction

1-1. Surfactants

Interfacial activity is the phenomenon where surface tension between two liquids or between a liquid and a solid is noticeably decreased by the addition of a certain reagent. This reagent that can lower the surface tension is generally called a surfactant. Surfactants are amphiphilic compounds, i.e., their molecules have both hydrophilic and hydrophobic components. According to the head group of their molecular structure, surfactants are classified as either ionic or nonionic. Ionic surfactants are further grouped depending on whether their head group is cationic or anionic. **Figure 1-1** shows the characteristic performance of each class of surfactant. As previously described, surfactants are adsorbed at the interface between water and other materials and can lower the surface tension of a solution. Because of their high efficiency for lowering surface tension, they are used in various applications, including detergents, cosmetics, dispersants, and foaming agents.[1–3]

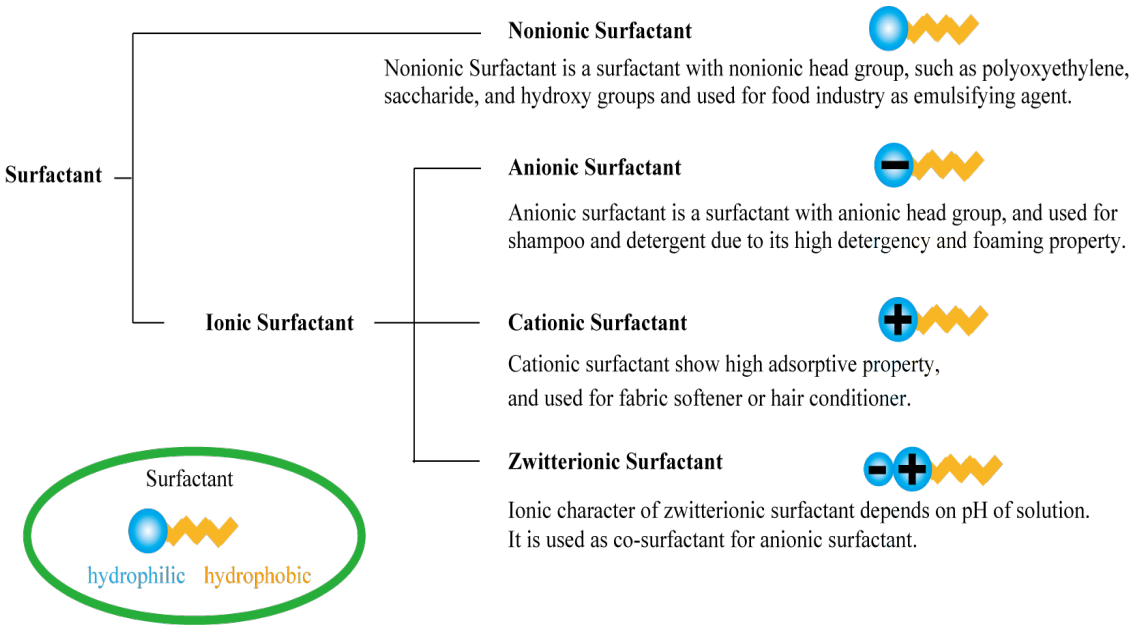

Figure 1-1. Classification of surfactants and their applications.

In addition to adsorption behavior, another important property of surfactants is aggregation. Under conditions where the interfaces of a solution are fully covered with adsorbed surfactants, surfactants start to self-aggregate by adding additional surfactant molecules to the system. This aggregate formed by surfactants is called a micelle. The critical micelle concentration (CMC) is the surfactant concentration where surfactants start to form self-aggregates. Self-aggregation occurs when surfactants, aggregating with each hydrophobic chain inside micelles, have an advantage in free energy over surfactants dispersed with their hydrophobic chain surrounded by water molecules. Therefore, surfactants form micelles with the hydrophilic head group in contact with surrounding water molecules and their hydrophobic carbon chain inside the micelle (**Figure 1-2**).

Moreover, surfactants exhibit various aggregate structures, such as micelles, vesicles, and reverse micelles, depending on the solvent structure, solution temperature, etc. The interaction between surfactants is dominated not by covalent or ionic binding, but rather by weaker interactions, such as van der Waals interaction, hydrogen bonding,

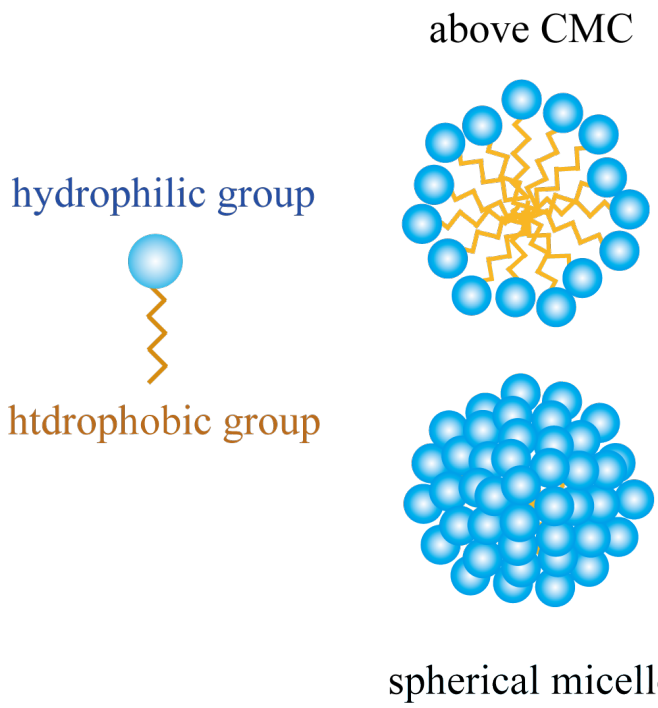

Figure 1-2. Aggregation behavior of surfactants at a concentration greater than the CMC.

or electrostatic interaction. Therefore, micelles fluctuate and easily change their structure depending on the solvent conditions. Because of their various structures and ability to fluctuate, they are used in various applications, e.g., as templates for mesoporous silica,[4] drag reduction,[5] and Drug Delivery System (DDS)[6]. Surfactants are also used as model molecules for biological lipids because biological lipids, which form biomembranes, also possess hydrophilic head groups and hydrophobic tails. Their aggregation structures are widely investigated to elucidate the correlation between a biomembrane's structure and its capabilities. For this reason, the correlation between the chemical structures of surfactants/additives and their aggregation structures is an important research topic.

1-2. Aggregation structures of surfactants

Surfactants form a large variety of aggregates in solution because of their weak molecular interactions. The most stable structure of surfactant aggregates depends on the chemical structure of the surfactant and its solution conditions. The structural transition of surfactant aggregates can be described by the geometrical restriction of surfactants. The packing parameter for a certain surfactant, p, is given by:[7]

$$p = \frac{v}{a_0 l_C} \tag{1.1}$$

where a_0, v, and l_C are the surface area of the head group, the volume fraction of the alkyl carbon chain, and the critical chain length of the alkyl carbon chain, respectively. Smaller aggregates are entropically favored. However, aggregates with structure larger than the shape geometrically limited by the packing parameter of the surfactants are energetically unfavorable. Thus, the relationship between the packing parameter, p, for each surfactant and its aggregation structure can be easily deduced (**Figure 1-3**). If the packing parameter is systematically changed, the aggregation structure can be controlled. Various methods have been developed for changing the packing parameter, e.g., changing the chemical structure of the surfactant, adding additives such as salts or alcohols, and mixing more than two surfactants.

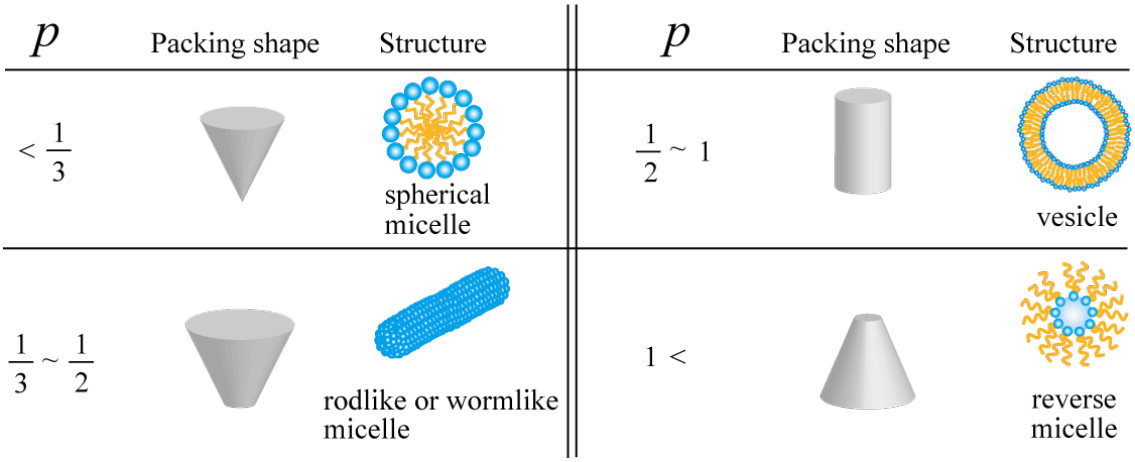

Figure 1-3. Relationship between the packing parameters of surfactants and their aggregation structure.

1-2-1. Wormlike micelles

Wormlike micelles or rodlike micelles are one of the various surfactant aggregate shapes. The word "wormlike micelle" is sometimes used to describe rodlike micelles that have grown to a length at which they begin to overlap. In 1951, Anacker and Debye experimentally proposed the existence of wormlike micelles on the basis of light-scattering experiments. Their study marked the beginning of the study of wormlike micelles.[8] In 1956, Pilpel described a sphere-to-rod transition that occurs with increasing electrolyte concentration.[9]

In 1987, Cates explained the growth and dynamics of wormlike micelles using mean field theory;[10] in the same year, Shikata et al. demonstrated that the rheological behavior of wormlike micelles can be described by the Maxwell model with a single relaxation time because of their weak interaction.[11] Mackintosh applied the mean field theory of wormlike micelles to a charged wormlike micelle system.[12] Experimental results of ionic surfactant systems have been described by this theory, and this theory is often applied in rheological studies.[13] According to the mean field theory, the growth of micelles is encouraged by an increase in surfactant concentration or a decrease of the solution temperature. The dominant factors for the growth of wormlike micelles are the end-cap energy and their surface charge. If the micelles exhibit high end-cap energy, the surfactants in the end-caps of wormlike micelles will possess higher free energy. As a

result, wormlike micelles grow to decrease the number of end-caps. If they have a high charge, wormlike micelles have difficulty growing because of electrostatic repulsions between surfactant molecules or micelles. The length of wormlike micelles is determined by a combination of these parameters.

1-2-2. Reverse micelles (microemulsions)

Reverse micelles (RMs) are water droplets stably dispersed by surfactants in oil. Therefore, RMs are generally formed in three-component systems (water/oil/surfactant). A RM is a type of microemulsion (ME) or nanoemulsion, swelling micelle. However, the word "reverse micelle" is used only for water-in-oil microemulsion systems, not for oil-in-water ME systems. In 1943, Schulman and Hoar reported RMs for the first time.[14] In general, RMs are water droplets homogeneously dispersed by surfactants resulting in a transparent solution. They are thermodynamically stable, and their size varies up to 100 nm. Therefore, their sizes do not reach the wavelength of visible light and their solutions remain transparent. Helfrich et al. expressed the formation mechanism of RMs by applying the curvature elastic-energy.[15] This theory has been used to express the physical properties of RMs.[16] On the other hand, Eastoe et al. reported that water-in-oil RMs stabilized by a gemini surfactant, dioctyl sulfosuccinate sodium salt (AOT), do not exhibit oil penetration to the surfactant shell, which experimentally indicates that RMs can be stably dispersed using gemini surfactants with higher packing parameters.[17]

For RM systems, organic solvents are used as the bulk phase. From an environmental point of view, the amount of volatile organic solvents used should be minimized. Therefore, there are numerous studies related to the use of supercritical carbon dioxide ($scCO_2$)[18] or room-temperature ionic liquids (RTILs).[19] The temperature and pressure of CO_2 systems are easily changed, and CO_2 is easily removed. On the other hand, RTILs possess numerous advantages, such as being nonflammable and nonvolatile.

1-3. Oligomeric surfactants

Oligomeric surfactants are surfactants with multiple hydrophobic groups and multiple hydrophilic groups per molecule (**Figure 1-4**). A normal surfactant is monomeric and has only one hydrophilic head group and one hydrophobic carbon chain.

In contrast, gemini or dimeric surfactants, the simplest oligomeric surfactants, contain two hydrophobic and hydrophilic groups, respectively. They exhibit greater efficiency for lowering surface tension and have a lower CMC than monomeric surfactants. Additionally, numerous researchers have reported that they can form various aggregates in aqueous solutions without the use of additives.[20] There exist two types of gemini surfactants: those that consist of only one head group and those that consist of two head groups. The typical example of the former type is AOT, which is an anionic gemini surfactant that exhibits a high packing parameter and is used to form stable RMs.[17] Monomeric surfactant can stabilize RMs when salts are added, whereas AOT can stabilize RMs in the absence of any salt. The formation of RMs is generally confirmed by cryogenic transmission electron microscopy (cryoTEM) or dynamic light scattering (DLS) measurements. As previously described, water-in-oil RMs can be stabilized by a gemini surfactant (AOT).[17] This behavior is also attributed to the high packing parameter of the gemini surfactant AOT.

Gemini surfactants with one head group have been used in organic solvent systems. However, their use in aqueous systems is difficult because of their high hydrophobicity. In fact, AOT has been reported to form vesicles in an aqueous solution at lower surfactant concentrations, resulting in a turbid solution.[23] Therefore, gemini surfactants

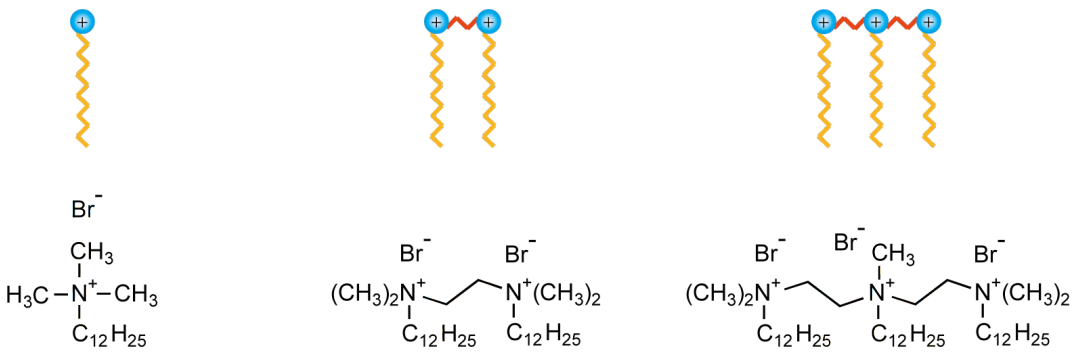

Figure 1-4. Representative structures of oligomeric surfactants that have been synthesized. [21–22]

with two hydrophilic head groups and two hydrophobic carbon chains have recently been synthesized for applications in aqueous systems or as model molecules. A typical example of a gemini surfactant with two head groups is 12-2-12, first synthesized by Zana in 1991.[21] This surfactant is more hydrophilic because of its two head groups and forms wormlike micelles in aqueous solutions.[24] Gemini surfactants can form wormlike micelles without the use of any additives, whereas monomeric surfactants form wormlike micelle in the presence of salts. This unique morphology is attributed to their high packing parameter or their higher end-cap energy.[25] The aggregation behaviors of gemini surfactants (*n*-*m*-*n*; *n*: hydrocarbon chain number, *m*: spacer chain number), e.g., the effect of the spacer or hydrocarbon chain length, the effect of a fluorine-substituted hydrocarbon chain, and the effect of head groups (cation or anion head), have been systematically investigated.[26] Furthermore, gemini surfactants have been recently reported to be useful for gene transfection because of their unique chemical structures.[27] They are also used for the synthesis of carbon nanotubes[28] and mesoporous silica[29] because of their unique aggregation behavior. Narrowly distributed particles have been successfully synthesized using gemini surfactants. Furthermore, their aggregation structure can be easily controlled at lower surfactant concentrations. For example, Silva et al. reported that gemini-surfactant-supported lipids form various aggregates (LipoPlex) in an aqueous solution.[30]

Other oligomeric surfactants that, like gemini surfactants, possess multiple hydrophilic heads and hydrophobic tails have also been synthesized. Trimeric surfactants exhibit lower CMCs and greater efficiencies for lowering surface tension than monomeric or gemini surfactants because of their extensive hydrophobic interactions. Furthermore, they have been reported to form branched wormlike micelles at lower surfactant concentrations than gemini surfactants.[22] Yan et al. have reported that highly ordered mesoporous silica can be synthesized using a cationic trimeric surfactant.[31] Trimeric surfactants with hydrophilic spacers have also been synthesized to overcome the problems associated with highly hydrophobic surfactants.[32] However, Wang et al. reported that gemini surfactants exhibit greater efficiency as pigment agents than trimeric surfactants because trimeric surfactants with hydrophilic spacer still exhibit strong hydrophobic interactions.[33] However, the aggregation structure of trimeric surfactants is easily controlled at lower surfactant concentrations because of

their high packing parameters. Understanding the characteristics of each surfactant is important for their application. However, there are few studies about the aggregation behavior of oligomeric surfactants because they are difficult to synthesize. Investigations of the aggregation structure of oligomeric surfactants are important for enabling their application.

1-4. Structural investigation of surfactant aggregation

Aggregates formed by surfactants have a nanoscale structure; observing the aggregation structure directly is therefore difficult. In recent studies, some effective methods for investigating nanoscale structures, e.g., cryoTEM, small-angle X-ray scattering (SAXS), small-angle neutron scattering (SANS), etc., have been used to observe the aggregation structure of surfactants. I describe the characteristics of each method in the following paragraphs.

(1) cryoTEM: The aggregation structure of surfactants can be observed in real-space. However, this method requires the preparation of thin films approximately 100 nm thick, which indicates that aggregates larger than 100 nm cannot be observed. For solutions with a viscosity too high to allow them to be prepared as a thin film or solutions that contain aggregates larger than 100 nm, freeze-fracture TEM (FF-TEM) can be used. In this method, the cold, sliced surface is shadowed with evaporated platinum and then coated with carbon. This metal replica is then observed by TEM. CryoTEM and FF-TEM are powerful methods for investigating nanoscale aggregation structures and do not lead to misunderstanding of the obtained structural information because they provide real-space observations. However, aggregation structures can be changed by freezing and cryoTEM images provide restricted local information. Furthermore, in-situ observations of the structure of surfactant aggregates under particular conditions, such as under flow, cannot be performed.

(2) Atomic force microscopy (AFM): AFM enables in-situ observations of surfactant aggregates. However, only the aggregation structure at a solid–liquid interface, e.g., on the silica substrate, can be observed. Therefore, AFM is a restricted method for investigating the aggregation behavior of surfactants.

(3) Static light scattering (SLS): The data obtained from SLS measurements is time- and space-averaged data that contains information in reciprocal space; such data must therefore be analyzed properly. Smaller-angle data, i.e., larger-scale information than that provided by SAXS or SANS, can be obtained from SLS measurements. It is appropriate for observing approximately 100 nm aggregates. Scattering data complements to microscopy measurements because scattering data is space-averaged data, whereas microscope images provide local information. Furthermore, TEM is a powerful method for observing the systems with sharp interface, while scattering method can evaluate the obscureness of interface as represented by density fluctuation.

(4) Dynamic light scattering (DLS): DLS measurements enable the sizes of aggregates to be estimated via a time correlation function. Therefore, DLS covers a wide range of size scales. However, obtaining an accurate estimation of particle size requires that a dilute solution with spherical particles be used.

(5) SAXS: Proper analysis of SAXS data is difficult because the obtained data is time- and space-averaged and provides information about the aggregation structure in reciprocal space. Compared with SANS measurements, SAXS measurements provided significant contrast of the scattering length density between the head groups and tail groups of surfactants. Therefore, information related to both the micelle core and shell can be obtained (**Figure 1-5**). Additionally, synchrotron SAXS measurements enable millisecond time-resolved measurements because they require less time than SANS or laboratory SAXS measurements.

(6) SANS: As is the case with SAXS, proper analysis of SANS data is difficult because the obtained data is time- and space-averaged and provides information about the aggregation structure in reciprocal space. Compared with SAXS, SANS requires longer measurement times and a larger amount of sample because the incident neutron intensity is weak. However, the neutron beam has good permeability. Therefore, SANS enables the in-situ investigation of structures under particular conditions because a thick quartz cell or aluminum cell can be used. In SANS measurements, almost only the

contrast between hydrogen atoms and other atoms can be observed (**Figure 1-6**). For this reason, the SANS data can be analyzed using a simple model. SANS measurements also have an advantage of low parasitic scattering and the possibility of changing contrasts. Contrast variation SANS can be performed by changing the ratio of deuterated solvent to normal solvent.

The structure of aggregates also can be determined using other methods, such as rheological measurements, spectroscopic measurements, etc. In previous studies of surfactant aggregates, the appropriate methods were selected according to the purpose of each study.

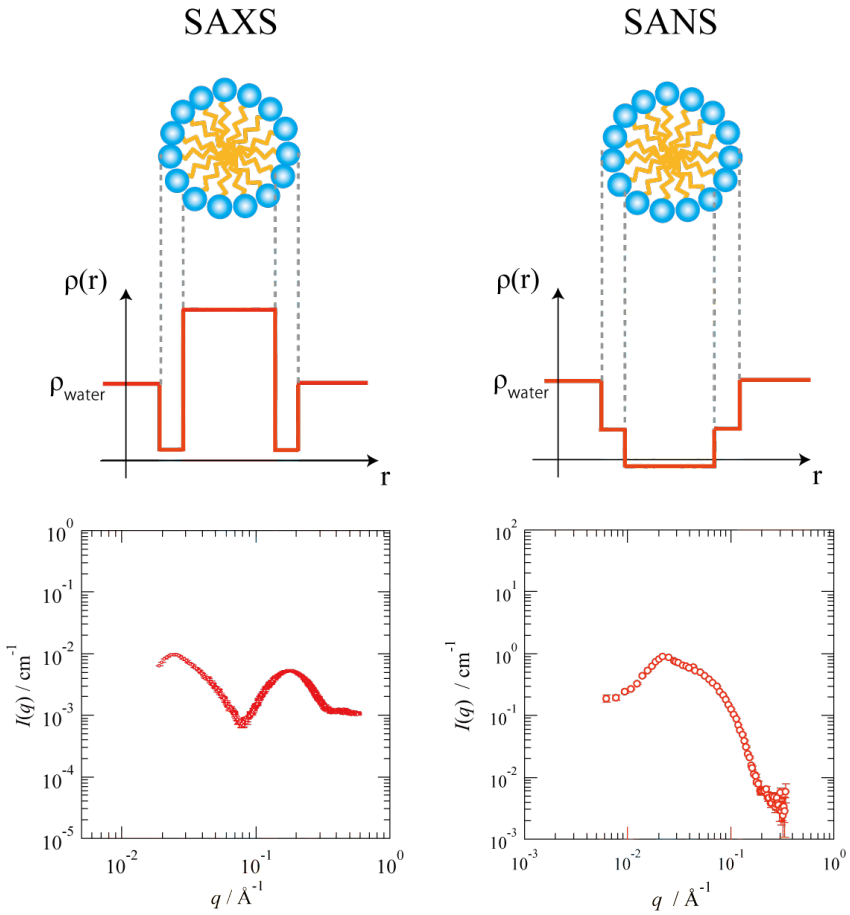

Figure 1-5. Upper figure: Comparison of the scattering-length density (ρ) for SAXS and SANS measurements. Lower figure: Comparison of the SAXS and SANS profiles for a micellar system.[34–35]

Self-aggregating surfactants have been used in various fields. For example, wormlike micelles are used in consumer products, as templates for mesoporous silica, and in enhanced oil recovery.[37] In contrast, RMs are commonly used to encapsulate labile hydrophilic molecules within their interior; they are therefore used to deliver drugs, enzymes, and DNA,[38–40] in cosmetic products,[41] and as nanoscale reactors.[42] The application of surfactant aggregates depends on their structures. Therefore, the literature contains numerous studies designed to elucidate the relationship between surfactants' aggregation and chemical structures.[26] In this thesis, scattering methods were mainly used to understand the in-situ aggregation structure of oligomeric surfactants.

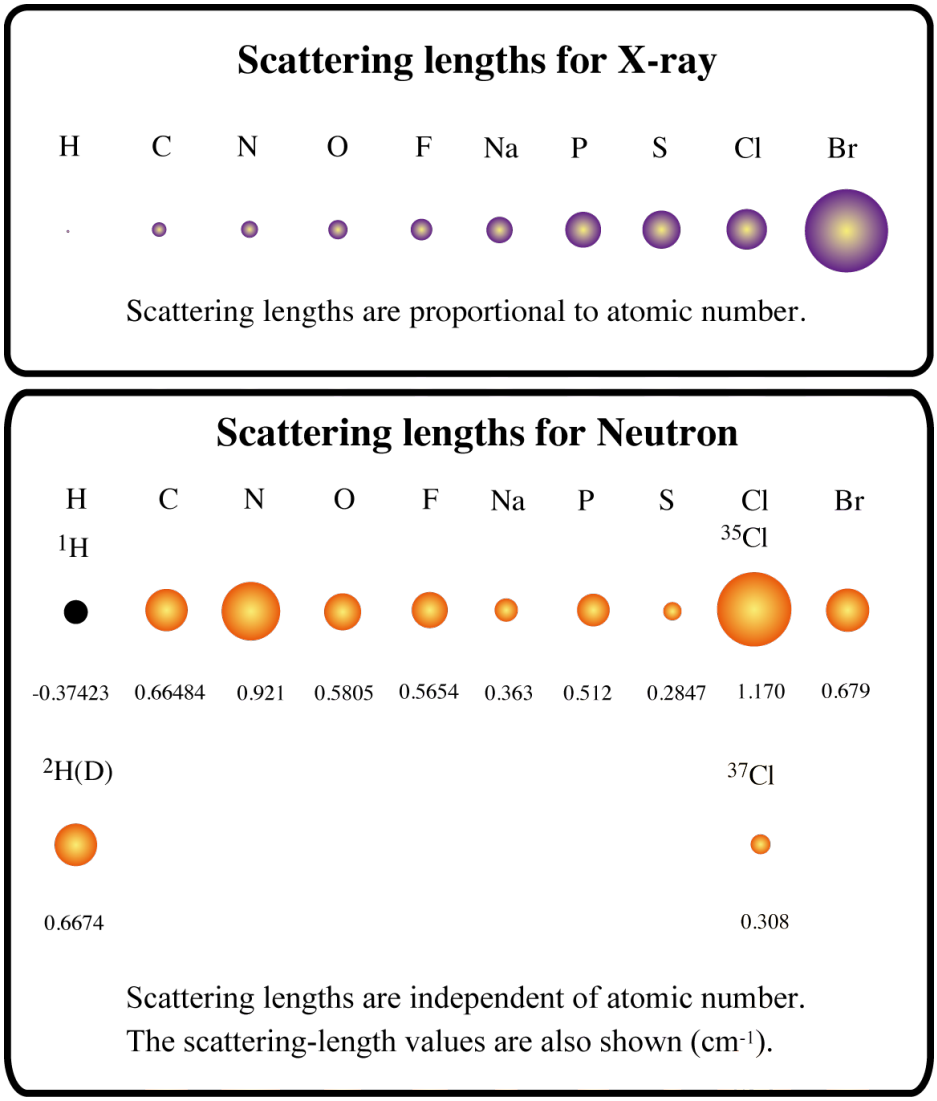

Figure 1-6. X-ray and neutron scattering lengths of various atoms.[36]

1-5. Outline of this thesis

In this thesis, the unique properties of aggregates formed by oligomeric surfactants were investigated. The following paragraphs summarize the contents of this thesis.

Chapter 2:

Because the synthesis of trimeric surfactants is more difficult than that of gemini surfactants, only a few studies on trimeric surfactant aggregates have been conducted. In this chapter, the novel quaternary ammonium star-shaped trimeric surfactants, tris(N-alkyl-N,Ndimethyl- 2-ammoniumethyl)amine bromides ($3C_n$trisQ, where n represents alkyl chain carbon number of 8, 10, 12, and 14) is used because they are easier to synthesize than previous ones. $3C_n$trisQ was derived from tris(2-aminoethyl)amine. Aggregation properties of the surfactants were evaluated by rheology, small angle neutron scattering (SANS), and cryogenic transmission electron microscopy (cryo-TEM). Furthermore, by using $3C_n$trisQ, the unique properties of wormlike micelles formed by oligomeric surfactants were discussed in the viewpoint of end-cap energy.

Chapter 3:

In chapter 3, the aggregation structure of trimeric surfactants in salt solution was investigated. Monomeric surfactants are known to show sphere-to-rod transition in the presence of organic salts. To clarify salt effect to aggregation structure for oligomeric systems, it is important to compare the structural behavior among monomeric, gemini, and trimeric surfactants. However, there are still few reports examining these trimeric surfactants.

In this chapter, the structural behavior of $3C_n$trisQ in the presence of NaSal was investigated. NaSal is a typical salt known to induce sphere-to-rod transition in lower salt concentration in monomeric or gemini surfactant systems. Therefore $3C_n$trisQ can show various aggregation structures in NaSal solution because $3C_n$trisQ show sphere-to-rod transition in the absence of salt, as described in chapter 2. Using small-angle X-ray scattering (SAXS) and rheological measurements, the structural

phase diagram of a 3C$_n$trisQ solution was determined by varying length of hydrocarbon chains of 3C$_n$trinsQ, a NaSal concentration, and a sample concentration.

Chapter 4:

In this chapter, oligomeric surfactants were used for water-in-ionic liquid (IL)-type reverse micelle (RM) systems. In this study, oligomeric surfactants are highly hydrophobic because of their multiple hydrocarbon chains and were therefore used in IL systems. IL-based RMs prepared using cationic or anionic surfactants provide an excellent reaction medium relative to conventional organic solvent systems. To our knowledge, however, IL-based RM systems without organic solvent have not been developed in an RM system with an ionic surfactant. Furthermore, the incorporation of organic solvents as one component in the system leads to a decrease in the IL mole fraction, which effectively limits the range of unique and novel properties of the ILs. In this study, the formation of water-in-IL RMs without organic solvents in an IL mixture of 1-octylimidazolium-based aILs and pILs with ionic oligomeric surfactants was reported. In the case of the organic-solvent-free system proposed here, this study focused on the variation in water-droplet size as a function of (1) the water concentration, C_W, and (2) the mole fraction of pIL, χ_{pIL}, which were characterized using DLS, SAXS, and SANS techniques.

References

(1) Yang, J. Viscoelastic Wormlike Micelles and Their Applications. *Curr. Opin. Colloid Interface Sci*., **2002**, 7**,** 276-281.

(2) Zana, R., *Surfactants Solutions: New Methods of Investigation*; MarcelDekker Inc., New York, 1987.

(3) Bikerman, J. J.; *Foams; Theory and Industrial Applications*, Reinhold, NY, 1953.

(4) Kim, W. J.; Yang, S. M. Preparation of Mesoporous Materials from the Flow-Induced Microstructure in Aqueous Surfactant Solutions. *Chem. Mater*. **2000,** 12, 3227-3235.

(5) Ezrahi, S.; Tuval, E.; Aserin, A.; Garti, N. *Daily Applications of Systems with Wormlike Micelles*. In *Giant Micelles*. R. Zana and E. W. Kaler. CRC Press, Boca Raton, 2007.

(6) Lawrence, M. J. Surfactant Systems: Their use in drug delivery. *Chem. Soc Rev.* **1994**, 23, 417-424.

(7) Israelachvili, J. N. *Intermolecular and Surface Forces,* Academic Press, London, 1992.

(8) Debye, P.; Anacker, E. W. Micelle Shape from Dissymmetry Measurements. *J. Phys. Chem.* **1951**, 55, 644-655.

(9) Pilpel, N. J. Viscoelasticity in Aqueous Soap Solutions. *J. Phys. Chem.* **1956**, 60, 779-782.

(10) Cates, M. E. Reptation of Living Polymers: Dynamics of Entangled Polymers in the Presence of Reversible Chain-Scission Reactions. *Macromolecules* **1987**, 20, 2289-2296.

(11) Shikata, T.; Hirata, H.; Kotaka, T. Micelle Formation of Detergent Molecules in Aqueous Media: Viscoelastic Properties of Aqueous Cetyltrimethylammonium Bromide Solutions. *Langmuir*, **1987**, 3, 1081-1086.

(12) Mackintosh, F. C.; Safran, S. A.; Pincus, P. A. Equilibrium size distribution of charged 'living' polymers. *J. Phys.: Condens. Matter 2*, **1990**, SA359-SA364.

(13) Helgeson, M. E.; Hodgdon, T. K.; Kaler, E. W.; Wagner, N. J. A systematic study of equilibrium structure, thermodynamics, and rheology of aqueous CTAB/$NaNO_3$ wormlike micelles. *Colloid Interface Sci.* **2010**, 349, 1–12.

(14) Hoar, T. P.; Schulman, J. H. Transparent Water-in-Oil Dispersions: the Oleopathic Hydro-Micelle. *Nature* **1943**, 152, 102–103.

(15) Helfrich, W. Elastic Properties of Lipid Bilayers: Theory and Possible Experiments. *NZ. Naturforsch C.* **1973**, 28, 11, 693–703.

(16) Farago, B.; Monkenbusch, M.; Goecking, K. D.; Richter, D.; Huang, J. S. Dynamics of Microemulsions as Seen by Neutron Spin Echo. *Physica B*. **1995**, 213&214, 712-717.

(17) Eastoe, J.; Hetherington, K. J.; Sharpe, D.; Dong, J.; Heenan, R. K.; Steytler, D. Films of Di-chained Surfactants in Microemulsions. *Colloids Surfaces A: Physicochem. Eng. Aspects* **1997**, 128, 209-215.

(18) Eastoe, J.; Gold, S.; Steyler, D. C. Surfactantts for CO_2. *Langmuir* **2006**, 22, 9832-9842.

(19) Moniruzzaman, M.; Kamiya, N.; Nakashima, K.; Goto, M. Formation of Reverse Micelles in a Room-Temperature Ionic Liquid. *ChemPhysChem* **2008**, 9, 689-692.

(20) Menger, F. M.; Keiper, J. S. Gemini Surfactants. *Angew. Chem. Int. Ed.* **2000**, 39, 1906-1920.

(21) Zana, R.; Benrraou, M.; Rueff, R. Alkanediyl-α, ω-bis(dimethylalky1ammonium bromide) Surfactants. 1. Effect of the Spacer Chain Length on the Critical Micelle Concentration and Micelle Ionization Degree. *Langmuir* **1991**, 7, 1072-1075.

(22) Danino, D.; Talmon, Y.; Levy, H.; Beinet, G.; Zana, R. Branched Threadlike Micelles in an Aqueous Solution of a Trimeric Surfactant. *Science* **1995**, 269, 1420-1421.

(23) Saha, R.; Verma, P. K.; Mitra, R. K.; Pal, S. K. Structural and Dynamical Characterization of Unilamellar AOT Vesicles in Aqueous Solutions and Their Efficacy as Potential Drug Delivery Vehicle. *Colloids Surf. B* **2011**, 88, 345-353.

(24) Schmitt, V.; Schosseler, F.; Lequeux, F. Structure of Salt-Free Wormlike Micelles: Signature by SANS at Rest and under Shear. *Europhys. Lett*. **1995**, 30, 31-36.

(25) In, M.; Warr, G. G.; Zana, R. Dynamics of Branched Threadlike Micelles. *Phys. Rev. Lett*. **1999**, 83, 11, 2278-2281.

(26) Han, Y.; Wang, Y. Aggregation Behavior of Gemini Surfactants and Their Interaction with Macromolecules in Aqueous Solution. *Phys. Chem. Chem. Phys*. **2011**, 13, 1939-1956.

(27) Kirby, A. J.; Camilleri, P., Engberts, J.; Feiters, M. C.; Nolte, R. J. M.; Soderman, O.; Bergsma, M.; Bell, P. C.; Fielden, M. L.; Rodriguez, C. L. G.; Guedat, P.; Kremer, A.; McGregor, C.; Perrin, C.; Ronsin, G.; Eijk, M. Gemini Surfactants: New Synthetic Vectors for Gene Transfection. *Angew. Chem. Int. Ed.* **2003**, 42, 1448-1457.

(28) Chen, L.; Xie, H.; Li, Y.; Yu, W. Applications of Cationic Gemini Surfactant in Preparing Multi-walled Carbon Nanotube Contained Nanofluids. *Colloids Surf. A* **2008**, 330, 176-179.

(29) Chen, Q.; Han, L.; Gao, C.; Che, S. Synthesis of Monodispersed Mesoporous Silica Spheres (MMSSs) with Controlled Particle Size Using Gemini Surfactant. *Micropor. Mesopor. Mater.* **2010**, 128, 203-212.

(30) Silva, S. G.; Oliveira, I. S.; Vale, M. C.; Marques, E. F. Serine-based Gemini Surfactants with Different Spacer Linkages: from Self-assembly to DNA Compaction, *Soft Matter*, **2014**, 10, 9352-9361.

(31) Yan, X.; Han, S.; Hou, W.; Yu, X.; Zeng, C.; Zhao, X.; Che, H. Synthesis of Highly Ordered Mesoporous Silica Using Cationic Trimeric Surfactant as Structure-directing Agent, *Colloids Surf. A* **2007**, 303, 219-225.

(32) Wu, C.; Hou, Y.; Deng, M.; Huang, X.; Yu, D.; Xiang, J.; Liu, Y.; Li, Z.; Wang, Y. Molecular Conformation-Controlled Vesicle/Micelle Transition of Cationic Trimeric Surfactants in Aqueous Solution, *Langmuir*, **2010**, 26 (11), 7922-7927.

(33) Wang, M.; Wu, C.; Tang, Y.; Fan, Y.; Han, Y.; Wang, Y. Interactions of Cationic Trimeric, Gemini and Monomeric Surfactants with Trianionic Curcumin in Aqueous Solution. *Soft Matter*, **2014**, 10, 3432-3440.

(34) Kusano, T.; Iwase, H.; Yoshimura, T.; Shibayama, M. Structural and Rheological Studies on Growth of Salt-Free Wormlike Micelles Formed by Star-Type Trimeric Surfactants. *Langmuir*, **2012**, 28, 16798-16806.

(35) Kusano, T.; Iwase, H.; Akutsu, K.; Yoshimura, T.; Shibayama, M. Structural Study on Aggregation Behavior of Star-Type Trimeric Surfactants in the Presence of Organic Salts. *Colloid Interface Sci.* **2014**, submitted.

(36) Sears, V. F. Neutron Scattering Length and Cross Sections. *Neutron News* **1992**, 3 (3), 26-37.

(37) Zana, R.; Kaler, E. W. *Giant Micelles*. CRC Press: Boca Raton, 2007

(38) Vrignaud, S.; Anton, N.; Gayet, P.; Benoit, J.; Saulnier, P. Reverse Micelle-loaded Lipid Nanocarriers: A Novel Drug Delivery System for the Sustained Release of Doxorubicin Hydrochloride. *Eur. J. Pharm. Biopharm*. **2011**, 79, 197-204.
(39) Moniruzzaman, M.; Kamiya, N.; Goto, M. Activation and Stabilization of Enzymes in Ionic Liquids. *Org. Biomol. Chem.* **2010**, 8, 2887-2899.
(40) Park, L.; Maruyama, T.; Goto, M. DNA Hybridization in Reverse Micelles and Its Application to Mutation Detection. *Analyst*, **2003**, 128, 161-165.
(41) Azeem, A.; Rizwan, M.; Ahmad, F. J.; Khan, Z. I.; Khar, R. K.; Aqil, M.; Talegaonkar, S. Emerging Role of Microemulsions in Cosmetics. *Recent Pat. Drug. Deliv. Formul.* **2008**, 2, 275-289.
(42) Uskokovic, V.; Drofenik, M. Synthesis Of Materials Within Reverse Micelles. Surf. Rev. Lett. **2005**, 12 (2), 239-277.

Chapter 2

Aggregation Behavior of Star-Type Trimeric Quaternary Ammonium Bromide Surfactants in Aqueous Solutions

2-1. Introduction

The growth of wormlike micelles in the presence of salts has been investigated using small-angle neutron scattering (SANS), rheological measurements, cryo-transmission electron microscopy (cryo-TEM), and molecular dynamics simulations.[1-7] It has been suggested that in the formation of wormlike micelles, counterions provided by the salts decrease the electrostatic interactions between the charges of the surfactant headgroups and induce sphere-to-rod transitions. Mackintosh et al. described the length of wormlike micelles as a function of the surface charges, temperature, radius, and end-cap energy (E_C) using mean-field theory[8] and qualitatively explained the effects of the added salts on micellar growth. Micellar growth depends strongly on the surface charges and E_C. Therefore, the effects of surface charges on wormlike micellar growth have been systematically investigated as a means for controlling the length of wormlike micelles. For example, the effects of the headgroups, organic salts, inorganic salts, and mixing of surfactants on the transition or growth of micelles have been studied.[3, 9-16] The structural formation of salt-free micelles consisting

of cationic surfactants and anions have also been extensively investigated. A variety of structures, such as wormlike micelles, vesicles, and lamellar systems have been observed.[17, 18] In salt-free systems, the structure is mainly determined by the surface charges of the cation-anion aggregates and the structure of the anions. Li et al. discussed the structure of aggregates in relation to the chain lengths of anions,[17] while Hao et al. observed the formation of nanodiscs and multi-lamellar structures depending on the ratio of the cations and anions.[18] They attributed the structural changes to intercalation of anions into cationic surfactants. It should be noted that charge effects remain significant, even for these salt-free systems.

These studies have suggested that wormlike micelles grow lengthwise by decreasing the surface charges, and that surface charges inhibit the growth of wormlike micelles. To elucidate the growth mechanism of wormlike micelles formed using a cationic surfactant in an aqueous solution, it is therefore necessary to study the effects of both surface charges and E_C. Although the effects of surface charges on wormlike micellar growth have been extensively studied, few studies have been reported on the effect of the E_C.[19, 20]

Because the synthesis of trimeric surfactants is more difficult than that of gemini surfactants, only a few studies of trimeric surfactant aggregates have been conducted.[21, 22] Herein, the synthesis of novel quaternary ammonium star-shaped trimeric surfactants, tris(N-alkyl-N,N-dimethyl-2-ammoniumethyl)amine bromides ($3C_n$trisQ, where n represents an alkyl chain carbon number of 8, 10, 12, or 14), from tris(2-aminoethyl)amine is described. The aggregation properties of the surfactants were evaluated by determining their rheological properties and using SANS and cryo-TEM. In addition, the unique properties of the wormlike micelles formed by the oligomeric $3C_n$trisQ, surfactants were investigated considering their E_C.

2-2. Experimental section

2-2-1. Materials

Tris(2-aminoethyl)amine, *n*-octyl iodide, *n*-decyl iodide, *n*-dodecyl iodide, and *n*-tetradecyl bromide were obtained from Tokyo Chemical Industry Co., Ltd. (Tokyo, Japan). Formaldehyde (35%) and formic acid (85%) solutions were purchased from

Nacalai Tesque, Inc. (Kyoto, Japan). Acetone, ethanol, ethyl acetate, hexane, methanol, hydrochloric acid (35%), and sodium hydroxide were obtained from Kanto Chemicals Co., Inc. (Tokyo, Japan). All chemicals were reagent-grade commercial materials and used without further purification.

2-2-2. Synthesis of tris(N-alkyl-N,N-dimethyl-2-ammoniumethyl)-amine bromides (3C*n*trisQ)[23]

①Tris(2-aminoethyl)amine (48.6 g, 0.33 mol) was added slowly to a stirred solution of formaldehyde (6.1 mol) and formic acid (5.6 mol) at room temperature, and the mixture was refluxed for 12 h. Concentrated hydrochloric acid was then added to the mixture, and the solution was heated on a water bath for 3 h. After the solution was concentrated on a rotary vacuum evaporator, the residual solid was washed twice with methanol and dried under reduced pressure to give tris(N,N-dimethyl-2-aminoethyl)amine hydrochloride as a white solid in 65% yield. tris(N,N-dimethyl-2-aminoethyl)-amine hydrochloride (10.0 g, 0.029 mol) was added slowly to 400 mL of methanol containing sodium hydroxide (16 g), and the solution was stirred while heating for 2–3 h. After the solvent was removed by evaporation, acetone was added to the residue, and the solution was filtered to remove the inorganic precipitate. The evaporation of acetone yielded ② tris(N,N-dimethyl-2-aminoethyl)amine as a brown liquid.

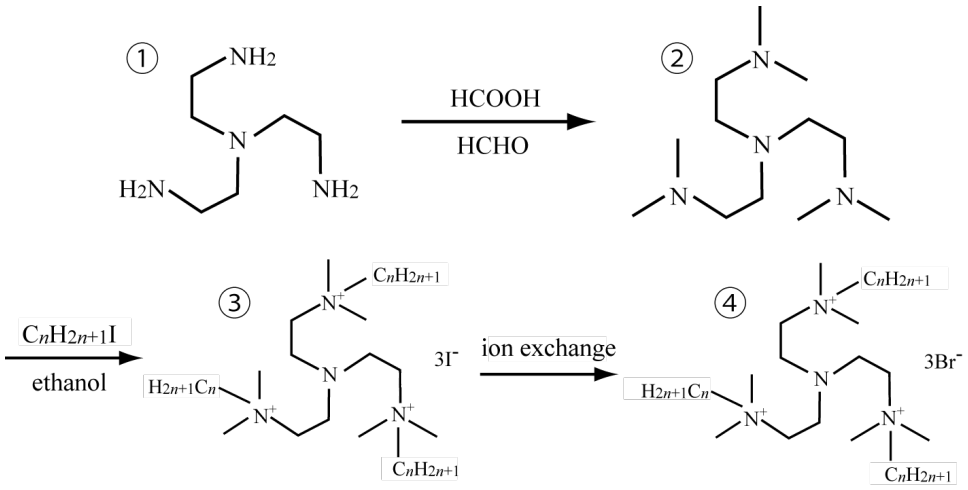

Figure 2-1. Synthetic route for the preparation of 3C*n*trisQ trimeric surfactants

Next, n-octyl iodide (n = 8), n-decyl iodide (n = 10), n-dodecyl iodide (n = 12), or n-tetradecyl bromide (n = 14) (0.174 mol) was added to a stirred solution of tris(N,N-dimethyl-2-aminoethyl)amine in approximately 200 mL of ethanol. Each mixture was refluxed for over 40 h. After the solvent was evaporated under reduced pressure, each residue was washed several times first with ethyl acetate and then with hexane and recrystallized from a mixture of ethyl acetate and ethanol to give the corresponding ③ tris(N-alkyl-N,N-dimethyl-2-ammoniumethyl)amine iodide or bromide as white solids. The yields were 74%, 76%, 82%, and 45% for n = 8, 10, 12, and 14, respectively.

To prepare the bromides for n = 8, 10, and 12, each iodide was dissolved in methanol and passed through a Dowex 1-X8 anion-exchange column (50–100 mesh) in order to exchange the iodide ions for bromide ions. After the eluent was evaporated under reduced pressure, each residue was washed with ethyl acetate, recrystallized from a mixture of ethyl acetate and ethanol, and dried under reduced pressure to afford 3C$_n$trisQ (n = 8, 10, and 12) as white solids.

^{1}H NMR ($CDCl_3$): δ 0.882 (t, 18H, CH_3–$(CH_2)_{n-1}$–N^+), 1.26 (m, (6n–18)H, CH_3–$(CH_2)_{n-3}$–CH_2–CH_2–N^+), 1.71 (m, 6H, CH_3–$(CH_2)_{n-3}$–CH_2–CH_2–N^+), 3.37 (s, 18H,–N^+–$(CH_3)_2$), 3.43 (t, 6H, CH_3–$(CH_2)_{n-3}$–CH_2–CH_2–N^+), 3.63 (t, 6H,–N–CH_2–CH_2–N^+–), 4.13 ppm (t, 6H,–N–CH_2–CH_2–N^+–).

Elemental analysis:

3C$_8$trisQ. Calculated for $C_{36}H_{81}N_4Br_3$ H_2O: C, 52.23; H, 10.11; N, 6.77. Found: 52.08; H, 10.73; N, 6.82.

3C$_{10}$trisQ. Calculated for $C_{42}H_{93}N_4Br_3$ H_2O: C, 55.32; H, 10.50; N, 6.14. Found: 55.20; H, 11.11; N, 6.36.

3C$_{12}$trisQ. Calculated for $C_{48}H_{105}N_4Br_3$ H_2O: C, 57.88; H, 10.83; N, 5.62. Found: 57.39; H, 11.02; N, 5.54.

3C$_{14}$trisQ. Calculated for $C_{54}H_{117}N_4Br_3$: C, 61.06; H, 11.10; N, 5.27. Found: 60.53; H, 11.58; N, 5.25.

2-2-3. Characterization

Except when used in the SANS experiment, the surfactant solutions were prepared using Milli-Q Plus water (resistivity = 18.2 MΩ·cm), and the analyses were performed

at 25 ± 0.5 °C. The surfactant solutions for the SANS measurements were prepared with deuterium oxide (D_2O), and the analyses were performed at 28 ± 0.5 °C.

Surface tension measurements

The surface tensions of aqueous solutions of the star-shaped trimeric surfactants were determined using a Krüss K122 tensiometer and the Wilhelmy plate technique. The surface excess concentration (Γ) in $mol \cdot m^{-2}$ and the area occupied by each molecule (A) of each trimeric surfactant at the air/solution interface were calculated using the classic Gibbs adsorption isotherm equations:[24] $\Gamma = -(1/iRT)(d\gamma/d\ln C)$ and $A = 1/(N\Gamma)$. Here γ is the surface tension, C is the surfactant concentration, R is the gas constant (8.31 J K^{-1} mol^{-1}), T is the absolute temperature, and N is Avogadro's number. The value of i in the equation for the trimeric surfactants was assumed to be 4, which is the number of possible species assuming complete dissociation in solution.

Rheological measurements

Rheological measurements were conducted by a stress control rheometer (MCR-501, Anton Paar, Austria) using a cone plate with a radius of 25.0 mm and a cone angle of 1°. The shear rate ($\dot{\gamma}$) and angular frequency (ω) ranged from 0.01 to 1000 s^{-1} and 0.1 to 100 s^{-1}, respectively. The sample temperature was maintained at 25 ± 0.03 °C.

SANS

SANS analyses were performed on the SANS-U instrument at the research reactor (JRR-3) at the Japan Atomic Energy Agency, Tokai, Japan. The sample-to-detector distances (SDDs) were 1.03 m and 8 m. The neutron wavelength was set at 7 Å with a wavelength distribution ($\Delta\lambda/\lambda$) of 0.11. The q-range was 0.005 to 0.3 $Å^{-1}$, where the magnitude of the scattering vector q is defined by $q = 4\pi\sin(\theta/2)/\lambda$ (λ and θ represent the wavelength and the scattering angle, respectively). "High intensity" focusing SANS (FSANS) analyses were performed using a stack of 55 biconcave MgF_2 lenses with a source aperture of 20 mm and a sample aperture of 15 mm. Details of the FSANS analyses on the SANS-U instrument have been described elsewhere.[25] All of the analyses were performed at ambient temperature (28 ± 0.5 °C). The results were corrected for the detector efficiency, solid-angle, and background scattering, and the

scattering intensity was converted to the absolute intensity per sample volume using a secondary low-density polyethylene standard.

SANS data analysis

In general, the SANS intensity of particle systems is described by:

$$I(q) = n_p(\Delta\rho)^2 V_p P(q) S(q), \tag{2.1}$$

where n_p, $\Delta\rho$, V_p, $P(q)$ and $S(q)$ are the number of particles per unit volume, the scattering contrast, the volume of a single particle and the form and structure factors, respectively. In the present study, the values for n_p and V_p were obtained as fitting parameters. The scattering contrast $\Delta\rho$ is defined as the difference in the scattering length densities of the micellar particles produced by the surfactant (ρ_{micelle}) and the water (ρ_{w}):

$$\Delta\rho = \rho_{\text{micelle}} - \rho_{\text{w}} \tag{2.2}$$

Assuming the penetration of water molecules into the micelle, the value of ρ_{micelle} is expressed as follows:

$$\rho_{\text{micelle}} = \frac{\sum b_{\text{surfactant}} + n_{\text{w}} \sum b_{\text{w}}}{v_{\text{surfactant}} + n_{\text{w}} v_{\text{w}}} \tag{2.3}$$

where $b_{\text{surfactant}}$ and b_{w} are the total scattering lengths of the surfactant and water, respectively, and $v_{\text{surfactant}}$ and v_{w} are the molecular volumes of the surfactant and water, respectively. Because the chemical components of $3C_{12}$trisQ and a water molecule are known, the scattering lengths and volumes can be estimated as $b_{\text{surfactant}} = -0.1575 \times 10^{-3}$ Å^{-2}, $b_{\text{w}} = 1.918 \times 10^{-3}$ Å^{-2}, $v_{\text{surfactant}} = 1511.2$ Å^3, and $v_{\text{w}} = 30.3$ Å^3. The parameter n_{w} denotes the number of water molecules per surfactant molecule inside the micelles.

As shown previously, in aqueous solutions $3C_{12}$trisQ forms ellipsoidal micelles at low concentrations and rodlike (wormlike) micelles at high concentrations.[23] The form factor $P(q)$ of a homogeneous ellipsoid with minor axis R_1 and major axis R_2 is given by:

$$P_{\text{ellip}}(q) = 9\int_0^1 \left(\frac{J_1(qR_s)}{qR_s} \right)^2 \mathrm{d}x \tag{2.4}$$

where $J_1(x)$ is the first order Bessel function of x. R_{s} is defined as

$$R_s = R_1\left[1 + x^2\left(u^2 - 1\right)\right]^{1/2} \tag{2.5}$$

where u is the axis ratio (R_2/R_1). In an aqueous solution, when the $3C_{12}$trisQ aggregates are spherical micelles, the value of u is 1. On the other hand, the form factor $P(q)$ of a homogeneous rod with radius R_C and full length L is given by

$$P_{\mathrm{rod}}(q) = \int_0^{\frac{\pi}{2}} \left[\frac{2J_1(R_C q \sin\alpha)}{R_C q \sin\alpha} \frac{\sin(Lq\cos\alpha/2)}{Lq\cos\alpha/2} \right]^2 \sin\alpha \mathrm{d}\alpha . \tag{2.6}$$

The structure factor $S(q)$ for a charged micellar system is calculated by applying a rescaled mean spherical approximation as proposed by Hayter and Penfold. This Hayter–Penfold $S_{\mathrm{HP}}(q)$ makes use of a model for charged hard spheres with electrostatic screening determined by the Debye screening length l_{D} of the solution.[26] For an asymmetric particle, such as an ellipsoid or a rod, the structure factor $S'(q)$ is used to correct for the anisotropic shape. Therefore, $S'(q)$ is given by[19]

$$S'(q) = 1 + \frac{\left|\langle F(q)\rangle\right|^2}{\langle |F(q)|\rangle^2} \left(S_{\mathrm{HP}}(q) - 1\right) \tag{2.7}$$

where $F(q)$ is the scattering amplitude.

Considering instrumental smearing, the obtained scattering curves $I_{\mathrm{res}}(q)$ can be described as

$$I_{\mathrm{res}}(q) = \int_0^{\infty} I(q) R(q') dq' \tag{2.8}$$

The resolution function $R(q')$ is approximately defined by a Gaussian function:

$$R(q') = \frac{1}{\sqrt{2\pi}\Delta q(q')} \exp\left[-\frac{(q'-q)^2}{2(\Delta q(q'))^2} \right] \tag{2.9}$$

where $\Delta q(q')$ is the standard deviation of q and given by

$$\Delta q(q') = q' \sqrt{\left(\frac{\Delta\lambda}{\lambda}\right)^2 + \left(\Delta\theta \cot\left(\sin^{-1}\left(\frac{\lambda q'}{4\pi}\right)\right)\right)^2} \tag{2.10}$$

where $\Delta\lambda/\lambda$ and $\Delta\theta$ are the wavelength and angular resolution, respectively. The $\Delta\theta$ values are determined by convolution of the direct beam intensity distribution. The reported values for $\Delta\lambda/\lambda$ = 0.11 and $\Delta\theta$ = 1.224 and 3.518 with SDDs of 8 and 1.03 m, respectively, were used.[25]

cryo-TEM

A small amount (3–5 μL) of sample aqueous solution was placed on a TEM copper grid covered by a porous carbon film, and the excess solution on the grid was blotted with filter paper to form a thin liquid film. The grid was then immediately plunged into liquid propane (−180 °C) cooled by liquid nitrogen in a cryofixation apparatus (LEICA, Reichert KF- 80) in order to fix the liquid water as vitreous ice. Next, the ice was transferred into the specimen stage of a cryo-TEM (JEOL, JEM-2100F(G5)) operated at an acceleration voltage of 200 kV through its cryotransfer apparatus cooled by liquid nitrogen. The specimen stage was cooled using liquid helium, and the specimen was maintained at −269 °C during observation

2-3. Results and discussion

2-3-1. Synthesis

The synthesis of the 3C$_n$trisQ trimeric surfactants and determination of their critical micelle concentrations (CMCs) were mainly performed by Prof. Yoshimura at Nara Women's University. Tris(*N*,*N*-dimethyl-2-aminoethyl)amine was reacted with *n*-alkyl iodides (except for n = 14) in order to obtain the star-type cationic trimeric surfactants in high yields via substitution of all three amines. The use of *n*-alkyl iodides afforded the trimeric surfactants in high yields and less time than when *n*-alkyl bromides were used. Determination of the surface tension using these trimeric surfactants with iodide counterions was attempted, but they did not sufficiently dissolve in water, and no

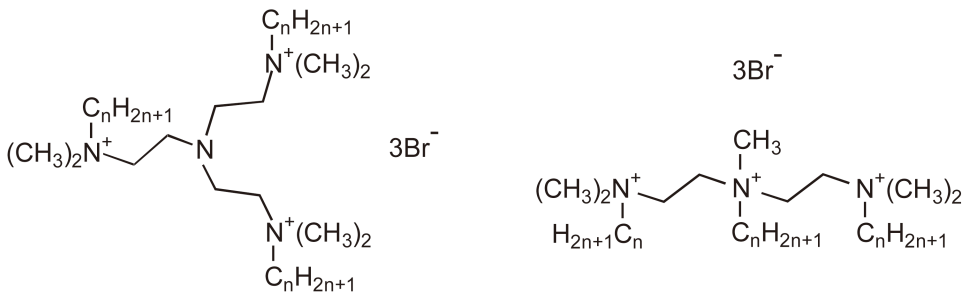

3C*n*trisQ ***n*-2-*n*-2-*n***

Figure 2-2. Chemical structures of star-shaped quaternary ammonium bromide trimeric surfactants, 3C$_n$trisQ, and liner-type trimeric surfactants, *n*-2-*n*-2-*n*.

breakpoints could be obtained in the surface tension versus concentration plots. Therefore, to improve their water solubility, the counterions of the trimeric surfactants with n = 8, 10, and 12 were exchanged with bromide ions using Dowex 1-X8, and the bromo 3C$_n$trisQs were used for the analyses described below (**Figure 2-2**). It should also be noted that these star-type trimeric surfactants 3C$_n$trisQ were obtained in higher yields and more simply than previously reported linear trimeric surfactants (n-2-n-2-n).[27]

2-3-2. Krafft temperature and CMC

Clear aqueous solutions of the star-type trimeric surfactants (0.20 wt%) were prepared by dissolving each surfactant in hot water and placing the solutions in a refrigerator at ~5 °C for at least 24 h. The temperature of the cooled surfactant solution was then raised gradually with constant stirring, and the conductance (κ) was measured every 0.5 to 1.0 °C (data not shown). Abrupt changes in the κ versus temperature plots were not observed because the Krafft temperatures of the star-type trimeric surfactants 3C$_n$trisQ are below 5 °C. The surfactant solutions were clear and no visual precipitates were observed. Therefore, the three quaternary ammonium headgroups gave the

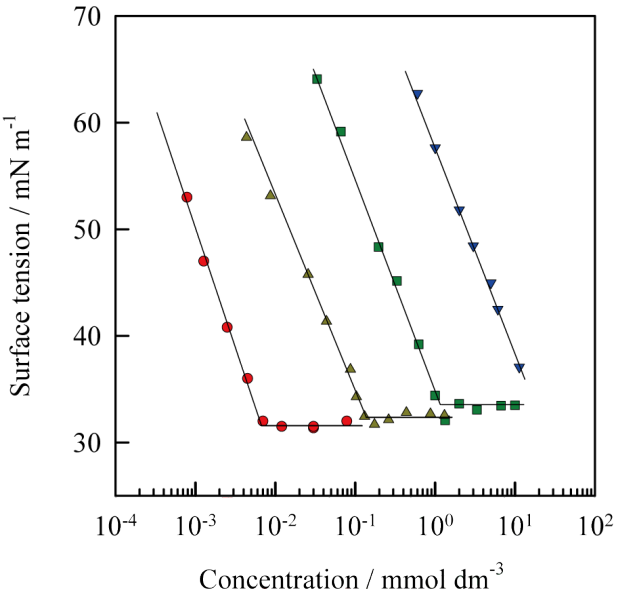

Figure 2-3. Variation in surface tension with surfactant concentration for 3C$_n$trisQ at 25 °C: ▼ (blue), n = 8; ■ (green), 10; ▲ (yellow), 12; ● (red), 14.[23]

$3C_n$trisQ surfactants good water solubilities at 25 °C, despite the three long hydrocarbon chains, even when n = 14.

The surface tensions for the $3C_n$trisQ surfactants with n = 8, 10, 12, and 14 at 25 °C were determined and are plotted as a function of concentration in **Figure 2-3**. The surface tensions for the surfactants with n = 10, 12, and 14 decreased with increasing concentration, reaching clear breakpoints that were taken to be their CMCs. Unfortunately, for the shortest chain length n = 8, the CMC could not be determined from the plot. In this case, due to the short chain length, micelles did not form in solution, even at the highest concentration studied, and the solution simply became turbid. In addition, the surface tension and CMC data were compared to those of corresponding monomeric, gemini, and linear trimeric surfactants, as listed in Table 2-1. The data include the CMC, surface tension at the CMC (γ_{CMC}), surface excess concentration (Γ), and area occupied by each surfactant molecule (A). The data for $3C_{12}$trisQ were compared to results for the trimeric surfactants C_{12}TAB (dodecyltrimethylammonium bromide, monomeric),[28,29] 12-2-12 (1,2-bis(dodecyldimethylammonium)ethane bromide, gemini),[28,30] and 12-*s*-12-*s*-12 (*s* represents spacer chain lengths of 2, 3, and 6; linear).[27, 28, 31.] As can be seen in Table 2-1, $3C_{12}$trisQ exhibited a CMC value lower than those of the corresponding monomeric and gemini surfactants. It is noteworthy that the CMC decreased by 1 order of magnitude for each additional hydrocarbon chain-hydrophilic headgroup. This result signified that the trimeric surfactants had excellent micelle-forming ability at low concentrations due to the increased hydrophobicity provided by the three hydrocarbon chains. On the other hand, the CMC of star-like $3C_{12}$trisQ was slightly higher than that of linear 12-2-12-2-12. This result was in line with our assumption that $3C_{12}$trisQ, based on tris(2-aminoethyl)amine, would have greater hydrophilicity due to the presence of the tertiary amine. In addition, $3C_{12}$trisQ exhibited a CMC lower than those of other linear cationic trimeric surfactants with spacers, such as *trans*-1,4-buten-2-ylene, *m*-xylylene, and *p*-xylylene (0.36, 0.28, and 0.29 mmol·dm^{-3}, respectively),[32] and two star-type cationic trimeric surfactants with three amide groups in the spacers (0.20 and 0.33 mmol·dm^{-3}),[33] although their counterions were chloride ions. Plots of the hydrocarbon chain length as a function of the logarithm of the CMC values for the

star-type trimeric surfactants 3C$_n$trisQ are compared with those of the monomeric,[34] gemini,[35] and linear-type trimeric[27] surfactants in **Figure 2-4**.

Table 2-1. The Critical Micelle Concentration, the Surface Tension at the CMC, the Surface Excess Concentration, and the Area Occupied per Molecule at the Air/Solution Interface for the Trimeric Surfactants 3C$_n$trisQ as well as for Monomeric Surfactants and Oligomeric Quaternary Ammonium Bromides at 25 °C[23]

Surfactant	cmc (mmol dm^{-3})	γ_{cmc} (mN m^{-1})	$10^6\Gamma$ (mol m^{-2})	A (nm^2 / molecule)
3C$_8$trisQ	-	-	0.875	1.9
3C$_{10}$trisQ	1.17	33.4	0.883	1.88
3C$_{12}$trisQ	0.139	32.3	0.82	2.03
3C$_{14}$trisQ	0.00647	32.1	0.97	1.7
C$_{12}$TAB	14 [a], 16 [b]	38.6 [a], 39 [b]	3.42 [a]	0.49 [a]
12-2-12	0.9 [a], 0.967 [c]	31.4 [a], 32.4 [c]	2.31 [a]	0.72 [a], 1.00 [c]
12-2-12-2-12	0.08 [a], 0.065 [d]	36.4 [d]	1.29 [a], 1.11 [d]	1.28 [a], 1.49 [d]
12-3-12-3-12	0.14 [e]		1.75 [e]	1.47 [e]
12-6-12-6-12	0.28 [e]		0.7 [e]	2.49 [e]

[a] Ref 28, [b] from Ref 29, [c] from Ref 30, [d] from Ref 27, [e] from Ref 31.

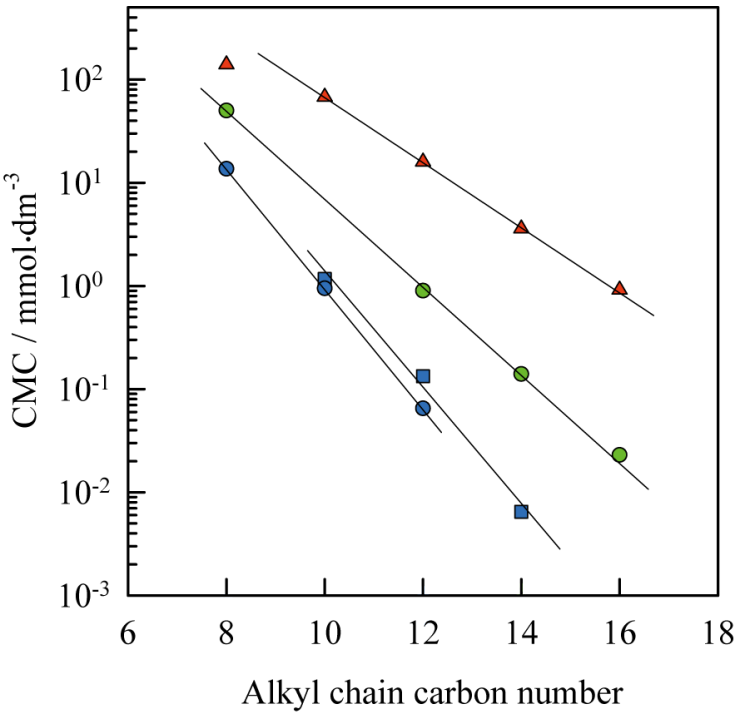

Figure 2-4. Relationships between the CMC and the hydrocarbon chain length for star-type trimeric 3C$_n$trisQ, [23] C$_n$TAB (monomeric),[34] *n*-2-*n* (gemini),[35] and *n*-2-*n*-2-*n* (linear-type trimeric):[27] □ (blue), 3C$_n$trisQ; △ (red), C$_n$TAB; ○ (green), *n*-2-*n*; ○ (blue), *n*-2-*n*-2-*n*.

It is generally known that the CMC decreases logarithmically as the carbon number (*n*) in the hydrocarbon chain of a homologous series increases, and the relation can be expressed by the so-called Klevens equation as log CMC = $A - Bn$, where A and B are constants specific to the homologous series under constant conditions (temperature, pressure, and other parameters). The relation for the star-type 3C$_n$trisQ surfactants was linear for hydrocarbon chain lengths from 10 to 14, and the slope was quite close to that for the previously investigated linear-type trimeric series[27]. That is, the B values were 0.31, 0.40, 0.58, and 0.56 for C$_n$TAB, *n*-2-*n*, *n*-2-*n*-2-*n*, and 3C$_n$trisQ, respectively, and increased as the number of chains increased, indicating that the variation in the CMC values with chain length was much greater for the trimeric surfactants. However, when the total carbon number in the hydrocarbon chains was taken into account, the effect of chain length on the CMC of the trimeric surfactants was similar to that on the gemini surfactants and less than that for the monomeric compounds.

Based on these data, it was found that the longer the chain length and the greater the chain number in the surfactants, the lower the CMC. This behavior may be attributed to thermodynamics, because there is less entropic loss in the formation of the micelles for the surfactants with longer chain lengths and greater chain numbers.[32,37]

2-3-3. Alkyl chain length dependence of aggregation structures.

The dependence of aggregate formation by the $3C_n$trisQ surfactants on the alkyl chain length was investigated. It is known that rheological behavior depends on the shape of the aggregates formed by surfactants in solution.[38,39] Therefore, the effect of the shapes of the aggregates formed by the different $3C_n$trisQ surfactants on their shear behavior of aqueous solutions were investigated using rheological measurements. The shear-rate dependence of the viscosity was determined at two concentrations of the star-type $3C_n$trisQ (n = 10, 12, and 14) trimeric surfactants, and the results are plotted in **Figure 2-5**. Data for pure water are also shown as solid lines for reference. Notably, for the $3C_{10}$trisQ solutions at 2.93 and 5.85 mmol·dm^{-3} (2.5 and 5.0 times the CMC, respectively), the shear-rate dependence of the viscosity was the same as that for water. Therefore, aggregation did not affect the solution viscosity. Based on previous findings, the shapes of the aggregates were assumed to be spherical or ellipsoidal micelles.[39,40] In addition, the behavior of the viscosity of a $3C_{12}$trisQ solution at 3.48 mmol·dm^{-3} (25 times the CMC) was also similar to that for water, indicating that spherical micelles were formed in solution. However, when the concentration was increased to 27.8 mmol·dm^{-3} (200 times the CMC), the viscosity of the $3C_{12}$trisQ solution decreased with increasing shear-rate, which is known as shear thinning and is a typical behavior for solutions containing rodlike or wormlike micelles[5,41] and chain-like polymers.[42] These results implied a spherical micelle-to-rodlike micelle transition as the concentration increased. This transition was also observed using SANS, cryo-TEM, and dynamic viscoelasticity analyses for gemini surfactants with dodecyl chains.[43,21] Details of the spherical micelle-to-rodlike micelle transition for $3C_{12}$trisQ are described in section 2-3-4 based on the results of SANS and cryo-TEM analyses. It should also be noted that both $3C_{14}$trisQ solutions at 0.162 and 1.62 mmol·dm^{-3} (25 and 250 times the CMC, respectively) were more viscous than water but their viscosities did not change as the shear-rate increased. The viscosity of $3C_{14}$trisQ was much lower than that of $3C_{12}$trisQ,

due to the different concentrations used for the analyses of the two surfactant solutions. It is possible that higher viscosities for aqueous $3C_{14}$trisQ solutions with higher $3C_{14}$trisQ concentrations may be obtained, even if all of the surfactant does not dissolve in water.

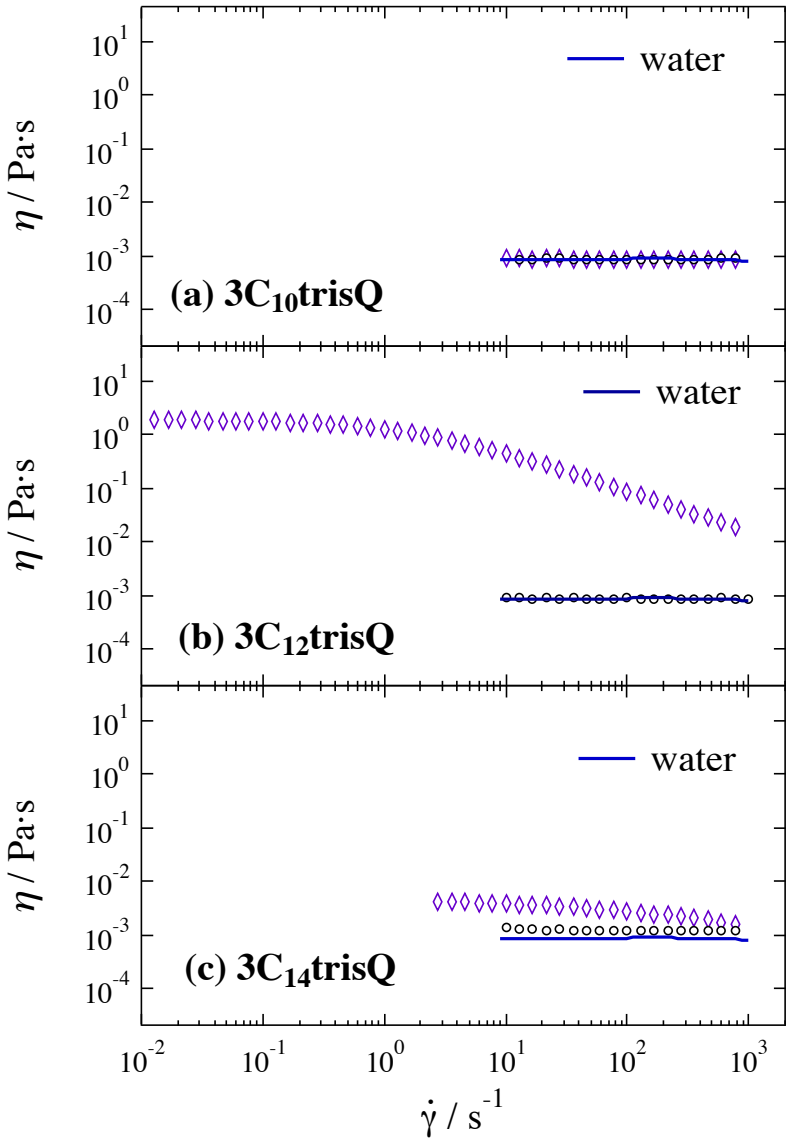

Figure 2-5. Shear-rate dependence of the viscosity for star-type trimeric surfactants $3C_n$trisQ (n = 10, 12, and 14) in aqueous solutions: (a) n = 10 (○(black), 2.93; ◊ (purple), 5.85 mmol·dm^{-3}), (b) n = 12 (○(black), 3.48; ◊ (purple), 27.8 mmol·dm^{-3}), and (c) n = 14 (○(black), 0.162; ◊ (purple), 1.62 mmol·dm^{-3}).[44]

SANS analyses were then performed in order to determine the structures of the aggregates formed in solution by the $3C_n$trisQ surfactants with n = 10, 12, and 14 (**Figure 2-6**). The $3C_{10}$trisQ and $3C_{12}$trisQ surfactants exhibited peak profiles in the q-range 0.02 $Å^{-1} < q < 0.05$ $Å^{-1}$. These peaks were attributed to repulsive inter-particle interactions between the micelles because the micelle surfaces were charged. With increasing surfactant concentration, these peak positions (indicated by arrows in fig. 2-6) shifted to higher q values. On the other hand, the SANS profiles for $3C_{14}$trisQ contained no peaks. That is, the SANS profiles at both concentrations showed $I(q) \sim q^{-1}$ in the low q-range ($q < 0.06$ $Å^{-1}$) and $I(q) \sim q^{-4}$ in the high q-range ($q > 0.06$ $Å^{-1}$), indicating that $3C_{14}$trisQ formed rodlike or wormlike micelles.

The scattering curves were fitted for $3C_n$trisQ with n = 10, 12, and 14 (fitted curves in fig. 2-6). As shown in **Figure 2-5a**, the shear-rate dependence of the viscosity indicated that $3C_{10}$trisQ formed spherical or ellipsoidal micelles in solution. Therefore, the theoretical scattering function for charged ellipsoidal particles was fit to a model (equations 2.2, 2.3, and 2.4). For $3C_{10}$trisQ, the R_1 and u values were estimated to be R_1 = 1.62 nm and u = 0.55 at 2.93 mmol·dm^{-3} (2.5 times the CMC), and R_1 = 1.71 nm and u = 0.51 at 5.85 mmol·dm^{-3} (5 times the CMC). For $3C_{12}$trisQ, according to the results of the rheological measurements, spherical or ellipsoidal micelles were also expected to be formed at 3.48 mmol·dm^{-3} (25 times the CMC). Therefore, the model fit was performed using the scattering function for charged ellipsoidal particles and calculated using equations 2.2, 2.3, and 2.4. The values for R_1 and u were estimated to be 1.93 nm and 0.44, respectively, using this model-fitting analysis. On the other hand, at 27.8 mmol·dm^{-3} (200 times the CMC), the rheological behavior of $3C_{12}$trisQ suggested the formation of wormlike micelles in aqueous solution. (The aggregation behavior and sphere-to-rod transition of $3C_{12}$trisQ is discussed in section 2-3-4).

To confirm the structures of the aggregates formed by $3C_{12}$trisQ, cryo-TEM observations were performed by Prof. Kurata and Dr. Ogawa at Kyoto University. Cryo-TEM analysis enables the direct visualization of aggregates in the thin layers of a vitrified specimen of a solution. Cryo-TEM micrographs for $3C_{12}$trisQ at concentrations of 13.9 and 27.8 mmol·dm^{-3} (100 and 200 times the CMC, respectively) are shown in **Figure 2-7**. Cryo-TEM observations were also attempted using a 6.95 mmol·dm^{-3} solution; however, the micrograph did not clarify due to the low concentration. At 13.9

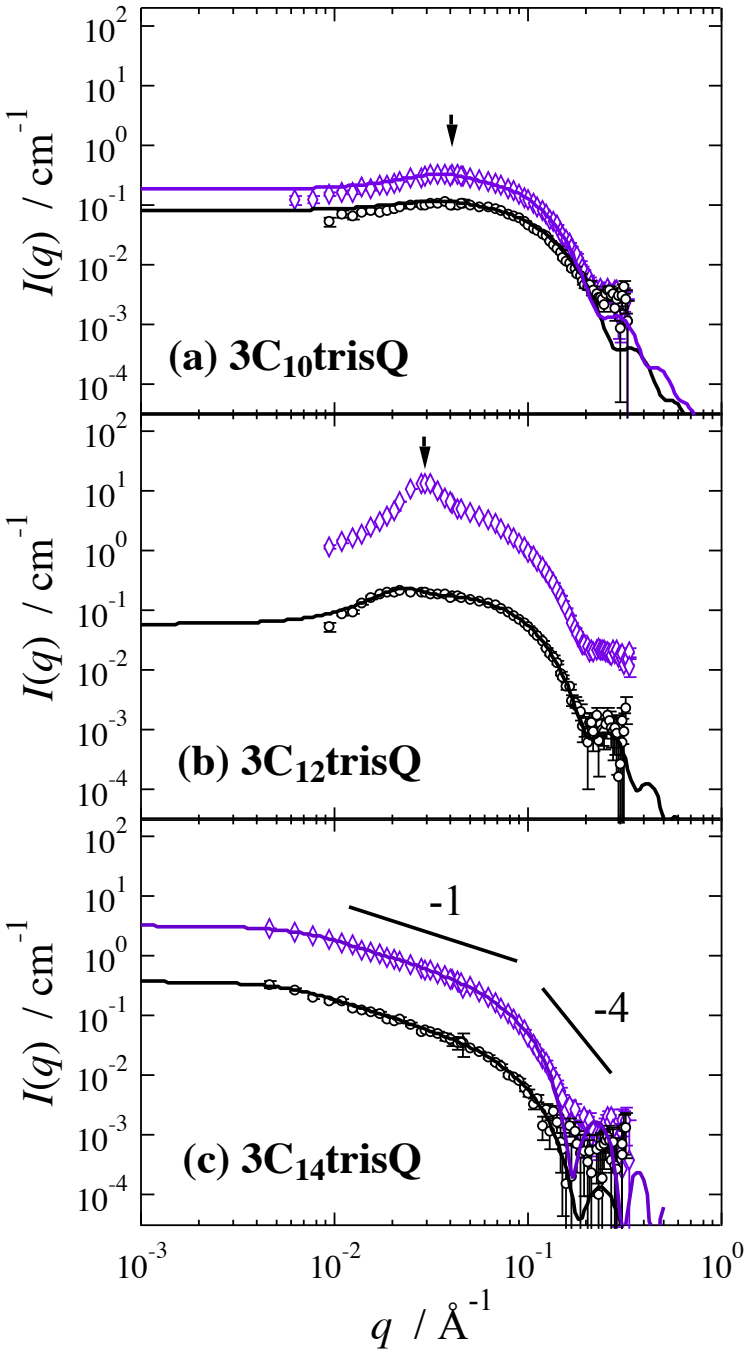

Figure 2-6. SANS profiles and fitted curves for the star-type trimeric surfactants 3C$_n$trisQ (n = 10, 12, and 14) in aqueous solutions: (a) n = 10 (○(black), 2.93; ◊ (purple), 5.85 mmol·dm^{-3}), (b) n = 12 (○(black), 3.48; ◊ (purple), 27.8 mmol·dm^{-3}), and (c) n = 14 (○(black), 0.162; ◊ (purple), 1.62 mmol·dm^{-3}). The solid lines represent the best-fit theoretical scattering functions.[44]

mmol·dm^{-3}, threadlike micelles with very few branches were clearly observed, and the length and number of the micelles increased with increasing concentration. The rod length, L, of the threadlike micelles determined via SANS analysis was expected to be approximately the same as the persistence length or mesh size because the cryo-TEM data suggested that the micelles had longer contour lengths. Zana et al. reported that linear-type quaternary ammonium salt trimeric surfactants (12-*s*-12-*s*-12) form branched threadlike micelles for $s = 3$[4,7] and spheroidal micelles for $s = 67$ in solution. In addition, the shapes of these micelles were similar to those of the corresponding gemini surfactants 12-*s*-12 with spacer chain lengths s = 2–12.[43,22] Star-shaped oligomeric surfactants, including $3C_{12}$trisQ, are capable of forming such structures because the multiple hydrocarbon chains of these surfactants can adopt different relative orientations in the micelles. Furthermore, the strong coulomb repulsions between the multiple quaternary ammonium headgroups may lead to an increase in the curvature of the surfactant film, which in turn favors branched threadlike micelles.

For $3C_{14}$trisQ, the SANS profiles indicated the presence of rodlike particles at both the concentrations. In addition, peak profiles were not observed (i.e., $S(q) \approx 1$). Therefore, model fitting was performed using only the form factor of the rod particles (equation 2.5), and the Rc values were estimated to be 2.26 and 2.13 nm at 0.162 (25 times the CMC) and 1.62 (250 times the CMC) mmol·dm^{-3}. According to the literature,[45] the scattering profile for rodlike particles indicates a crossover from q^{-1} behavior to constant (i.e., q_0) behavior in the lower q regions (Guinier q-region). However, this crossover was not observed in the actual SANS results, and therefore the length (L) of the rodlike micelles for $3C_{14}$trisQ was expected to be more than 25 nm (= $1/q_{min}$, where q_{min} is the lowest accessible q limit).

2-3-4. Sphere-to-rod transition of $3C_{12}$trisQ.

As mentioned in the previous section, $3C_{12}$trisQ exhibited a sphere-to-rod transition with increasing surfactant concentration, while the aggregation structures of $3C_{10}$trisQ and $3C_{14}$trisQ were independent of the surfactant concentration. Therefore, the structural transition of $3C_{12}$trisQ was investigated in detail using SANS and rheological analyses.

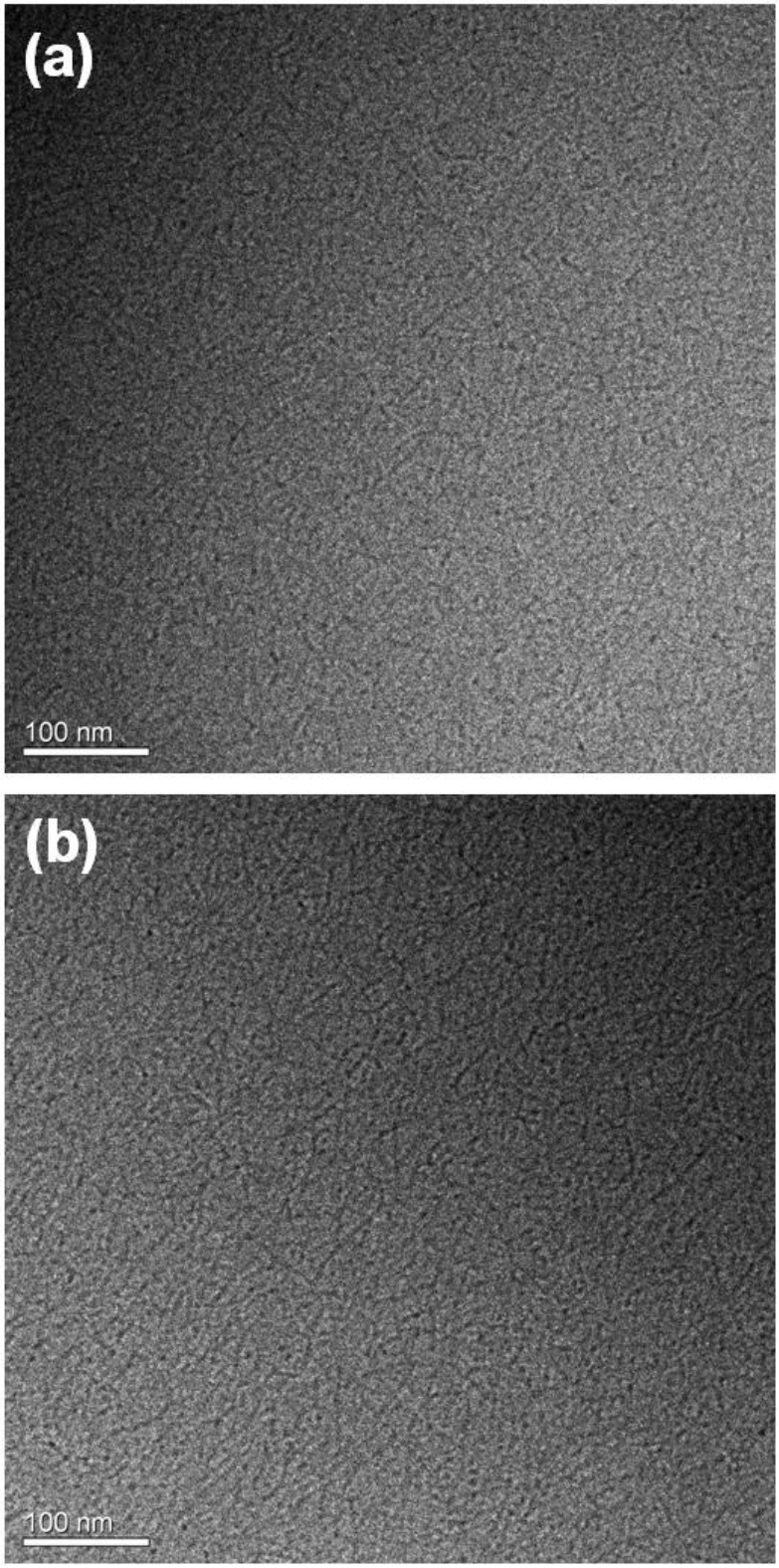

Figure 2-7. Cryo-TEM images for $3C_{12}$trisQ in solution: (a) 13.9 mmol·dm^{-3} and (b) 27.8 mmol·dm^{-3}.[44]

i) SANS study

Figure 2-8 shows the SANS profiles for aqueous $3C_{12}$trisQ solutions with volume fractions (ϕ) ranging from 0.0034 (C_M = 0.0035 mol·dm^{-3}) to 0.0272 (C_M = 0.0278 mol·dm^{-3}). All of the SANS profiles for $3C_{12}$trisQ exhibited broad peak profiles in the q-range from 0.02 to 0.05 Å^{-1} that were attributed to the electrostatic repulsion between the surface charges of the micelles.

According to a previous SANS study of the aggregation behavior of cationic gemini surfactants,[46] the sphere-to-rod transition of micelles can be easily elucidated by analyzing the ϕ-dependence of the SANS peak-position (q_m). **Figure 2-8b** shows the ϕ-dependence of q_m. With increasing ϕ from 0.0034 (C_M = 0.00348 mol·dm^{-3}) to 0.0102 (C_M = 0.0104 mol·dm^{-3}) the peak-positions shifted to higher q values, while there was a shift to lower q values when ϕ was between 0.0102 (C_M = 0.0104 mol·dm^{-3}) and 0.0170 (C_M = 0.0174 mol·dm^{-3}). Further increases in ϕ (from 0.0170 to 0.0272) caused these peak-positions to shift to higher q values. This behavior of $3C_{12}$trisQ was also observed in gemini surfactant (12-2-12) solutions.[46]

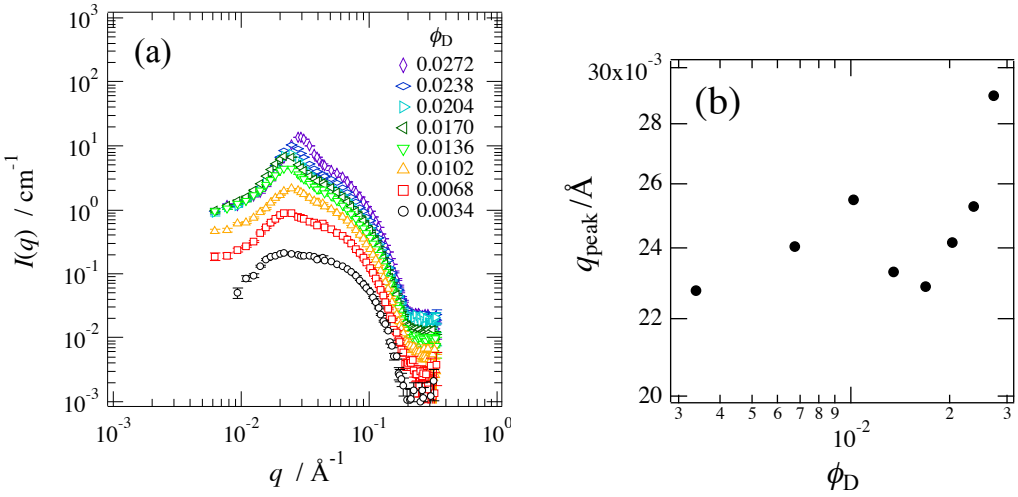

Figure 2-8. (a) Variation of SANS profiles for $3C_{12}$trisQ in aqueous solution with varying volume fractions (ϕ_D) from 0.0034 (C_M = 0.0035 mol·dm^{-3}) to 0.0272 (C_M = 0.0278 mol·dm^{-3}). (b) ϕ-dependence of the SANS peak-positions observed in the q-range of 0.02 Å^{-1} < q < 0.05 Å^{-1}.[44]

ii) Rheological measurements

Figure 2-9a shows the dependence of the viscosity of aqueous $3C_{12}$trisQ solutions with ϕ values ranging from 0.0034 (C_M = 0.0035 mol·dm^{-3}) to 0.0272 (C_M = 0.0278 mol·dm^{-3}) on the shear rate. An experimental result for water is also shown for reference. At $\phi \leq 0.0068$ (C_M = 0.0070 mol·dm^{-3}), the viscosity of the aqueous $3C_{12}$trisQ solutions was nearly independent of the shear viscosity and similar to that of water. At ϕ values ranging from 0.0102 (C_M = 0.0104 mol·dm^{-3}) to 0.0170 (C_M = 0.0174 mol·dm^{-3}), the viscosity was higher than that of water, but remained independent of the shear rate. However, at ϕ values ranging from 0.0204 (C_M = 0.0209 mol·dm^{-3}) to 0.0272 (C_M = 0.0278 mol·dm^{-3}), the viscosity monotonically decreased with increasing shear rate, which is a well-known phenomenon called "shear thinning." This behavior is typical for wormlike micelles[39, 40] and chain-like polymers.[47] Therefore, the results of the rheological analysis suggested that wormlike micelles were formed by $3C_{12}$trisQ at ϕ values ranging from 0.0204 (C_M = 0.0209 mol·dm^{-3}) to 0.0272 (C_M = 0.0278 mol·dm^{-3}).

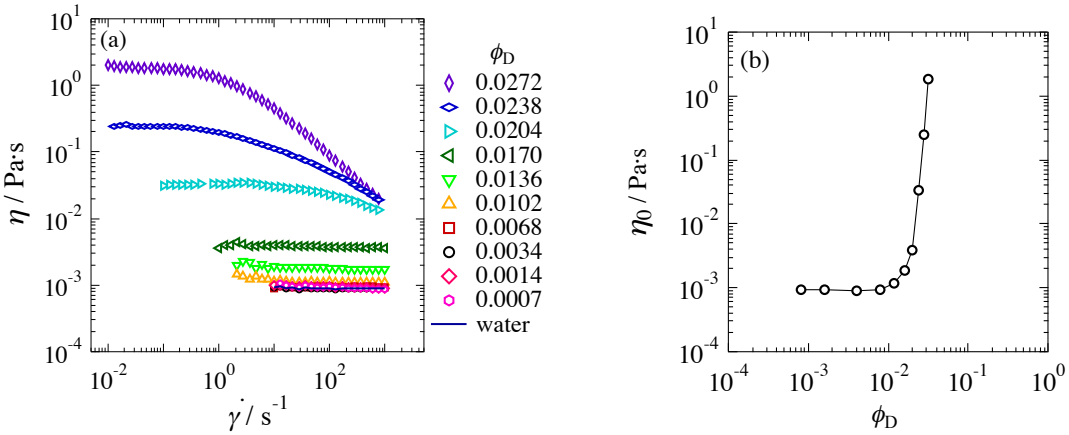

Figure 2-9. (a) Shear-rate dependence of the viscosity of aqueous $3C_{12}$trisQ solutions with volume fractions (ϕ) ranging from 0.0007 (C_M = 0.0007 mol·dm^{-3}) to 0.0272 (C_M = 0.0278 mol·dm^{-3}). (b) ϕ-dependence of the zero-shear viscosity of aqueous $3C_{12}$trisQ solutions obtained by extrapolating the viscosity to the zero-shear region. [44]

Figure 2-9b shows the ϕ-dependence of the zero-shear viscosity (η_0) for the aqueous $3C_{12}$trisQ solutions estimated by extrapolating the viscosity to a zero-shear rate ($\dot{\gamma} = 0$). As can be seen in the figure, η_0 was constant at $\phi \leq 0.0068$ ($C_M = 0.0070$ mol·dm^{-3}), began to gradually increase at $\phi = 0.0102$ ($C_M = 0.0104$ mol·dm^{-3}), and then rapidly increased at $\phi = 0.0204$ (0.0209 mol·dm^{-3}). This behavior indicated that wormlike micelles were formed by $3C_{12}$trisQ, and at ϕ values between 0.0102 (C_M = 0.0104 mol·dm^{-3}) and 0.0272 ($C_M = 0.0278$ mol·dm^{-3}), the wormlike micelles grew in size with increasing ϕ.

Many rheological studies have shown that wormlike micelle systems exhibit unique viscoelastic behaviors; for instance, the behavior of entangled wormlike micellar solutions can be represented by a Maxwell model with a single relaxation time, while the behavior of short wormlike micellar solutions resembles that of flexible polymer solutions.[11] Therefore, viscoelastic measurements were performed using aqueous $3C_{12}$trisQ solutions with ϕ values ranging from 0.0007 ($C_M = 0.0007$ mol·dm^{-3}) to 0.0272 ($C_M = 0.0278$ mol·dm^{-3}). **Figure 2-10** shows the ϕ-dependence of the storage modulus G' and the loss modulus G" for aqueous $3C_{12}$trisQ solutions with ϕ values of 0.0204 ($C_M = 0.0209$ mol·dm^{-3}) and 0.0272 ($C_M = 0.0278$ mol·dm^{-3}) as representative results. At $\phi \leq 0.0170$ ($C_M = 0.0174$ mol·dm^{-3}), the ω-dependence of the G" values for the aqueous $3C_{12}$trisQ solutions was similar to that for water. At ϕ values ranging from 0.0204 ($C_M = 0.0209$ mol·dm^{-3}) to 0.0238 ($C_M = 0.0243$ mol·dm^{-3}), the G" values were higher than the storage modulus values G', which implied that the rheological behavior of these $3C_{12}$trisQ solutions was the same as that of the pure liquid surfactant. However, at $\phi = 0.0272$ ($C_M = 0.0278$ mol·dm^{-3}), the results indicated the G' and G" crossover point. Prior to the crossover point, the solutions exhibited aqueous behavior with G" greater than G', but beyond the crossover point (ω = ca. 5 s^{-1}); the aggregate structure became predominantly elastic. This viscoelastic behavior of the $3C_{12}$trisQ solutions at ϕ = 0.0238 ($C_M = 0.0243$ mol·dm^{-3}) and $\phi = 0.0272$ ($C_M = 0.0278$ mol·dm^{-3}) are similar to those for cetyltrimethylammonium bromide solutions in the presence of low sodium salicylate concentrations[3] (i.e., typical for wormlike micelles).

iii) Surfactant concentration dependence of $3C_{12}$trisQ aggregation structures

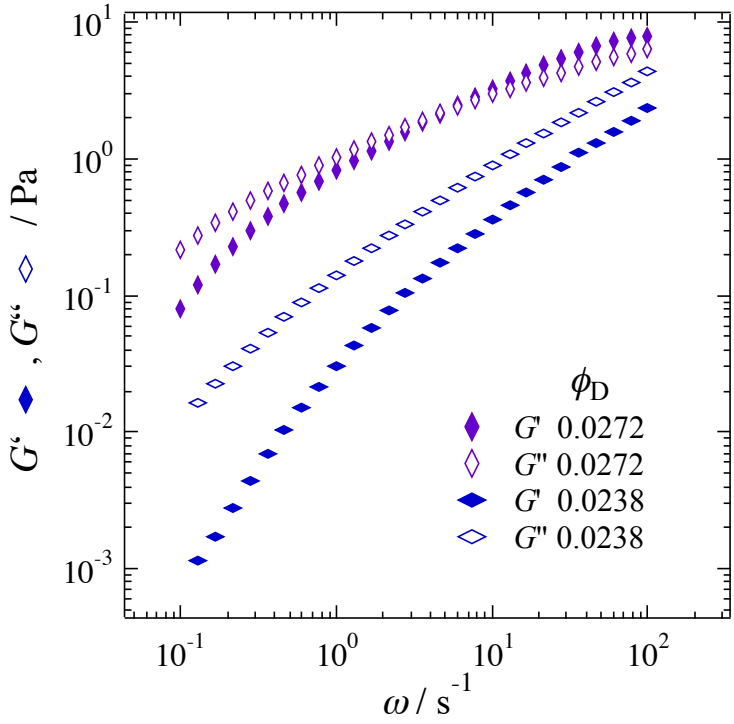

Figure 2-10. Storage modulus G’ and the loss modulus G” for aqueous $3C_{12}$trisQ solution with ϕ = 0.0238 (C_M = 0.0243 mol·dm^{-3}) and ϕ = 0.0272 (C_M = 0.0278 mol·dm^{-3}) as a function of the angular frequency. [44]

As indicated in the previous section, the $3C_{12}$trisQ aggregates formed ellipsoidal micelles at ϕ = 0.0034 (C_M = 0.0035 mol·dm^{-3}) and rodlike (wormlike) micelles at ϕ = 0.0272 (C_M = 0.0278 mol·dm^{-3}), suggesting a sphere-to-rod transition in the $3C_{12}$trisQ solutions. Therefore, the aggregation behavior of $3C_{12}$trisQ (such as the sphere-to-rod transition and wormlike micellar growth) as a function of the sample volume fraction was further investigated.

The combination of SANS and rheological analysis results revealed the aggregation behavior of $3C_{12}$trisQ in aqueous solutions. According to the ϕ-dependence of the SANS peak-position q_m (shown in fig. 2-8b) and of the zero-shear viscosity (shown in fig. 2-9b), the aggregate behavior of $3C_{12}$trisQ in aqueous solutions can be classified into three ϕ-regions; ϕ-region (I), where $\phi \leq$ 0.0068 (CMC × 50, C_M = 0.0070 mol·dm^{-3}), ϕ-region (II), where 0.0102 (CMC × 75, C_M = 0.0104 mol·dm^{-3}) $\leq \phi \leq$ 0.0170 (CMC × 100, C_M = 0.0174 mol·dm^{-3}), and ϕ-region (III), where 0.0204 (CMC ×

150, C_M = 0.0209 mol·dm^{-3}) ≤ ϕ ≤ 0.0272 (CMC × 200, C_M = 0.0278 mol·dm^{-3}). The features of each region were then compared with the properties of monomeric and gemini surfactants in aqueous solutions.

ϕ-Region (I); ϕ ≤ 0.0068 (CMC × 50, 0.00695 mol·dm^{-3}). The viscosity analysis results shown in fig. 2-9a indicate that the dependence of the viscosity on the shear rate was similar to that of water, implying that 3C$_{12}$trisQ formed small aggregates, i.e., spherical micelles, in aqueous solution.

ϕ-Region (II); 0.0102 (CMC × 75, 0.0104 mol·dm^{-3}) ≤ ϕ ≤ 0.0170 (CMC × 125, 0.0174 mol·dm^{-3}). In fig. 2-9, it can be seen that the SANS peak-position q_m shifted to lower q values with increasing ϕ in ϕ-region (I), while it shifted to higher q values in ϕ-region (II). Specifically, in ϕ-region (II), the shear rate dependence of the viscosity (shown in fig. 2-9a) for 3C$_{12}$trisQ was higher than that of water, and it behaved as a Newtonian fluid (Newtonian plateaus were observed). The zero-shear viscosity asymptotically increased with increasing ϕ. These results correspond with observations for gemini surfactant wormlike micelle solutions. Thus, it can be concluded that in ϕ-region (II), the aggregation behavior of 3C$_{12}$trisQ is similar to that of the gemini (12-2-12) surfactant in an aqueous solution, i.e., wormlike micelles are formed, and their length increases with increasing ϕ.

ϕ-Region (III); 0.0204 (CMC × 150, 0.0209 mol·dm^{-3}) ≤ ϕ ≤ 0.0272 (CMC × 200, 0.0278 mol·dm^{-3}). Fig. 2-9a clearly shows that the 3C$_{12}$trisQ solution in ϕ-region (III) exhibited shear thinning, suggesting that 3C$_{12}$trisQ produced long, wormlike micelles in the aqueous solution. The remarkable increase in the zero-shear viscosity (seen in fig. 2-9b) corresponded to the growth of wormlike micelles and overlapping wormlike micelles.[36]

iv) Model-fitting analysis for the SANS results

To investigate the growth of the micelles, a model-fitting analysis for the 3C$_{12}$trisQ SANS results was performed. Model-fitting results for the 3C$_{12}$trisQ solution at ϕ = 0.0034 (C_M = 0.0035 mol·dm^{-3}) and ϕ = 0.0272 (C_M = 0.0279 mol·dm^{-3}) were reported previously.[45] In ϕ-region (I), according to the ϕ-dependence of the q_m value and the zero-shear viscosity, the 3C$_{12}$trisQ aggregates were spherical (or ellipsoidal) micelles in these aqueous solutions. Considering the results obtained in previous SANS studies of

various cationic surfactants,[1-4] a charged ellipsoidal particle model was assumed; the scattering function for this model is represented by equations 2.4, 2.5, and 2.7.

In ϕ-region (II), the viscosity and SANS analysis results indicated that $3C_{12}$trisQ formed wormlike (or rodlike) micelles in aqueous solutions. Theoretically, the form factor $P(q)$ for wormlike micelles should exhibit asymptotic behavior (q^{-2}) in the low q-region and q^{-1} in the medium q-region. However, these SANS profile features were not observed for $3C_{12}$trisQ due to the combined peak-profile, i.e., structure factor $S(q)$. Therefore, structural information on the flexibility and length of the wormlike micelles was absent in the present SANS results, which is a notable problem for salt-free cationic surfactant solutions. As a result, in this case model-fitting analyses were performed using a theoretical scattering function for the charged rod particle model. The form factor $P(q)$ for rod particles with radius R_c and length L is given by equation 2.6. The structure factor $S(q)$ was calculated using the Hayter–Penfold method based on the rescaled mean spherical approximation (equation 2.7).

In ϕ-region (III), the viscosity data clearly indicated that wormlike micelles overlapped in the aqueous solutions. Consequently, a charged rod particle model could not be applied for model-fitting analysis because the Hayter–Penfold structure factor $S(q)$ (equation 2.7) assumes a small anisotropic degree for each particle. However, as a reference, the model-fitting analysis was carefully performed using a charged rod particle model in order to compare the calculated results with the experimental results for this ϕ-region.

Figure 2-11 shows both the best-fit theoretical scattering curves and experimental SANS profiles for $3C_{12}$trisQ in aqueous solutions. The theoretical scattering functions appropriately fitted all of the experimental results. Interestingly, the SANS profiles for the $3C_{12}$trisQ solutions in ϕ-region (III) were also in agreement with the theoretical SANS curve calculated using a charged rodlike particle. However, it should be noted that when a long charged rodlike model expressed using a random phase approximation (RPA) and PRISM-type interactions was assumed,[48] the SANS profiles for the $3C_{12}$trisQ solutions could not be simulated.

The details of these results are not discussed herein because these model-fitting functions may not be applicable to $3C_{12}$trisQ solutions in ϕ-region (III). An extensive study of overlapping wormlike micelles for $3C_{12}$trisQ solutions in ϕ-region (III) using

other techniques, such as computer simulations and Cryo-TEM observations, must be conducted. **Figures 2-12a–d** show the ϕ dependence of the structural parameters, including the radius (R), length (L), number of water molecules per surfactant molecule inside the micelles (n_w), and Debye screening length (l_D), obtained from the model-fitting analysis of the SANS results.

Fig. 2-12a shows the ϕ-dependence of the radius (R) of the micelles obtained from the model-fitting analysis, which corresponded to the minor axis (R_1) of an ellipsoid particle in ϕ-region (I) and the cross-sectional radius (R_c) of a rodlike particle in ϕ-regions (II) and (III). The obtained R values were nearly constant and ranged from 18.4 to 20.0 Å. As a reference, the fully extended length of the hydrocarbon chain l_c can be estimated using the Tanford formula:[49]

$$l_c = 1.54 + 1.265n_c \quad (\text{Å}) \tag{2.11}$$

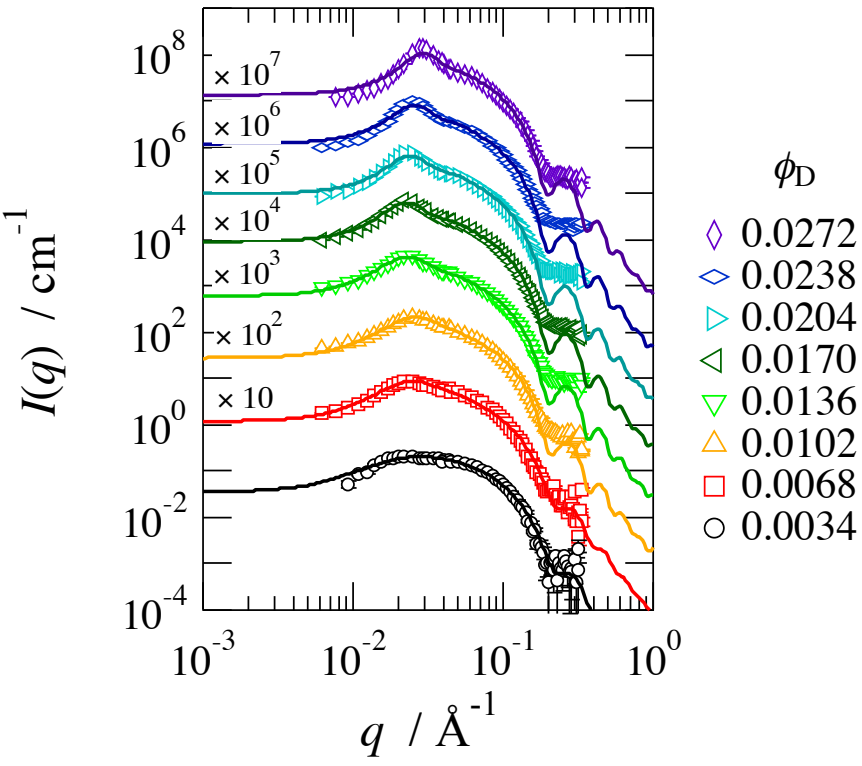

Figure 2-11. Comparison of the experimental scattering profiles (symbols) and best-fit calculated scattering curves (solid lines) for aqueous $3C_{12}$trisQ solutions. The profiles are vertically shifted to avoid overlap.[44]

where n_c is the number of carbon atoms in the hydrocarbon chain. The value of l_c was estimated using equation 2.11 to be 16.7 Å for n_c = 12, which was smaller than the R value obtained from the model-fitting analysis. However, considering the length of the hydrophilic group, the value obtained in the model-fitting analysis was appropriate, and the analysis was therefore properly performed. As a result, it was confirmed that the R values were not dependent on the sample volume fraction.

The behavior of water molecules in micelles formed from cationic surfactants during sphere-to-rod transitions and micellar growth has not been discussed extensively.[39] In the present study, however, the number of water molecules in the cationic surfactant micelles was successfully estimated, and the behavior of the water molecules during the sphere-to-rod transition and micellar growth was also observed. The number of water molecules per surfactant molecule inside the micelles (n_w) was estimated from the scattering contrast ($\Delta\rho$) using equations 2.2 and 2.3. fig. 2-12c shows the ϕ-dependence of n_w for the $3C_{12}$trisQ micelles. The n_w values systematically decreased from 51.4 to 17.1 with increasing ϕ. Bound water (the hydrated head of the surfactant) and free water in the micelles were not been distinguished because the SANS results could only be fitted using the uniform spherical particle model. Approximately 34 water molecules were excluded prior to the sphere-to-rod transition and micellar growth due to the high density of surfactant molecules in wormlike micelles.

Fig. 2-12d shows the ϕ-dependence of the Debye screening length l_D. The l_D value decreased from 155.8 to 47.3 Å with increasing ϕ. This decrease was caused by the increasing electrostatic screening of the surfactant solutions due to the growth of the wormlike micelles.

The aggregation number (N_{agg}) was estimated from the model-fitting parameters using the following equation:

$$N_{agg} = \frac{V_{micelle}}{(v_{surfactant} + n_w v_w)} \tag{2.12}$$

where $V_{micelle}$ is the volume of one micelle and $v_{surfactant}$ and v_w are the molecular volume of the surfactant and D_2O, respectively. **Figure 2-13** shows the ϕ-dependence of N_{agg} estimated using equation 2.12. The N_{agg} of $3C_{12}$trisQ wormlike micelles obeyed the power law $N_{agg} \sim \phi^{1.23}$ at ϕ values ranging from 0.0034 (C_M = 0.0035 mol·dm^{-3}) to

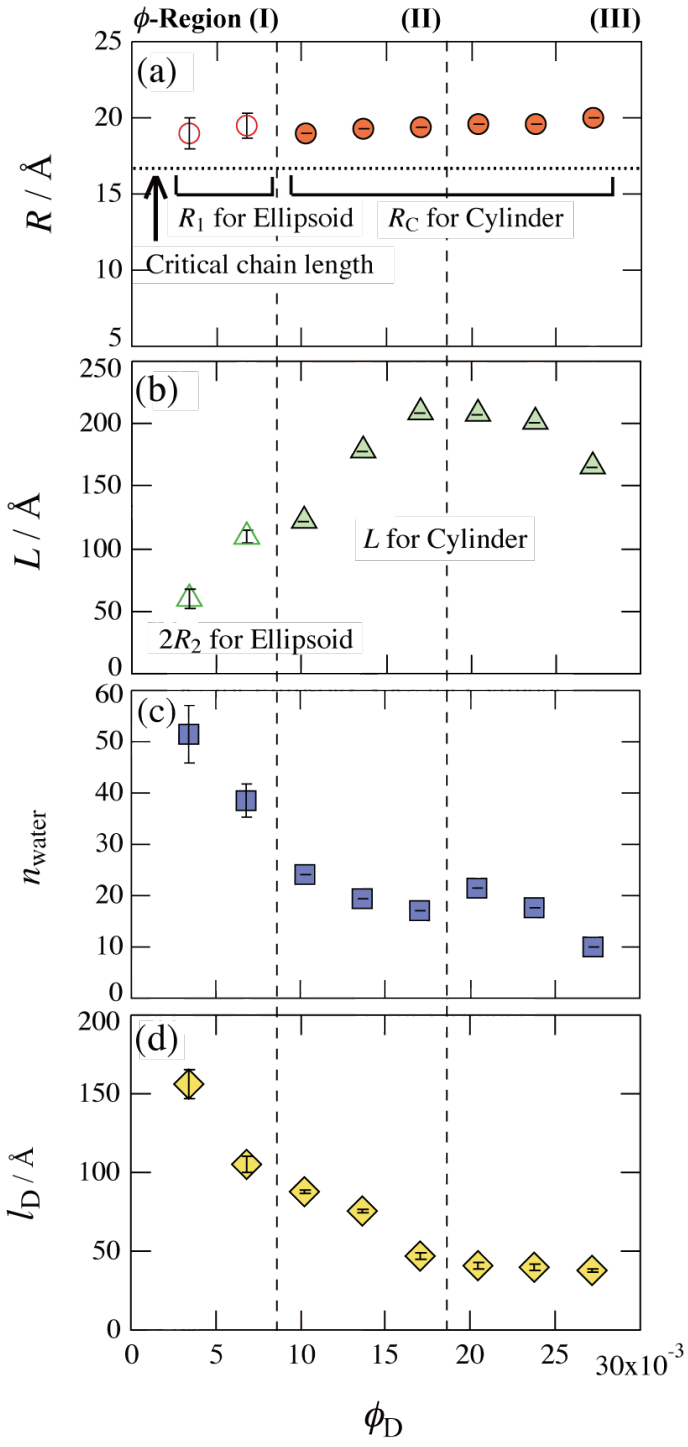

Figure 2-12. Volume fraction (ϕ) dependence of the structural parameters obtained from the model-fitting analysis of the SANS results: (a) radius (R); (b) length (L); (c) number of water molecules per surfactant molecule inside the micelles (n_w); and (d) Debye screening length (l_D).[44]

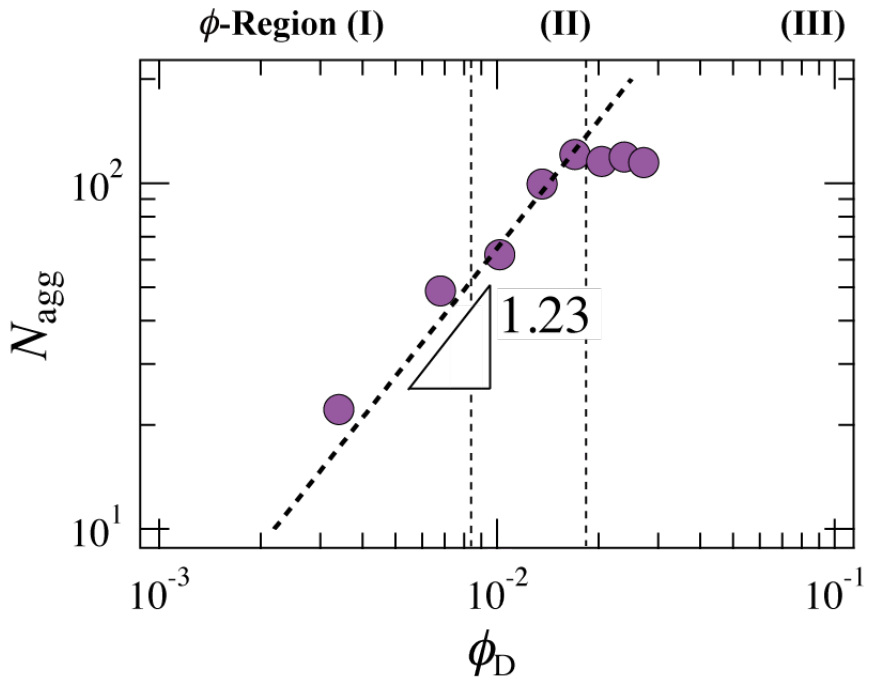

Figure 2-13. Volume fraction (ϕ) dependence of the aggregation number (N_{agg}) for $3C_{12}$trisQ micelles estimated using the fitting parameters (radius, length, and number of water molecules per surfactant molecule inside the micelles). [44]

0.0170 (C_M = 0.0174 mol·dm^{-3}). It is known that the exponent of the power law is affected by the surface charge of the micelles, with values of 0.5 ($\phi^{0.5}$) for nonionic micelles and 1.4 ($\phi^{1.4}$) for cationic gemini surfactants (12-2-12) reported in the literature.[46] Unsurprisingly, the exponent for the $3C_{12}$trisQ micelles was similar to that for the gemini surfactant (12-2-12) micelles because both the surfactants have the same number of valence electrons per hydrocarbon chain.

2-3-5. Mechanism of wormlike micelle formation: differences among trimeric, gemini, and monomeric surfactants

Next, the structural transition of $3C_{12}$trisQ was compared to those of gemini and monomeric surfactants in order to elucidate the micelle growth mechanism for trimeric surfactants. For charged wormlike micelles, wormlike micellar growth contributes to two scission energies: the micellar surface charge and the E_C of the micelles.[8] When the scission energy (E_{sciss}) of a wormlike micelle is sufficiently high, the length of the

micelle increases. According to the literature, in a semi-dilute solution, the zero-shear viscosity (η_0) of a charged wormlike micelle depends on both the E_C and the effective charge number per unit length of the wormlike micelle (υ^*):[21]

$$\eta_0 \propto \phi \exp\left(\frac{E_{\text{sciss}}}{2k_BT}\right) \propto \phi \exp\left[\frac{E_C}{2k_BT} - \frac{l_B R \upsilon^{*2}}{2}\phi^{-0.5}\right] \tag{2.13}$$

where l_B is the Bjerrum length and R is the radius of the micelles. To evaluate the combined effect of the micellar surface charge and the E_C on wormlike micellar growth, the contributions of each factor were estimated for $3C_{12}$trisQ from the ϕ-dependence of the zero-shear viscosity (fig. 2-9b) using the R value estimated from the model-fitting analysis (fig. 2-12a). These results were compared with those for gemini (12-2-12) and monomeric (DTAB) surfactants with the same hydrocarbon chain lengths (12).

Figure 2-14 shows the ϕ-dependence of the zero-shear viscosity for aqueous solutions of $3C_{12}$trisQ, 12-2-12, DTAB, and DTAB with added NaSal. At lower volume fractions, the zero-shear viscosities (η_0) were nearly constant, while at higher volume fractions the viscosities increased rapidly with increasing ϕ. The volume fraction for which the viscosity increases significantly is referred to as the "on-set volume fraction (ϕ^*)." Under salt-free conditions, the ϕ-dependence of the η_0-behavior for the $3C_{12}$trisQ solutions was similar to that for the 12-2-12 solutions. On the other hand, the ϕ^* value for the $3C_{12}$trisQ solutions was slightly lower than that for the 12-2-12 solutions and significantly lower than that for the DTAB solutions. These results indicated that wormlike micelles were formed by $3C_{12}$trisQ at lower volume fractions than for DTAB. In addition, the rate of increase in η_0 for the DTAB solutions in the absence of NaSal was similar to those for the $3C_{12}$trisQ and 12-2-12 solutions, while the rate of increase in η_0 for the DTAB solution with added NaSal was lower ($\eta_0 \sim \phi^a$, with a = 14.22 for $3C_{12}$trisQ, 9.45 for 12-2-12, 8.31 for DTAB, and 2.94 for DTAB in the presence of NaSal). This rate reduction was caused by the screening of the micellar surface charges by the salt.[14] It should be noted that the effects of charges are dominant for structural transitions in surfactant/salt systems in a manner similar to that for mixed cation/anion systems.

Additional information can be obtained by rewriting equation 2.13 as follows:

$$2\ln\left[\frac{\eta_0}{\phi}\right] \propto \frac{E_C}{k_BT} - l_B R v^{*2}\phi^{-0.5} \tag{2.14}$$

The values for E_C and v^* for wormlike micelles in an aqueous surfactant solution can be obtained from a fitting analysis for the plot of $2\ln(\eta_0/\phi)$ versus $\phi^{0.5}$ assuming that the entangled wormlike micelles overlap. Therefore, curve fitting analyses were performed using the results in the overlapped ϕ-regions: 0.0204 (CMC × 150, C_M = 0.0209 mol·dm^{-3}) ≤ ϕ ≤ 0.0272 (CMC × 200, C_M = 0.0278 mol·dm^{-3}) for 3C_{12}trisQ: 0.023 (CMC × 40, C_M = 0.0387 mol·dm^{-3}) ≤ ϕ ≤ 0.035 (CMC × 60, C_M = 0.0569 mol·dm^{-3}) for 12-2-12; and 0.23 (CMC × 47, C_M = 0.746 mol·dm^{-3}) ≤ ϕ ≤ 0.47 (CMC × 95, C_M = 1.52 mol·dm^{-3}) for DTAB. The plots of $2\ln[\eta_0/\phi]$ versus $\phi^{0.5}$ for the three surfactants and their fitting results are presented in **Figure 2-15**. The v^* values were found to be 0.23 Å^{-1} for 3C_{12}trisQ, 0.22 Å^{-1} for 12-2-12, and 0.25 Å^{-1} for DTAB, indicating that they were independent of the molecular structure.

The E_C values were found to be (50.2 ± 1.14) k_BT for 3C_{12}trisQ, (41.4 ± 1.3) k_BT for 12-2-12, and (11.7 ± 1.24) k_BT for DTAB. Unlike the v^* values, the E_C for the wormlike micelles depended on the molecular structure; the E_C value for the 3C_{12}trisQ wormlike micelles was much higher than that for the DTAB micelles and slightly higher than that for the 12-2-12 micelles.

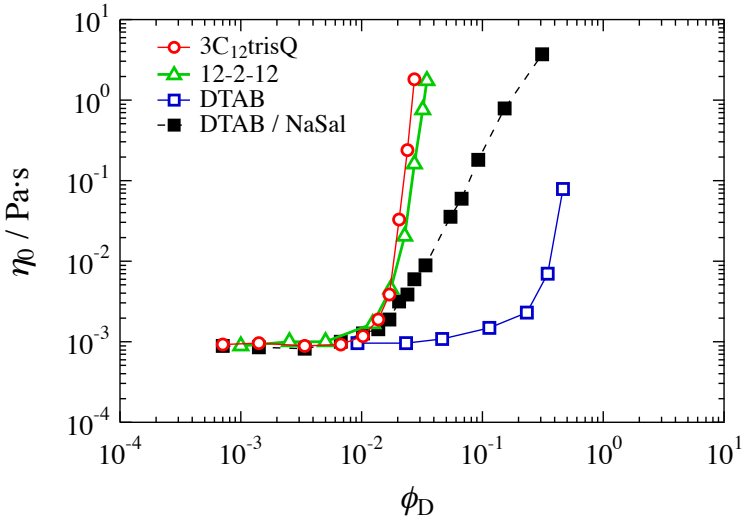

Figure 2-14. Volume fraction (ϕ) dependence of the zero-shear viscosity (η_0) for aqueous solutions of 3C_{12}trisQ, 12-2-12, DTAB, and DTAB with NaSal. [44]

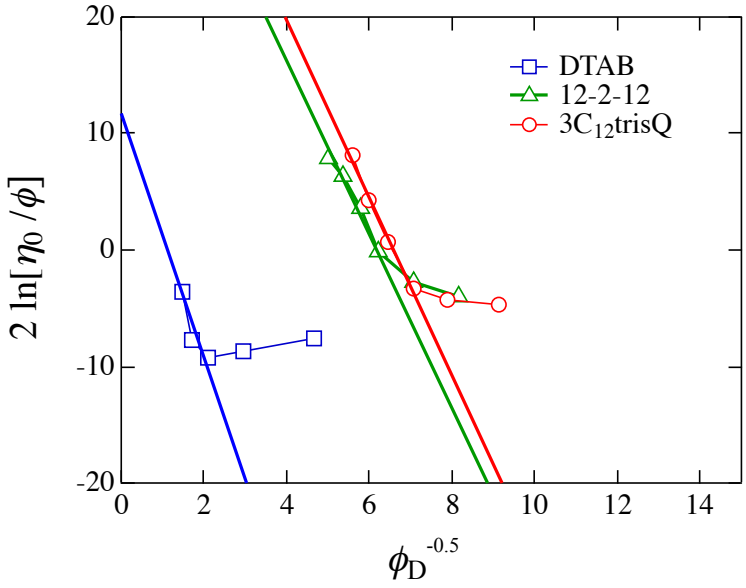

Figure 2-15. Plots of $2\ln[\eta_0/\phi]$ versus $\eta_0/\phi^{0.5}$ obtained using equation 2.14 for $3C_{12}$trisQ (circles), 12-2-12 (triangles), and DTAB (squares). The solid lines represent the fitting results obtained using model functions.[44]

Finally, to accurately estimate the difference in the scission energies (E_{sciss}) for $3C_{12}$trisQ and 12-2-12, the temperature dependence of the zero-shear viscosity of these two surfactants was determined. **Figure 2-16** shows the Arrhenius plots of the zero-shear viscosity for $3C_{12}$trisQ and 12-2-12 at the same volume fraction (ϕ). E_{sciss} was obtained from the slope of the Arrhenius plot generated using equation 2.13. Notably, the E_{sciss} value for $3C_{12}$trisQ ((52.0 ± 1.93) k_BT) was slightly higher than that for 12-2-12 ((46.6 ± 0.70) k_BT). These results support the ϕ–dependence of the zero-shear viscosity.

A comparison of the Arrhenius plots for $3C_{12}$trisQ and 12-2-12 indicated that $3C_{12}$trisQ readily formed wormlike micelles at lower volume fractions than 12-2-12. The main difference in the molecular structures of these surfactants is the number of spacer chains per molecule. Thus, it can be concluded that the spacer between the surfactant molecules increases the E_C and promotes the growth of wormlike micelles because an increase in the number of spacer chains limits intramolecular motion. The linear surfactant 12-2-12-2-12 readily precipitates in solution and thus to our knowledge

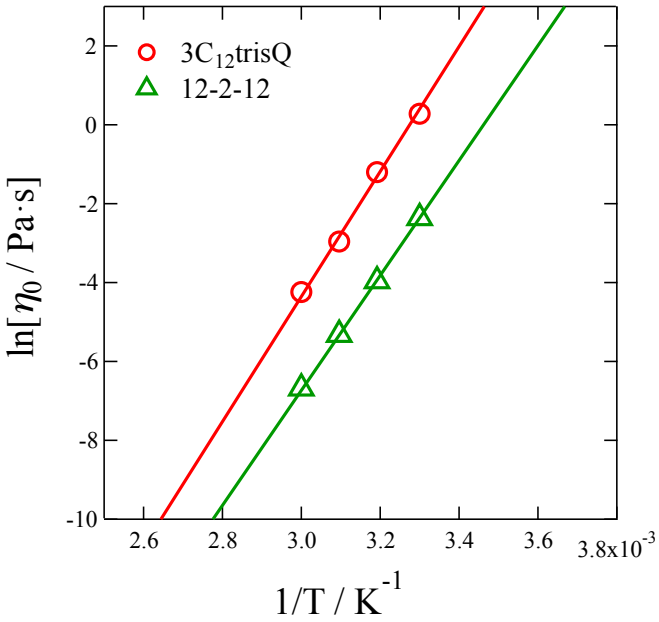

Figure 2-16. Arrhenius plots of the zero-shear viscosity of aqueous $3C_{12}$trisQ (circles) and 12-2-12 (triangles) solutions at a given ϕ.[44]

there have been no reports on structural transitions for this surfactant. According to In et al., the E_C of the linear surfactant 12-3-12-3-12 ((83 ± 7) k_BT) is approximately twice that of 12-3-12 ((43 ± 5) k_BT).[36] On the other hand, the E_C of $3C_{12}$trisQ is (50.2 ± 1.14) k_BT, which is much less than that of 12-3-12-3-12 and close to that of 12-3-12 ((43 ± 5) k_BT) and 12-2-12 ((41.4 ± 1.3) k_BT). The smaller value for the E_C of $3C_{12}$trisQ compared to that of 12-3-12-3-12 can be explained by the fact that star-type surfactants can form a more round shape than linear trimeric surfactants (12-3-12-3-12), resulting in a lower E_C. In fact, the occupied area per molecule at the air/solution interface, A, is largest for $3C_{12}$trisQ (A = 2.03 nm^2/ molecule) among the three evaluated surfactants (12-2-12-2-12: A = 1.28 nm^2/ molecule; 12-3-12-3-12: A = 1.47 nm^2/ molecule).[23]

2-4. Conclusions

In this chapter, the synthesis of novel star-type cationic trimeric surfactants consisting of three hydrocarbon chains, three quaternary ammonium headgroups, and a tris(2-aminoethyl)amine spacer was described. These surfactants were very soluble in

water despite having three hydrocarbon chains in each molecule. The relation between the logarithm of the CMC and the hydrocarbon chain length was linear, as is observed for conventional monomeric and gemini surfactants. The aggregation state of the trimeric surfactants in solution was significantly influenced by their hydrocarbon chain lengths and concentrations; that is, for n = 10, ellipsoidal micelles formed; for n = 12, the ellipsoidal micelles transformed to threadlike micelles with increasing concentration; and for n = 14, threadlike micelles formed at low concentrations and no transitions were observed as the concentration increased.

Furthermore, the structural transition of aggregates of the star-type trimeric surfactant $3C_{12}$trisQ was investigated using SANS and rheological analyses. The combination of SANS and rheological data revealed that $3C_{12}$trisQ exhibited a sphere-to-rod transition in the absence of salts. Wormlike micellar growth was observed with increasing volume fraction. It was also found that wormlike micellar growth accompanied the extrusion of water from the micelles. Using results from the analysis of the volume fraction dependence of the zero-shear viscosity, the surface charge per unit length and E_C for the wormlike micelles formed by $3C_{12}$trisQ, gemini (12-2-12), and monomeric (DTAB) surfactants were evaluated. The surface charge per unit length was independent of the molecular structure, while the E_C for $3C_{12}$trisQ and 12-2-12 were significantly higher than that for DTAB. These results indicated that wormlike micelles were readily formed in the $3C_{12}$trisQ and 12-2-12 solutions at lower concentrations. The main difference in the molecular structures of $3C_{12}$trisQ and 12-2-12 is the number of spacer chains. Therefore, it appears that spacers increase the E_C and promote the growth of wormlike micelles. It is thought that the number of spacer chains limits intra-molecular motion. In addition, star-type trimeric surfactants ($3C_{12}$trisQ) can form a more round shape than linear trimeric surfactants and thus exhibit a lower E_C.

To date, a large number of gemini surfactants have been designed and synthesized by many researchers, and their adsorption and aggregation properties have been investigated. However, there are very few reports on trimeric and tetrameric surfactants, which represent a natural extension of gemini surfactants.[27, 28, 31-33, 50-58] This lack of study is likely due to the greater difficulty associated with the design and synthesis of oligomeric surfactants such as $3C_n$trisQ compared with gemini surfactants, which can

be prepared relatively easily. The results in this study may aid future investigations of the structure-performance relations for new oligomeric surfactants with novel structures. They should also help to explain the adsorption and aggregation behavior of the different types of trimeric surfactants that have already been reported. In addition, because the synthetic approach to these star-type trimeric surfactants relatively simple, the preparation and investigation of additional, novel, trimeric surfactants is now expected.

References

(1) Joshi, J. V.; Aswal, V. K.; Goyal, P. S., Effect of Sodium Salicylate on The Structure of Micelles of Different Hydrocarbon Chain Lengths. *Physica B* **2007,** 391, 65-71.

(2) Kuperkar, K.; Abezgauz, L.; Danino, D.; Verma, G.; Hassan, P. A.; Aswal, V. K.; Varade, D.; Bahadur, P., Viscoelastic Micellar Water/CTAB/$NaNO_3$ Solutions: Rheology, SANS and Cryo-TEM Analysis. *J. Colloid Interface Sci.* **2008,** 323, 403-409.

(3) Aswal, V. K.; Goyal, P. S., Counterions in The Growth of Ionic Micelles in Aqueous Electrolyte Solutions: A Small-Angle Neutron Scattering Study. *Phys. Rev. E* **2000,** 61, (3), 2947-2953.

(4) Helgeson, M. E.; Hodgdon, T. K.; Kaler, E. W.; Wagner, N. J., A Systematic Study of Equilibrium Structure, Thermodynamics, and Rheology of Aqueous CTAB/$NaNO_3$ Wormlike Micelles. *J. Colloid Interface Sci.* **2010,** 349, 1-12.

(5) Croce, V.; Cosgrove, T.; Maitland, G.; Hughes, T.; Karlsson, G., Rheology, Cryogenic Transmission Electron Spectroscopy, and Small-Angle Neutron Scattering of Highly Viscoelastic Wormlike Micellar Solutions. *Langmuir* **2003,** 19, 8536-8541.

(6) Ali, A. A.; Makhloufi, R., Effect of Organic Salts on Micellar Growth and Structure Studied by Rheology. *Colloid Polym. Sci.* **1999,** 277, 270-275.

(7) Sangwai, A. V.; Sureshkumar, R., Coarse-Grained Molecular Dynamics Simulations of the Sphere to Rod Transition in Surfactant Micelles. *Langmuir* **2011,** 27, 6628-6638.

(8) MacKintosh, F. C.; Safran, S. A.; Pincus, P. A., Equilibrium Size Distribution of Charged 'Living' Polymers. *J. Phys. : Condens. Matter* **1990,** 2, SA359-SA364.

(9) Rodrigues, R. K.; da Silva, M. A.; Sabadini, E., Worm-like Micelles of CTAB and Sodium Salicylate under Turbulent
Flow. *Langmuir* **2008,** 24, 13875-13879.

(10) Kumar, S.; Kirti.; Kumari, K.; Din, K., Role of Alkanols in Micellar Growth: A Viscometric Study. *J. Am. Oil. Chem. Soc.* **1995,** 72, (7), 817-821.

(11) Shikata, T.; Hirata, H.; Kotaka, T., Micelle Formation of Detergent Molecules in Aqueous Media. 2. Role of Free Salicylate Ions on Viscoelastic Properties of Aqueous

Cetyltrimethylammonium Bromide-Sodium Salicylate Solutions. *Langmuir* **1988,** 4, 354-359.

(12) Deguchi, K.; Meguro, K., The effects of Inorganic Salts and Urea on the Micellar Structure of Nonionic Surfactant. *J. Colloid Interface Sci.* **1975,** 50, (2), 223-227.

(13) Yu, D.; Huang, M.; Lin, Y.; Jiang, L.; Huang, J.; Wang, Y., Effects of Inorganic and Organic Salts on Aggregation Behavior of Cationic Gemini Surfactants. *J. Phys. Chem. B* **2010,** 114, 14955-14964.

(14) Fan, H.; Yan, Y.; Li, Z.; Xu, Y.; Jiang, L.; Xu, L.; Zhang, B.; Huang, J., General Rules for the Scaling Behavior of Linear Wormlike Micelles Formed in Catanionic Surfactant Systems. *J. Colloid Interface Sci.* **2010,** 348, 491-497.

(15) Grillo, I.; Penfold, J., Self-Assembly of Mixed Anionic and Nonionic Surfactants in Aqueous Solution. *Langmuir* **2011,** 27, 7453-7463.

(16) Meng, Q.; Kou, Y.; Ma, X.; Liang, Y.; Guo, L.; Ni, C.; Liu, K., Tunable Self-Assembled Peptide Amphiphile Nanostructures. *Langmuir* **2012,** 28, 5017-5022.

(17) Li, H.; Wieczorek, S. A.; Xin, X.; Kalwarczyk, T.; Ziebacz, N.; Szymborski, T.; Holyst, R.; Hao, J.; Gorecka, E.; Pociecha, D., Phase Transition in Salt-Free Catanionic Surfactant Mixtures Induced by Temperature. *Langmuir* **2010,** 26, (1), 34-40.

(18) Hao, J.; Yuan, Z.; Liu, W.; Hoffman, H., Aggregation Transition from Nanodisks to Equilibrium among Vesicles and Disks. *J. Phys. Chem. B* **2004,** 108, 19163-19168.

(19) Hirata, H.; Hattori, N.; Ishida, M.; Okabayashi, H.; Frusaka, M.; Zana, R., Small-Angle Neutron-Scattering Study of Bis(quaternary ammonium bromide) Surfactant Micelles in Water. Effect of the Spacer Chain Length on Micellar Structure. *J. Phys. Chem.* **1995,** 99, 17778-17784.

(20) Oelschlaeger, C.; Schopferer, M.; Scheffold, F.; Willenbacher, N., Linear-to-Branched Micelles Transition: A Rheometry and Diffusing Wave Spectroscopy (DWS) Study. *Langmuir* **2009,** 25, 716-723.

(21) Zana, R.; Talmon, Y. Dependence of Aggregate Morphology on Structure of Dimeric Surfactants. *Nature* **1993**, 362, 228−230.

(22) Bernheim-Groswasser, A.; Zana, R.; Talmon, Y. Sphere-Tocylinder Transition in Aqueous Micellar Solution of a Dimeric (Gemini) Surfactant. *J. Phys. Chem. B* **2000**, 104, 4005−4009.

(23) Yoshimura, T.; Kusano, T.; Iwase, H.; Shibayama, M.; Ogawa, T.; Kurata, H., Star-Shaped Trimeric Quaternary Ammonium Bromide Surfactants: Adsorption and Aggregation Properties. *Langmuir* **2012,** 28, 9322-9331.

(24) Rosen, M. *J. Surfactants and Interfacial Phenomena*, 3rd ed.; John Wiley and Sons: New York, 2004.

(25) Iwase, H.; Endo, H.; Katagiri, M.; Shibayama, M., Modernization of the Small-Angle Neutron Scattering Spectrometer SANS-U by Upgrade to A Focusing SANS Spectrometer. *J. Appl. Cryst.* **2011,** 44, 558-568.

(26) Hayter, J. B.; Penfold, J., An Analytic Structure Factor for Macroion Solutions. *Molecular Physics* **1981,** 42 (1), 109-118.

(27) Yoshimura, T.; Yoshida, H.; Ohno, A.; Esumi, K. Physicochemical Properties of Quaternary Ammonium Bromide-Type Trimeric Surfactants. *J. Colloid Interface Sci.* **2003**, 267, 167-172.

(28) Esumi, K.; Taguma, K.; Koide, Y. Aqueous Properties of Multichain Quaternary Cationic Surfactants. *Langmuir* **1996**, 12, 4039-4041.

(29) Rosen, M. J.; Mathias, J. H.; Davenport, L. Aberrant Aggregation Behavior in Cationic Gemini Surfactants Investigated by Surface Tension, Interfacial Tension, and Fluorescence Methods. *Langmuir* **1999**, 15, 7340-7346.

(30) Menger, F. M.; Keiper, J. S.; Mbadugha, B. N. A.; Caran, K. L.; Romsted, L. S. Interfacial Composition of Gemini Surfactant Micelles Determined by Chemical Trapping. *Langmuir* **2000**, 16, 9095-9098.

(31) In, M.; Bec, V.; Aguerre-Chariol, O.; Zana, R. Quaternary Ammonium Bromide Surfactant Oligomers in Aqueous Solution: Selfassociation and Microstructure. *Langmuir* **2000**, 16, 141-148.

(32) Laschewsky, A.; Wattebled, L.; Arotcaréna, M.; Habib-Jiwan, J.-L.; Rakotoaly, R. H. Synthesis and Properties of Cationic Oligomeric Surfactants. *Langmuir* **2005**, 21, 7170-7179.

(33) Wu, C.; Hou, Y.; Deng, M.; Huang, X.; Yu, D.; Xiang, J.; Liu, Y.; Li, Z.; Wang, Y. Molecular Conformation-Controlled Vesicle/Micelle Transition of Cationic Trimeric Surfactants in Aqueous Solution. *Langmuir* **2010**, 26, 7922-7927.

(34) Rosen, M. *J. Surfactants and Interfacial Phenomena*, 3rd ed.; John Wiley and Sons: New York, 2004.

(35) Zana, R.; Lévy, H. Alkanediyl-α,ω-bis(dimethylalkylammonium bromide) Surfactants (dimeric surfactants). Part 6. CMC of the Ethanediyl-1,2-bis(dimethylalkylammonium bromide) Series. *Colloids Surf. A* **1997**, 127, 229-232.

(36) Zana, R. Dimeric and Oligomeric Surfactants. Behavior at Interfaces and in Aqueous Solution: a Review. *Adv. Colloid Interface Sci*. **2002**, 97, 205-253.

(37) Rosen, M. J.; Aronson, S. Standard Free Energies of Adsorption of Surfactants at the Aqueous Solution/Air Interface from Surface Tension Data in the Vicinity of the Critical Micelle Concentration. *Colloids Surf*. **1981**, 3, 201-208.

(38) Afifi, H.; Karlsson, G.; Heenan, R. K.; Dreiss, C. A. Solubilization of Oils or Addition of Monoglycerides Derives the Formation of Wormlike Micelles with an Elliptical Cross-Section in Cholesterol-Based Surfactants: a Study by Rheology, SANS, and Cryo-TEM. *Langmuir* **2011**, 27, 7480-7492.

(39) Takeda, M.; Kusano, T.; Matsunaga, T.; Endo, H.; Shibayama, M.; Shikata, T. Rheo-SANS Studies on Shear-Thickening/Thinning in Aqueous Rodlike Micellar Solutions. *Langmuir* **2011**, 27, 1731-1738.

(40) Löf, D.; Schillén, K.; Torres, M. F.; Müller, A. J. Rheological Study of the Shape Transition of Block Copolymer-Nonionic Surfactant Mixed Micelles. *Langmuir* **2007**, 23, 11000-11006.

(41) Dreiss, C. A. Wormlike Micelles: Where Do We Stand? Recent Developments, Linear Rheology and Scattering Techniques. *Soft Matter* **2007**, 3, 956-970.

(42) Goodeve, C. F. A general Theory of Thixotropy and Viscosity. *Trans. Faraday Soc* **1939**, 35, 342-358.

(43) Danino, D.; Talmon, Y.; Zana, R. Alkanediyl-α,ω-bis-(dimethylalkylammonium bromide) surfactants (dimeric surfactants). 5. Aggregation and Microstructure in Aqueous Solutions. *Langmuir* **1995**, 11, 1448-1456.

(44) Kusano, T.; Iwase, H.; Yoshimura, T.; Shibayama, M. Structural and Rheological Studies on Growth of Salt-Free Wormlike Micelles Formed by Star-Type Trimeric Surfactants *Langmuir* **2012**, 28, 16798-16806

(45) Shibayama, M.; Nomura, S.; Hashimoto, T.; Thomas, E. L. Asymptotic Behavior and Lorentz Factor for Small-Angle Elastic Scattering Profiles from Preferentially Oriented Asymmetric Bodies. *J. Appl. Phys.* **1989**, 66, 4188-4197.

(46) In, M.; Bendjeriou, B.; Noirez, L.; Grillo, I., Growth and Branching of Charged Wormlike Micelles as Revealed by Dilution Laws. *Langmuir* **2010,** 26 (13), 10411-10414.

(47) Colby, R. H.; Boris, W. E.; Krause, W. E.; Dou, S., Shear Thinning of Unentangled Flexible Polymer Liquids. *Rheol. Acta.* **2007,** 46, 569-575.

(48) Zana, R.; Kaler, E. W., *Giant Micelles : Properties and Applications*. CRC Press: 2007; p 179-222.

(49) Tanford, C., *The Hydrophobic Effect*. Wiley: New York, 1980.

(50) Zana, R.; Levy, H.; Papoutsi, D.; Beinert, G. Micellization of Two Triquaternary Ammonium Surfactants in Aqueous Solution. *Langmuir* **1995**, 11, 3694-3698.

(51) Danino, D.; Talmon, Y.; Levy, H.; Beinert, G.; Zana, R. Branched Threadlike Micelles in an Aqueous Solution of a Trimeric Surfactant. *Science* **1995**, 269, 1420-1421.

(52) Kim, T. S.; Kida, T.; Nakatsuji, Y.; Ikeda, I. Preparation and Properties of Multiple Ammonium Salts Quaternized by Epichlorohydrin. *Langmuir* **1996**, 12, 6304-6308.

(53) Wattebled, L.; Laschewsky, A.; Moussa, A.; Habib-Jiwan, J.-L. Aggregation Numbers of Cationic Oligomeric Surfactants: a Timeresolved Fluorescence Quenching Study. *Langmuir* **2006**, 22, 2551-2557.

(54) Hou, Y.; Cao, M.; Deng, M.; Wang, Y. Highly-Ordered Selective Self-Assembly of a Trimeric Cationic Surfactant on a Mica Surface. *Langmuir* **2008**, 24, 10572-10574.

(55) Yoshimura, T.; Esumi, K. Physicochemical Properties of Ringtype Trimeric Surfactants from Cyanuric Chloride. *Langmuir* **2003**, 19, 3535-3538.

(56) Yoshimura, T.; Esumi, K. Physicochemical Properties of Anionic Triple-Chain Surfactants in Alkaline Solutions. *J. Colloid Interface Sci.* **2004**, 276, 450-455.

(57) Yoshimura, T.; Kimura, N.; Onitsuka, E.; Shosenji, H.; Esumi, K. Synthesis and Surface-Active Properties of Trimeric-Type Anionic Surfactants Derived from Tris(2-aminoethyl)amine. *J. Surfactants Deterg*. **2004**, 7, 67-74.

(58) Abdul-Raouf, M. E.-S.; Abdul-Raheim, A.-R. M.; Maysour, N. E.- S.; Mohamed, H. Synthesis, Surface-Active Properties, and Emulsification Efficiency of Trimeric-type Nonionic Surfactants Derived from Tris(2-aminoethyl)amine. *J. Surfactants Deterg*. **2011**, 14, 185-193.

Chapter. 3

Aggregation Structure of Star-Type Trimeric Surfactants in the Presence of Organic Salts

3-1. Introduction

In chapter 3, the aggregation structure of trimeric surfactants in salt solution was investigated. Monomeric surfactants are known to show sphere-to-rod transition in the presence of organic salts. Several studies compared formation mechanisms of wormlike micelles between monomeric surfactants with n = 12 in a solution with organic salts and 12-2-12 in a salt-free solution.[1-3] Mackintosh et al.[4] successfully explained the effects of added salts on wormlike micellar growth by using both surface charges and end-cap energy. In chapter 2, growth mechanisms of wormlike micelles formed by $3C_{12}$trisQ in an aqueous solution was also investigated by using SANS and rheological measurement, confirming the sphere-to-rod transition of the $3C_{12}$trisQ in a salt-free solution and the sphere-to-rod transition.[2, 5] Furthermore, It is also found that wormlike micelles formed by $3C_{12}$trisQ have a higher end-cap energy than gemini surfactant.[2]

The effect of salt on gemini surfactant aggregates in a solution has also been investigated.[6-9] Yu et al.[8] studied the effects of four kinds of salt on the aggregation behavior of gemini surfactants 12-4-12 and 12-4$(OH)_2$-12 by using NMR and SAXS. They found that the penetration of sodium salicylate (NaSal) anions and the charge neutralization of the surfactant by NaSal anions induced a micelle-to-vesicle transition. Lu et al.[9] concluded that 12-2-12(Et) can also form various structures in a salt (NaSal)

solution. To clarify salt effect to aggregation structure for oligomeric systems, it is important to compare the structural behavior among monomeric, gemini, and trimeric surfactants. However, there are still few reports examining these trimeric surfactants.

In this chapter, the structural behavior of 3C$_n$trisQ in the presence of NaSal was investigated. NaSal is a typical salt known to induce sphere-to-rod transition in lower salt concentration in monomeric or gemini surfactant systems. Therefore 3C$_n$trisQ can show various aggregation structures in NaSal solution because 3C$_n$trisQ show sphere-to-rod transition in the absence of salt, as described in Chapter 2. Using small-angle X-ray scattering (SAXS) and rheological measurements, the structural phase diagram of a 3C$_n$trisQ solution was determined by varying length of hydrocarbon chains of 3C$_n$trinsQ, a NaSal concentration, and a sample concentration.

3-2. Experimental section

3-2-1. Materials

In this study, trimeric surfactants, 3C$_n$trisQ with a hydrocarbon chain length (n) of 10, 12, and 14, respectively, in which the spacer chain length was 2, were used. The chemical structure of 3C$_n$trisQ was shown in **Figure 2-1**. 3C$_n$trisQ was synthesized as shown in chapter 2.[5] Sodium salicylate (NaSal) was used as salt.

3-2-2. SAXS measurement

SAXS measurements were carried out using the SAXS spectrometer installed on BL40B2 beamline at SPring-8, Hyogo, Japan.[10, 11] The X-rays wavelength was 0.7 Å, and the sample-to-detector distance was 2.1 m. The scattered X-rays from the samples were collected by an imaging-plate detector R-AXIS VII++ (Rigaku, Tokyo, Japan). The covered q-range was q = 0.008 – 0.6 Å^{-1}. The exposure time for each sample was 3 minutes. All measurements were performed at an ambient temperature. After circular averaging (using *Fit2d* software),[12] scattering from the solvent was subtracted correcting for the transmission.

3-2-2. HEXRD measurement

HEXRD measurements were performed at room temperature by using high-energy X-ray diffraction apparatus of BL04B2 beamline at SPring-8 (Japan Synchrotron Radiation Research Institute, JASRI, Japan). Monochrome 61.6 keV X-rays were obtained using a Si(220) monochromator. The exposure time for each sample was about 4.5 h.

3-2-3. Rheology measurement

The rheological experiments were performed using a stress control rheometer (MCR-501, Anton Paar, Austria) equipped with a cone plate of 25.0 mm radius and 1° cone angle. The shear-rate varied from 0.01 to 1000 s^{-1}. The sample temperature was controlled at 25.00 ± 0.03 °C.

3-3. Results and discussion

3-3-1. Hydrocarbon chain length and salt-concentration dependence of 3C$_n$trisQ aggregates in a solution

Figure 3-1 shows SAXS profiles for 3C$_n$trisQ in a solution with systematically varying n and the ratio of salt (C_S) to the surfactant (C_D) molar concentration (C_S/C_D). The C_D was fixed at 0.00558 M for 3C$_{10}$trisQ, 0.00695 M for 3C$_{12}$trisQ, and 0.00324 M for 3C$_{14}$trisQ, respectively. All SAXS profiles for the 3C$_n$trisQ solutions have two broad peaks at q = 0.01-0.05 $Å^{-1}$ and q = 0.2 $Å^{-1}$, indicating inter- and intra- micellar structure, respectively. The peak at q = 0.2 $Å^{-1}$ reflected differences of scattering length density between hydrophilic and hydrophobic portions within the micellar structures. For 3C$_n$trisQ, based on their chemical structure, the scattering length densities were estimated to be 1.46×10^{-5} $Å^{-2}$ for the hydrophilic head group, 7.11×10^{-6} $Å^{-2}$ for C$_{10}$, 7.15×10^{-6} $Å^{-2}$ for C$_{12}$, and 7.18×10^{-6} $Å^{-2}$ for C$_{14}$, respectively, The difference of scattering length density between hydrophilic and hydrophobic portions was sufficiently high, resulting in the broad peaks in the SAXS profiles.

i) 3C$_{10}$trisQ

In **Figure 3-1a**, SAXS profiles for 3C$_{10}$trisQ in a solution showed the inter-particle scattering peak around q = 0.03 $Å^{-1}$, which is attributed to the electrostatic repulsion

between surface charges of the micelles. In chapter 2, the SANS and rheology measurement results suggested that the $3C_{10}$trisQ (C_D = 0.00558 M) forms an ellipsoidal micelle in a solution in the absence of NaSal (i.e., $C_S/C_D = 0$). [16] With increasing C_S/C_D ratio, the SAXS intensity gradually increased in the q-range from 0.02 to 0.03 $Å^{-1}$ whereas this peak-potion (q_{m1}) was unchanged. This was due to the screening of electrostatic repulsion on micellar surfaces. In contrast, beyond this q-region (q > 0.03$Å^{-1}$), the SAXS profiles agreed with each other. These results indicate that ellipsoidal micelles were maintained in the range of C_S/C_D ratio from 0 to 0.18. The $3C_{10}$trisQ solution became isolable at $C_S/C_D > 0.18$.

ii) $3C_{12}$trisQ

In **Figure 3-1b**, except for $C_S/C_D = 0.8$, the SAXS profiles for the $3C_{12}$trisQ solution at C_D = 0.00695 M had two peaks around $q \sim 0.03$ $Å^{-1}$ and $q \sim 0.2$ $Å^{-1}$, respectively. At $C_S/C_D = 0$, the $3C_{12}$trisQ aggregates were ellipsoidal micelles in an aqueous solution.[5] With increasing C_S/C_D ratio, the peak-position (q_{m1}) at the lower q region monotonically changed. **Figure 3-2** shows the C_S/C_D-dependence of the q_{m1}-value in the q-range of $q \sim 0.01 - 0.02$ $Å^{-1}$. With increasing C_S/C_D ratio incrementally upward to 0.24 ($C_S/C_D \leq 0.24$), the q_{m1} shifted toward a lower q-value from 0.02 to 0.01 $Å^{-1}$ with slight increases in SAXS intensity, whereas the q_{m1} was nearly constant when C_S/C_D ranged between 0.24 and 0.66. At $C_S/C_D = 0.8$, on the other hand, the peak disappeared and the SAXS profiles showed asymptotic behaviors of q^{-2} in the q-range of $q \leq 0.03$ $Å^{-1}$. Simultaneously, a sharp peak appeared in the SAXS profile at $q = 0.19$ $Å^{-1}$. These results clearly indicated that $3C_{12}$trisQ forms multi-lamellar vesicles at $C_S/C_D = 0.8$. The repeat desistance (d) was estimated to be 33.05 Å with reference to the formula of $d = 2\pi/q$.

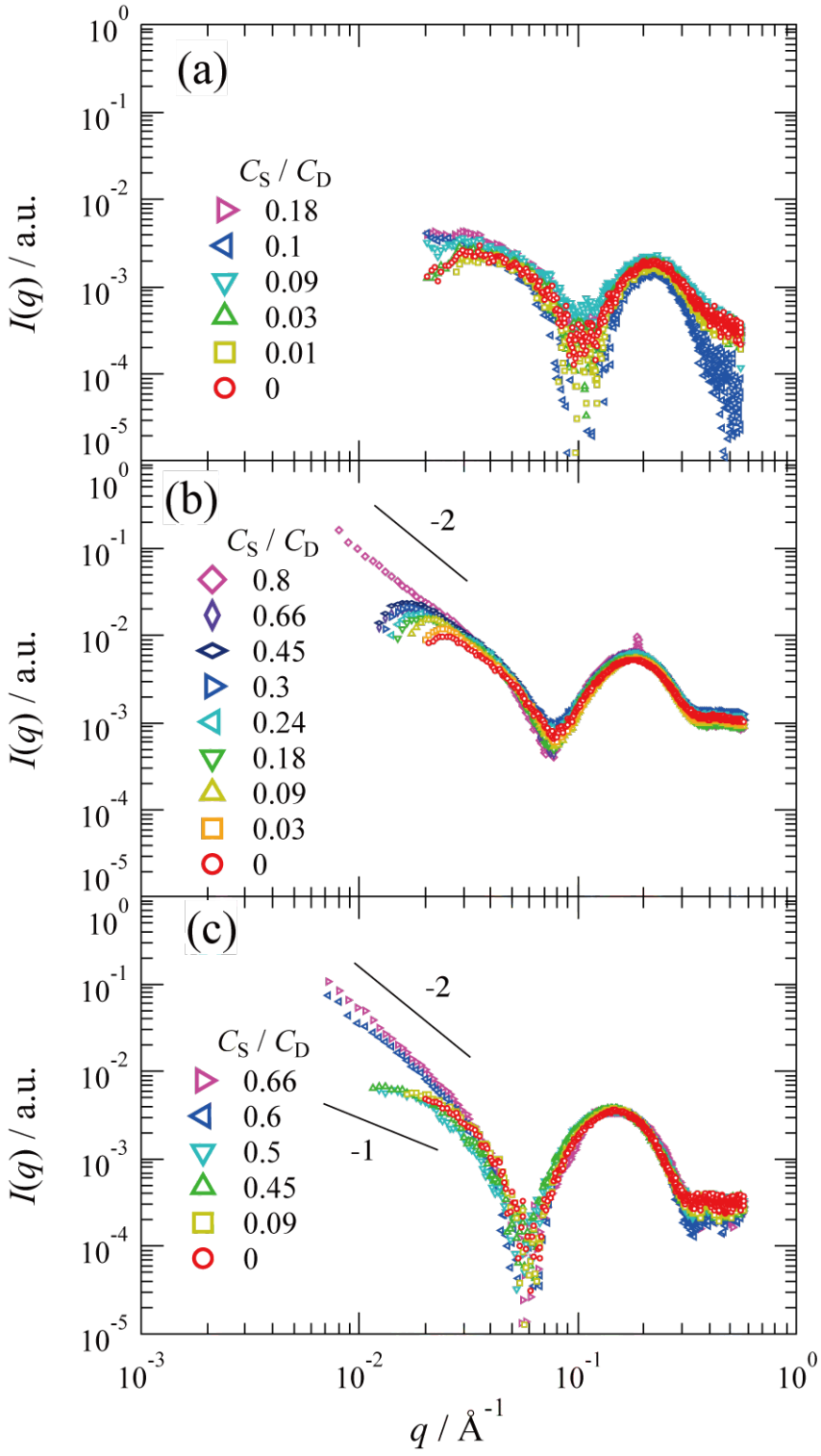

Figure 3-1. SAXS profiles for trimeric surfactant 3C$_n$trisQ (n = 10, 12 and 14) in salt (NaSal) solutions: (a) n = 10, (b) n = 12 and (c) n = 14 with varying the ratio of salt (C_S) to surfactant (C_D) concentration.[13]

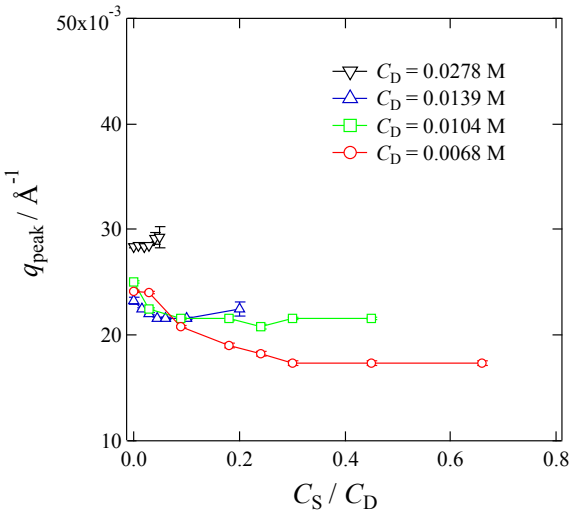

Figure 3-2. Salt (NaSal) concentration (C_S) dependence of the SAXS peak positions (q_{peak}) for $3C_{12}$trisQ observed in the q-range of 0.01 Å^{-1} < q < 0.05 Å^{-1}.[13]

Cationic surfactants are well known to show a micellar sphere-to-rod transition with adding NaSal.[14-18] Model-fitting analysis of scattering profiles is considered to be an effective method to reveal changes in micellar structures. However, when $3C_{12}$trisQ aggregates are wormlike micelles, it is currently impossible to perform a model-fitting analysis because the structure factor $S(q)$ corresponding to the peak profile at lower q-region remains unsolved. A PRISM structure factor $S_{PRISM}(q)$ was proposed for monomeric cationic surfactant solutions with a high salt concentration.[19] In contrast, both SAXS and SANS results for the $3C_{12}$trisQ solutions cannot be represented by the theoretical scattering using the $S_{PRISM}(q)$ with the rod model form factor $P(q)$. An alternative model, a Hayter-Penfold structure factor $S_{HP}(q)$ used in previous chapter, was used for various scattering data analysis for the charged particles.[20] However, when the micellar length L was much longer than the radius of cross-section R_C, i.e., L » R_C, it is not appropriate to use the $S_{HP}(q)$ for a model-fitting analysis of the wormlike micelles. In previous chapter, $S_{HP}(q)$ was used only as a reference in high surfactant concentration because trimeric surfactants form overlapped wormlike micelles. In et al.[1] examined sphere-to-rod transitions of various cationic surfactants including 12-2-12 and other type trimeric surfactants by analyzing SANS peak position (q_{m1}).

It is indicated that the changed tendency of the shear-rate dependence of viscosity was correlated with that of q_{m1}-behavior in the SANS result by combining analysis of SANS peak position and share-rate dependence of viscosity.[2] For cationic surfactants, the shear-rate dependence of viscosity obtained through rheological measurements clearly showed whether $3C_{12}$trisQ forms wormlike micelles in a solution. To confirm the formation of wormlike micelles, rheological measurements were performed. **Figure 3-3** shows the dependence of the viscosity on the shear-rate ($\dot{\gamma}$) for $3C_n$trisQ in a solution by varying C_S/C_D ratio. The viscosity behavior of $3C_{12}$trisQ strongly depended on the C_S/C_D ratio, while the viscosity behavior of $3C_{10}$trisQ was independent of the C_S/C_D ratio and the same as that for water because of smaller size of $3C_{10}$trisQ aggregates. At $C_S/C_D \leq 0.24$, the $\dot{\gamma}$-dependence of the viscosity for the $3C_{12}$trisQ solution was constant, and was in agreement with that of water, implying that $3C_{12}$trisQ aggregates are ellipsoidal micelles. At $C_S/C_D = 0.3$, changing the q_{m1}-behavior of the SANS profiles, the viscosity was higher than that of water while maintaining a constant-viscosity independent of the share-rate. This suggests formation of rodlike micelles in a solution according to previous finding. At $0.45 \leq C_S/C_D \leq 0.66$, on the other hand, the viscosity monotonically decreased with increasing $\dot{\gamma}$, which is a well-known phenomenon called "shear thinning" and is corresponded to formation of wormlike micelles.[2, 21-23] At $C_S/C_D = 0.8$, the viscosity dramatically decreased and was the same as that of water. This similar behavior in rheological behavior was observed for a cationic monomeric surfactant solution by adding 5-methyl salicylic acid,[24] suggesting that the $3C_{12}$trisQ aggregates formed vesicles at C_S/C_D =0.8. This is in agreement with the finding observed by SAXS.

iii) $3C_{14}$trisQ

In **Figure 3-1c**, the SAXS profiles for the $3C_{14}$trisQ solution had no peaks because the surfactant concentration (C_D) of $3C_{14}$trisQ was much lower than that of $3C_{10}$trisQ and $3C_{12}$trisQ. At $C_S/C_D \leq 0.5$, the SAXS profiles showed $I(q) \sim q^{-1}$ in the q-range of $q < 0.03$ Å^{-3}, indicating that $3C_{14}$trisQ formed rod or wormlike micelles in the solutions. At $0.6 \leq C_S/C_D \leq 0.66$, on the other hand, the power law behavior of q^{-2} was found to be in the q-range of $q < 0.03$ Å^{-1}, whereas a peak-profile was not observed in the q-range of 0.1 Å$^{-1} \leq q \leq 0.3$ Å^{-1}. The $3C_{14}$trisQ formed unilamellar vesicles in a solution at 0.6

$\leq C_S/C_D \leq 0.66$, owing to lower C_D in the $3C_{14}$trisQ solution. Similar to the $3C_{12}$trisQ solution, the SAXS results for the $3C_{14}$trisQ solution showed that the rodlike micelle-to-vesicle transitions escalated by increasing C_S/C_D ratio. **Figure 3-3c** shows the viscosity behavior of $3C_{14}$trisQ solution. The viscosity of $3C_{14}$trisQ solution was much smaller than that of $3C_{12}$trisQ, which is due to low surfactant concentration. In low salt concentration, the solutions showed shear thinning behavior originated from the rodlike structure, while they were the same as that for water in high salt concentration due to electrostatic screening of salt molecules.

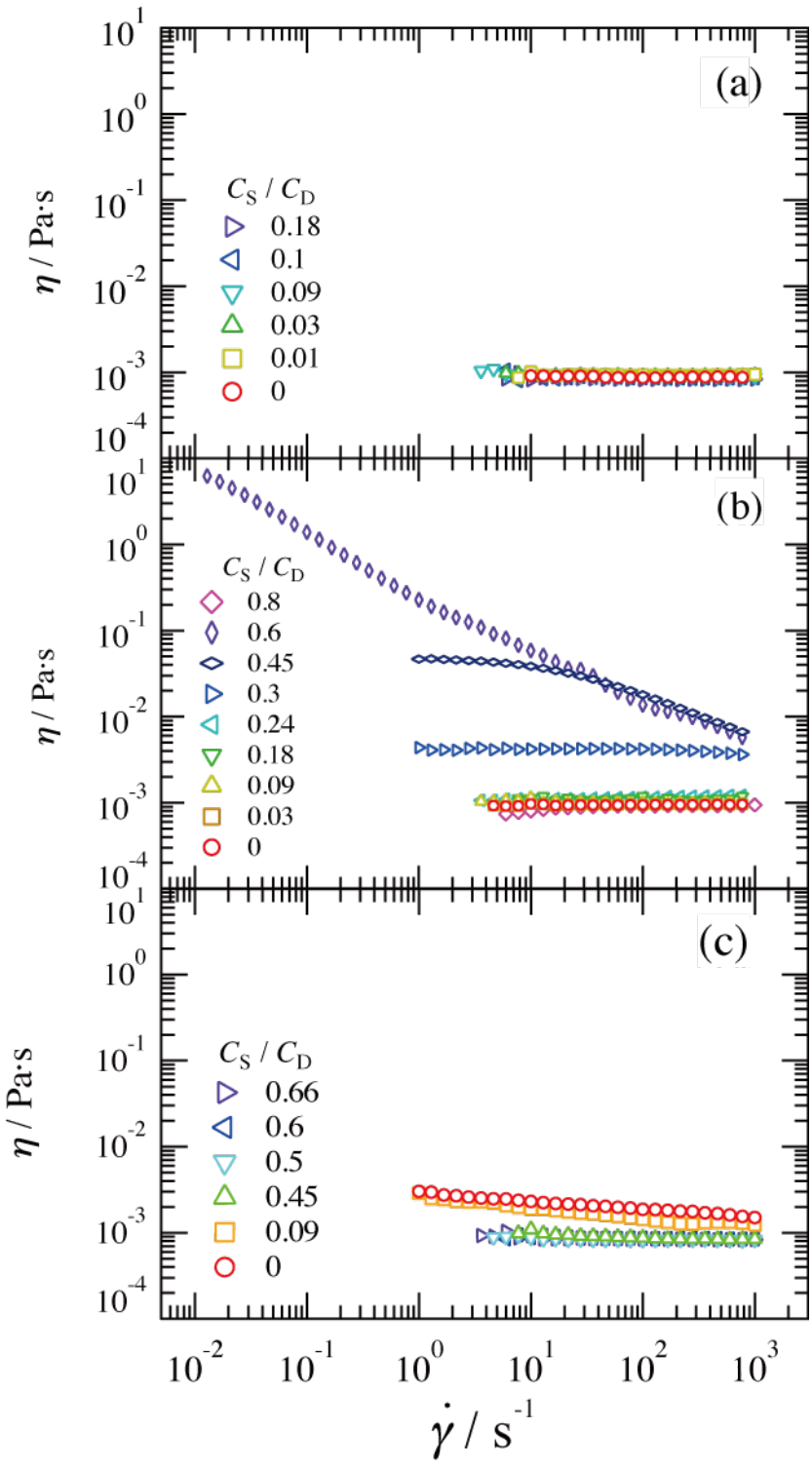

Figure 3-3. Shear-rate dependence ($\dot{\gamma}$) of viscosity (η) for trimeric surfactant (a) $3C_{10}$trisQ, (b) $3C_{12}$trisQ and (c) $3C_{14}$trisQ in salt (NaSal) solutions with varying the ratio of salt (C_S) to surfactant (C_D) molar concentration. [13]

3-3-2. Surfactant concentration dependence of aggregation structure of $3C_{12}$trisQ

In the subsection 3-3-1, it is found that $3C_{12}$trisQ aggregates depended on the NaSal concentrations in the solution. With increasing NaSal concentration, $3C_{12}$trisQ aggregates changed from spherical micelles to rodlike micelles (including wormlike micelles), and further to vesicles in solution. According to the results of chapter 2, even under salt-free conditions, the $3C_{12}$trisQ aggregates changed from spherical micelles to rodlike micelles, and formed the wormlike micelles in an aqueous solution in the C_D range of 0.0102 M $\leq C_D \leq$ 0.0278 M. Then, the structural transition of $3C_{12}$trisQ aggregates was studied with varying both surfactant and salt concentration.

Figure 3-4 shows the C_S/C_D-dependence of SAXS profiles for $3C_{12}$trisQ solutions at C_D = (a) 0.0104 M, (b) 0.0139 M, and (c) 0.0278 M, respectively. All SAXS profiles exhibited broad peaks in the q-range of 0.1 $Å^{-1} < q <$ 0.5 $Å^{-1}$. In this q-range, the SAXS profiles showed no change. In addition, at the lower q-region of q = 0.01 ~ 0.05 $Å^{-1}$, all SAXS profiles had broad peak profiles reflecting electrostatic repulsion between surface charges in the micelles. With increasing C_S/C_D, similar tendencies were observed in the C_S/C_D -dependences in the behavior of the peak-positions (q_{m1}) for $3C_{12}$trisQ solutions; the q_{m1}-values shifted toward lower q-values in the lower C_S/C_D range whereas those in the higher C_S/C_D range were almost constant.(fig. 3-2) With further increasing C_S/C_D, the $3C_{12}$trisQ were insoluble in water, namely the power law behavior of Q^{-2} was not observed on all SAXS profiles for $3C_{12}$trisQ solutions at C_D = 0.0104 M, 0.0139 M, and 0.0278 M.

Figure 3-5a shows the NaSal concentration dependence of the rheological behavior for $3C_{12}$trisQ solutions at C_D = 0.0104 M. The rheological behavior strongly depended on the NaSal concentration. At C_S/C_D = 0, the viscosity was higher than that for water, while the $\dot{\gamma}$-dependence of viscosity was almost constant. At C_S/C_D = 0.03, on the other hand, "shear thickening" was observed. These results suggest that rodlike micelles are formed at $C_S/C_D \leq$ 0.03. At 0.09 $\leq C_S/C_D \leq$ 0.45 where shear thinning was observed indicating that $3C_{12}$trisQ forms wormlike micelles. Therefore, the C_S/C_D-dependence shows micellar-growth of the $3C_{12}$trisQ aggregates with increasing NaSal concentration. Also, for C_D = 0.0139 M shown in fig. 3-5b, at 0 $\leq C_S/C_D \leq$ 0.045, the viscosity was higher than that for water, while the $\dot{\gamma}$-dependence of viscosity was nearly constant. At 0.06 $\leq C_S/C_D \leq$ 0.2, in addition, shear thinning was observed. This NaSal concentration

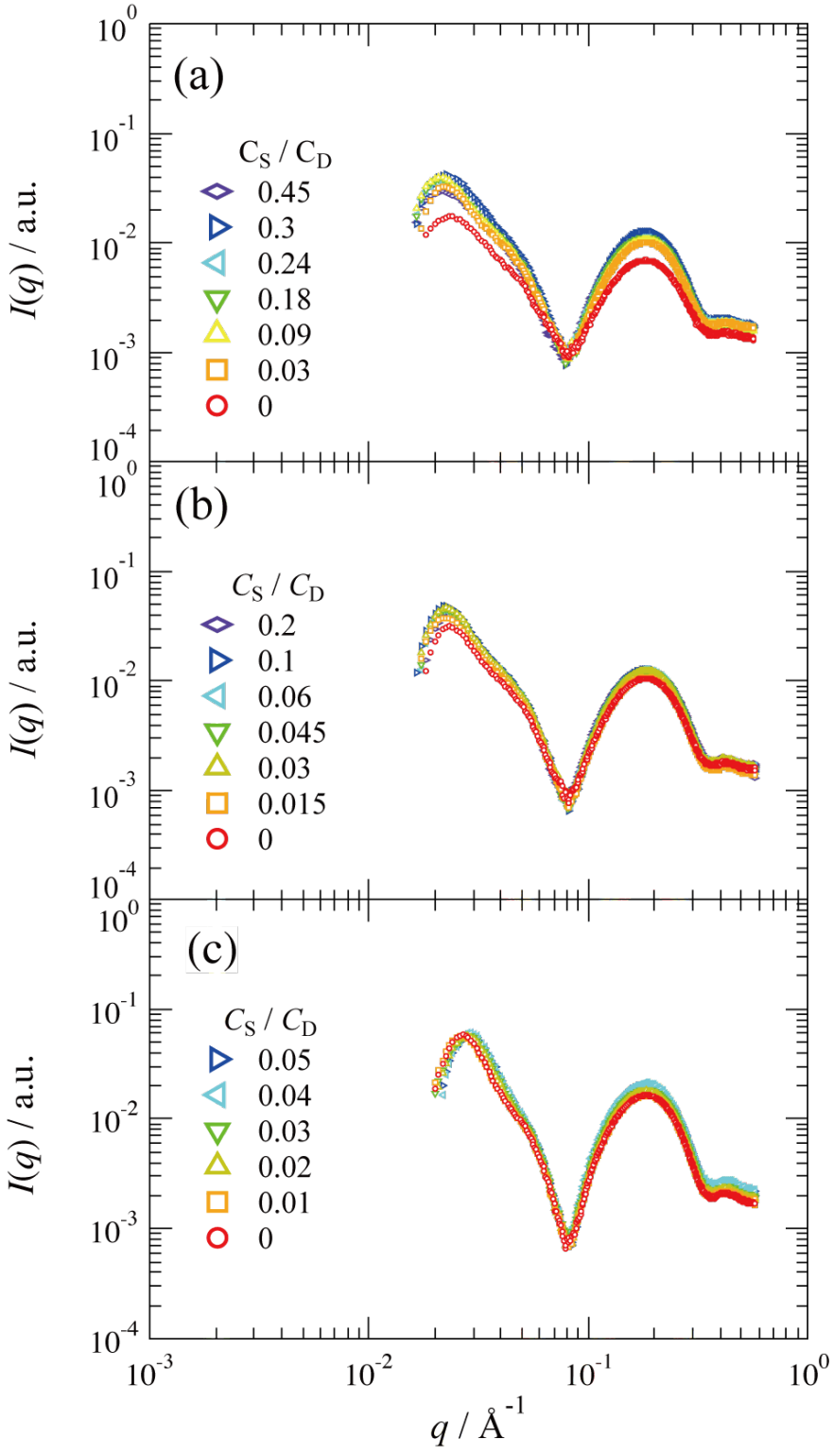

Figure 3-4. SAXS profiles for trimeric surfactant $3C_{12}$trisQ in salt (NaSal) solutions: (a) C_D = 0.0104 M, (b) C_D = 0.0139 M and (c) C_D = 0.0278 M with varying the ratio of salt (C_S) to surfactant (C_D) concentration. [13]

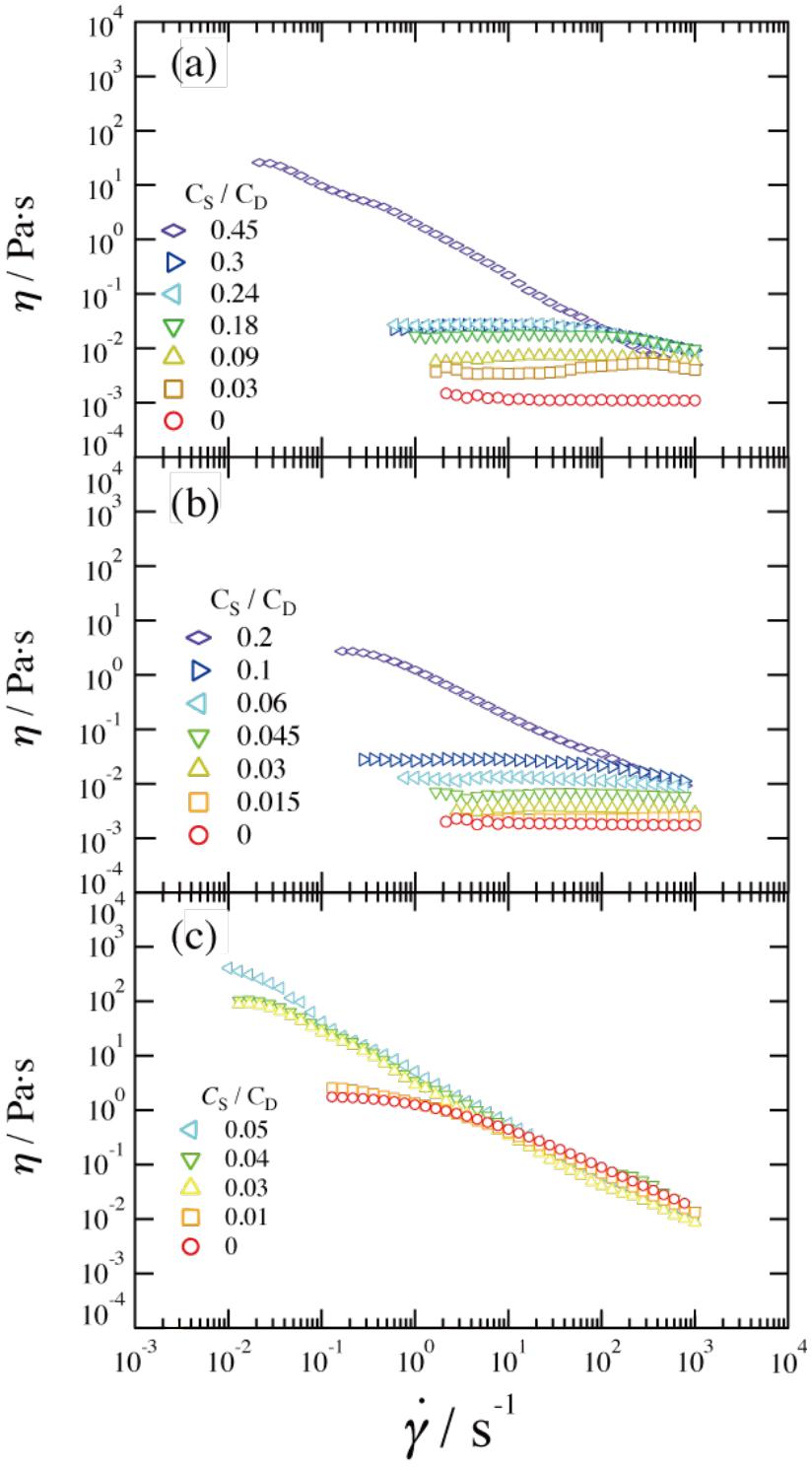

Figure 3-5. Shear-rate dependence ($\dot{\gamma}$) of viscosity (η) for trimeric surfactant $3C_{12}$trisQ in salt (NaSal) solutions: (a) C_D = 0.0104 M, (b) C_D = 0.0139 M and (c) C_D = 0.0278 M with varying the ratio of salt (C_S) to surfactant (C_D) volume fraction. [13]

in relation to its rheological behavior was in agreement with that for C_D = 0.0104 M shown in fig. 3-5a. For C_D = 0.0278 M, shown in fig. 3-5c, shear thinning was observed in the measured NaSal concentration indicating that $3C_{12}$trisQ forms wormlike micelles.

Both SAXS and rheological measurement clearly indicated that $3C_{12}$trisQ did not form vesicles at higher surfactant concentrations (C_D = 0.0104 M, 0.0139 M, and 0.0278 M). Beyond the NaSal solubility limits, (C_S^*), $3C_{12}$trisQ aggregates began to precipitate in the solution; C_S^* = 0.0055 M for C_D = 0.0104 M, C_S^* = 0.0040 for C_D = 0.0139 M, and C_S^* = 0.0020 for C_D = 0.0278 M, respectively, suggesting that the NaSal-solubility limit decreased by increasing C_D. This was accounted for through the hydrophobic interaction between surfactant molecules becoming higher due to the electrostatic screening of NaSal under high salt conditions resulting in increased $3C_{12}$trisQ precipitates.

3-4. Conclusion

The structural transition of aggregates of star-type trimeric surfactants ($3C_n$trisQ) in a solution was investigated by adding sodium salicylate (NaSal) using small-angle X-ray scattering (SAXS) and rheological measurements. It is found that depending on hydrocarbon chain length, NaSal concentration and sample concentration, the $3C_n$trisQ formed various aggregattion structures in solutions, such as ellipsoidal micelles, wormlike (rodlike) micelles, multi-lamellar vesicle, and unilamellar vesicles. **Figure 3-6** shows a structural phase diagram of aggregates formed by $3C_n$trisQ in a solution investigated in this study. The $3C_n$trisQ aggregates in a solution were significantly influenced by the hydrocarbon chain length and NaSal concentrations. $3C_{10}$trisQ formed ellipsoidal micelles in a solution independent of the NaSal concentration. $3C_{12}$trisQ at lower concentrations exhibited a structural transition from ellipsoidal micelles to rodlike or wormlike micelles and vesicles, with increasing NaSal concentration. $3C_{14}$trisQ also exhibited a wormlike micelle-to-vesicle transition.

The NaSal-induced structural transition of $3C_{12}$trisQ aggregates with varying surfactant concentration (C_D) was further investigated. **Figure 3-7** shows a structural phase diagram of aggregates formed by $3C_{12}$trisQ in solutions with varying both surfactant and NaSal concentrations. At the lower surfactant concentration ($C_D \leq$

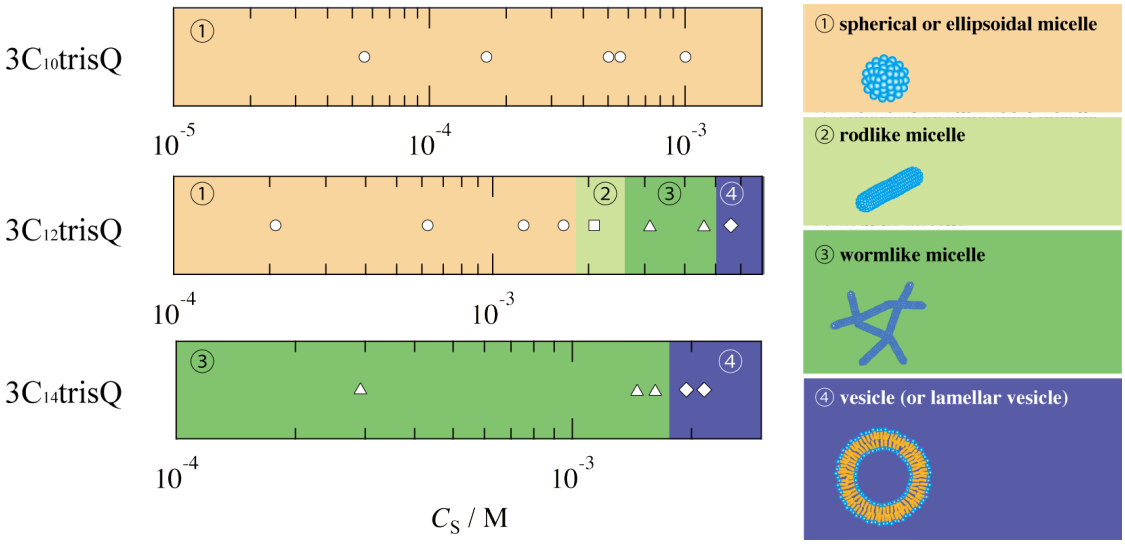

Figure 3-6. Schematic phase diagram of aggregates formed by trimeric surfactants, 3C$_n$trisQ, in salt (NaSal) solutions at 25 °C. [13]

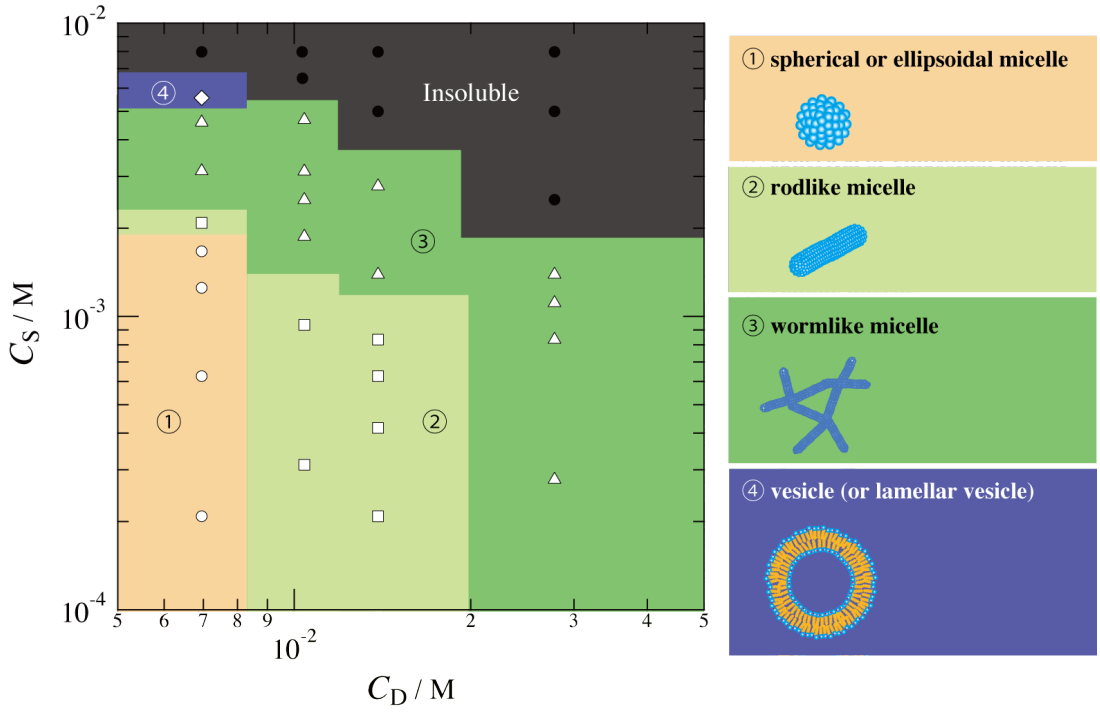

Figure 3-7. Schematic phase diagram of aggregates formed by trimeric surfactants, 3C$_{12}$trisQ, in salt (NaSal) solutions at 25 °C. [13]

0.00695 M), $3C_{12}$trisQ showed a structural transition from ellipsoidal micelles, though rodlike or wormlike micelles to vesicles by increasing NaSal concentration. In contrast, at a higher surfactant concentration of $C_D \geq 0.0139$ M, the $3C_{12}$trisQ did not form vesicles in the solution.

Finally, applications for $3C_n$trisQ was mentioned based on the present results. As described in the introduction, surfactants formed various type structures in a solution, such as wormlike micelles and vesicles. It is important to control the structure of surfactant aggregates in low surfactant concentrations. For $3C_{12}$trisQ solutions at C_D = 0.00324 M, it appeared to structural transition from ellipsoidal micelles, though rodlike or wormlike micelles to vesicles by increasing C_S. This C_D value is much lower than the critical micelle concentration of conventional surfactant. $3C_{14}$trisQ also formed the wormlike micelles and unilamellar vesicle in solutions at lower sample concentrations. Namely, the $3C_{12}$trisQ forms wormlike micelles and vesicles in solutions at lower sample concentrations compared to conventional surfactants. On the other hand, the solubility of $3C_{12}$trisQ in water is lower than gemini or monomeric surfactants due to its three hydrophobic chains. Therefore in next chapter, oligomeric surfactants were used in non-aqueous systems.

References

(1) In, M.; Bendjeriou, B.; Noirez, L.; Grillo, I., Growth and Branching of Charged Wormlike Micelles as Revealed by Dilution Laws. *Langmuir* **2010,** 26 (13), 10411-10414.

(2) Kusano, T.; Iwase, H.; Yoshimura, T.; Shibayama, M., Structural and Rheological Studies on Growth of Salt-Free Wormlike Micelles Formed by Star-Type Trimeric Surfactants. *Langmuir* **2012,** 28, 16798-16806.

(3) Ansari, W. H.; Aslam, J.; Siddiqui, U. S.; Din, K., Micellar Growth of m-2-m Type Gemini Surfactants (m = 10, 12, 14) with Higher Chain Length Alcohols / Amines (C6-C8) in the Absence and Presence of Organic Salts (Sodium Salicylate, Sodium Tosylate). *J. Mol. Liq.* **2012,** 174, 5-10.

(4) MacKintosh, F. C.; Safran, S. A.; Pincus, P. A., Equilibrium Size Distribution of Charged 'Living' Polymers. *J. Phys. : Condens. Matter* **1990,** 2, SA359-SA364.

(5) Yoshimura, T.; Kusano, T.; Iwase, H.; Shibayama, M.; Ogawa, T.; Kurata, H., Star-Shaped Trimeric Quaternary Ammonium Bromide Surfactants: Adsorption and Aggregation Properties. *Langmuir* **2012,** 28, 9322-9331.

(6) Wattebled, L.; Laschewsky, A., Effects of Organic Salt Additives on the Behavior of Dimeric ("Gemini") Surfactants in Aqueous Solution. *Langmuir* **2007,** 23, 10044-10052.

(7) Manet, S.; Karpichev, Y.; Bassani, D.; Kiagus-Ahmad, R.; Oda, R., Counteranion Effect on Micellization of Cationic Gemini Surfactants 14-2-14: Hofmeister and Other Counterions. *Langmuir* **2010,** 26 (13), 10645-10656.

(8) Yu, D.; Huang, M.; Lin, Y.; Jiang, L.; Huang, J.; Wang, Y., Effects of Inorganic and Organic Salts on Aggregation Behavior of Cationic Gemini Surfactants. *J. Phys. Chem. B* **2010,** 114, 14955-14964.

(9) Lu, T.; Huang, J.; Li, Z.; Jia, S.; Fu, H., Effect of Hydrotropic Salt on the Assembly Transitions and Rheological Responses of Cationic Gemini Surfactant Solutions. *J. Phys. Chem. B* **2008,** 112, 2909-2914.

(10) Inoue, K.; Oka, T.; Miura, K.; Yagi, N., Present Status of BL40B2 and BL40XU at SPring-8 (Beamlines for Small Angle X-ray Scattering). *AIP Conf. Proc.* **2004,** 705, 336-339.

(11) Masunaga, H.; Sasaki, S.; Tashiro, K.; Hanesaka, M.; Takata, M.; Inoue, K.; Ohta, N.; Yagi, N., Development of Synchrotron DSC/WAXD/SAXS Simultaneous Measurement System for Polymeric Materials at the BL40B2 in SPring-8 and its Application to the Study of Crystal Phase Transitions of Fluorine Polymers. *Polym. J.* **2007,** 39 (12), 1281-1289.

(12) Hammersley, A. P.; Svensson, S. O.; Hanfland, M.; Fitch, A. N.; Hausermann, D., Two-Dimensional Detector Software: From Real Detector to Idealised Image or Two-Theta Scan. *High Press. Res.* **1996,** 14, 235-248.

(13) Kusano, T.; Akutsu, K.; Iwase, H.; Yoshimura, T.; Shibayama, M., Structural Study on Aggregation Behavior of Star-Type Trimeric Surfactants in the Presence of Organic Salts. *J. Colloid Interf. Sci.* **2014,** submitted.

(14) Shikata, T.; Hirata, H.; Kotaka, T., Micelle Formation of Detergent Molecules in Aqueous Media: Viscoelastic Properties of Aqueous Cetyltrimethylammonium Bromide Solutions. *Langmuir* **1987,** 3, 1081-1086.

(15) Shikata, T.; Hirata, H.; Kotaka, T., Micelle Formation of Detergent Molecules in Aqueous Media. 2. Role of Free Salicylate Ions on Viscoelastic Properties of Aqueous Cetyltrimethylammonium Bromide-Sodium Salicylate Solutions. *Langmuir* **1988,** 4, 354-359.

(16) Inoue, T.; Inoue, Y.; Watanabe, H., Nonlinear Rheology of CTAB / NaSal Aqueous Solutions: Finite Extensibility of a Network of Wormlike Micelles. *Langmuir* **2005,** 21, (4), 1201-1208.

(17) Das, N. C.; Cao, H.; Kaiser, H.; Warren, G. T.; Gladden, J. R.; Sokol, P. E., Shape and Size of Highly Concentrated Micelles in CTAB / NaSal Solutions by Small Angle Neutron Scatering (SANS). *Langmuir* **2012,** 28 (33), 11962-11968.

(18) Rodrigues, R. K.; Silva, M. A.; Sabadini, E., Worm-like Micelles of CTAB and Sodium Salicylate under Turbulent Flow. *Langmuir* **2008,** 24 (24), 13875-13879.

(19) Zana, R.; Kaler, E. W., *Giant Micelles : Properties and Applications*. CRC Press: 2007; p 179-222.

(20) Hayter, J. B.; Penfold, J., An Analytical Structure Factor for Macroion Solutions. *Mol. Phys.* **1981,** 42, 109-118.

(21) Dreiss, C. A., Wormlike Micelles: Where Do We Stand? Recent Developments, Linear Rheology and Scattering Techniques. *Soft matter* **2007,** 3, 956-970.

(22) Takeda, M.; Kusano, T.; Matsunaga, T.; Endo, H.; Shikata, T.; Shibayama, M., Rheo-SANS Studies on Shear-Thickening/Thinning in Aqueous Rodlike Micellar Solutions. *Langmuir* **2011,** 27, (5), 1731-1738.

(23) Shrestha, R. G.; Shrestha, L. S.; Matsunaga, T.; Shibayama, M.; Aramaki, K., Lipophilic Tail Architecture and Molecular Structure of Neutralizing Agent for the Controlled Rheology of Viscoelastic Fluid in Amino-Acid Based Anionic Surfactant System. *Langmuir* **2011,** 27, 2229-2236.

(24) Davies, T. S.; Ketner, A. M.; Raghavan, S. R., Self-Assembly of Surfactant Vesicles that Transform into Viscoelastic Wormlike Micelles upon Heating. *J. Am. Chem. Soc.* **2006,** 128, 6669-6675.

Chapter 4

Water-in-Ionic Liquid Reverse Micelle Formation Using Oligomeric Surfactants

4-1. Introduction

In this chapter, oligomeric surfactants were used for water-in-ionic liquid (IL)-type RM systems. Oligomeric surfactants are highly hydrophobic because of their multiple hydrocarbon chains and were therefore used in IL systems. RMs in a conventional organic solvent system have been widely used in chemical reactions. However, the organic solvents used as the "oil" phase in RM formation are generally volatile, flammable, and toxic and therefore pose significant environmental problems. As alternatives to such conventional systems, thermodynamically stable water-in-IL RMs have been prepared using room-temperature ILs.[1–12] ILs are well known to possess novel and unique properties, including low volatility, high thermal stability, high designability, etc., and are thus used as a green solvent in the field of chemistry.[13, 14] In particular, the solvent properties of ILs can be easily varied by changing the chemical structure of ions and the combination of cation and anion[15–19] to give a water-in-IL RMs with novel and unique physicochemical properties. [20–24]

Focusing on water-in-IL systems, Gao et al. first reported that water-in-IL RMs are formed in a ternary system of 1-butyl-3-methylimidazolium tetrafluoroborate ([C_4

$_m$Im$^+$][BF_4^-]), Triton X-100 (neutral surfactant), and cyclohexane (organic solvent).[1] Such RMs in a ternary system, i.e., IL/organic solvent/neutral surfactant, have often been reported by some researchers, who have typically characterized them by varying the cation and anion species of the ILs. For neutral surfactants such as TritonX-100 and Tween 20, RMs can be formed in a system of IL and neutral surfactant in the absence of an organic solvent.[1, 2, 5, 25, 26] The development of organic-solvent-free systems is very important from an environment viewpoint and is thus desired in the field of chemistry. Goto et al. also reported that water-in-IL RMs are stably formed in typical aprotic ILs (aILs) when AOT is used as an anionic surfactant and hexanol is used as an organic solvent, [12, 13] resulting in successful activation and stabilization of enzymes in the RMs.[7, 27] Rai et al. recently reported the formation of water-in-IL RMs stabilized by zwitterionic surfactants (SB-12) in aILs containing ethanol.[12] IL-based RMs prepared using cationic or anionic surfactants provide an excellent reaction medium relative to conventional organic solvent systems.[4, 27] To our knowledge, however, unlike systems with neutral surfactants, organic-solvent-free systems have not been developed in an RM system with an ionic surfactant. Furthermore, the incorporation of organic solvents as one component in the system leads to a decrease in the IL mole fraction, which effectively limits the range of unique and novel properties of the ILs.

In this study, the formation of water-in-IL RMs without organic solvents in an IL mixture of 1-octylimidazolium-based aILs and pILs with anionic surfactant AOT was reported. In the case of the organic-solvent-free system proposed here, this study focused on the variation in water-droplet size as a function of (1) the water concentration, C_W, and (2) the mole fraction of pIL, χ_{pIL}, which were characterized using DLS, SAXS, and SANS techniques.

4-2. Experimental section

4-2-1. Materials

Figure 4-1 shows the chemical structures of the compounds used in this study. The aIL, 1-octyl-3-methylimidazolium bis(trifluoromethanesulfonyl)amide ([$C_{8\ m}$Im$^+$][TFSA$^-$]) was synthesized from *N*-methylimidazole and 1-bromoalkane according to the method reported in the literature.[19, 28] The pILs 1-alkylimidazolium bis(trifluoromethanesulfonyl)-

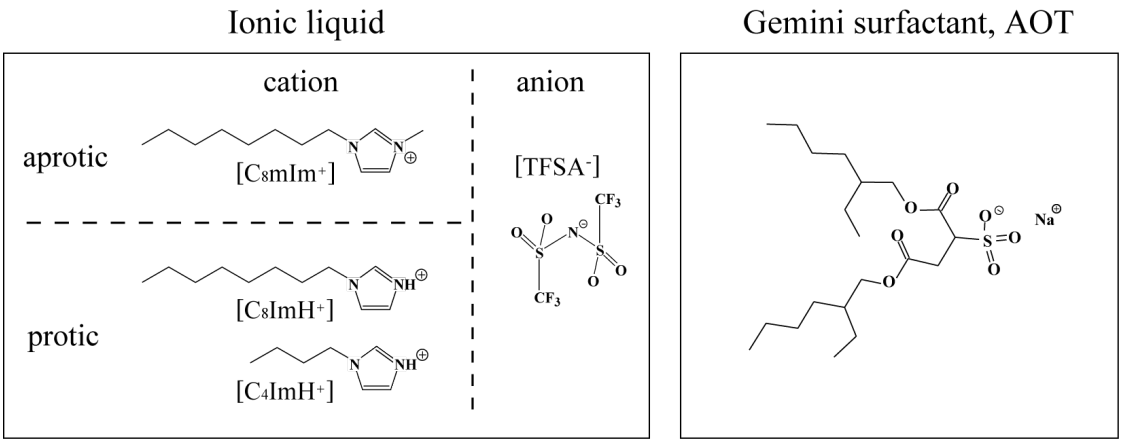

Figure 4-1. Chemical structures of imidazolium-based aprotic ($[C_{8\ m}Im^+][TFSA^-]$) and protic ionic liquids ($[C_{8\ m}ImH^+][TFSA^-]$ and $[C_{4\ m}ImH^+][TFSA^-]$) and ionic surfactant AOT.

amide ($[C_nImH^+][TFSA^-]$ (n = 4 and 8)) were prepared by mixing 1-alkylimidazole and HTFSA in acetonitrile and stirring the solutions for 24 h; the solvent was subsequently removed under a reduced pressure. For SANS measurements, a deuterated ionic liquid, d_{20}-$[C_{8\ m}Im][TFSA]$, was used. Previous paper describes the process for preparing the deuterated IL.[19] The synthesized d_{20}-$[C_{8\ m}Im][TFSA]$ was characterized by ^{1}H NMR, and the degree of deuteration was 98%. For SLS/DLS measurements, AOT was added to the solvent (neat IL or an aIL/pIL mixture) and was stirred for 1 day, followed by the addition of water with rigorous stirring for 30 min.

4-2-2. Light scattering

DLS measurements were conducted using an ALV5000 DLS/SLS apparatus (ALV, Germany). The temperature of the samples was maintained at 25 ± 0.03 °C. A 22 mW He–Ne laser with a wavelength λ of 632.8 nm was used as the light source. In the DLS measurements, the intensity correlation functions were obtained over a period of 60 s at θ = 90°. The hydrodynamic radius, R_h, of the RMs was obtained by both cumulant and CONTIN analyses[29] on the basis of the Stokes–Einstein equation, where the viscosities and the refractive indices of the mixtures were independently measured in our laboratory with an Abbe refractometer (DR-A1, ATAGO, Japan) and a rheometer (MCR-501, Anton

Paar, Austria); the viscosities and refractive indices were measured as functions of the mole fraction of pIL, χ_{pIL}, to the total ILs (**Figure 4-2**).

4-2-3. Small-angle X-ray scattering (SAXS)

SAXS experiments were conducted on the BL03XU beamline at SPring-8, Hyogo, Japan. In SAXS measurements, a monochromated X-ray beam with a wavelength λ of 1.00 Å was used as incident beam at room temperature, and the scattered X-rays were counted at sample-to-detector distances (SDDs) of 1.2 and 4.2 m by an imaging-plate detector (R-AXIS VII++, Rigaku Corp., Tokyo, Japan) with 3000 × 3000 pixel arrays and a pixel size of 0.1 mm pixel^{-1}. The obtained two-dimensional (2D) data was circularly averaged and corrected for dark current, background (cell) scattering, and transmittance. The obtained scattering data was normalized to the absolute intensity scale using a glassy carbon secondary standard.

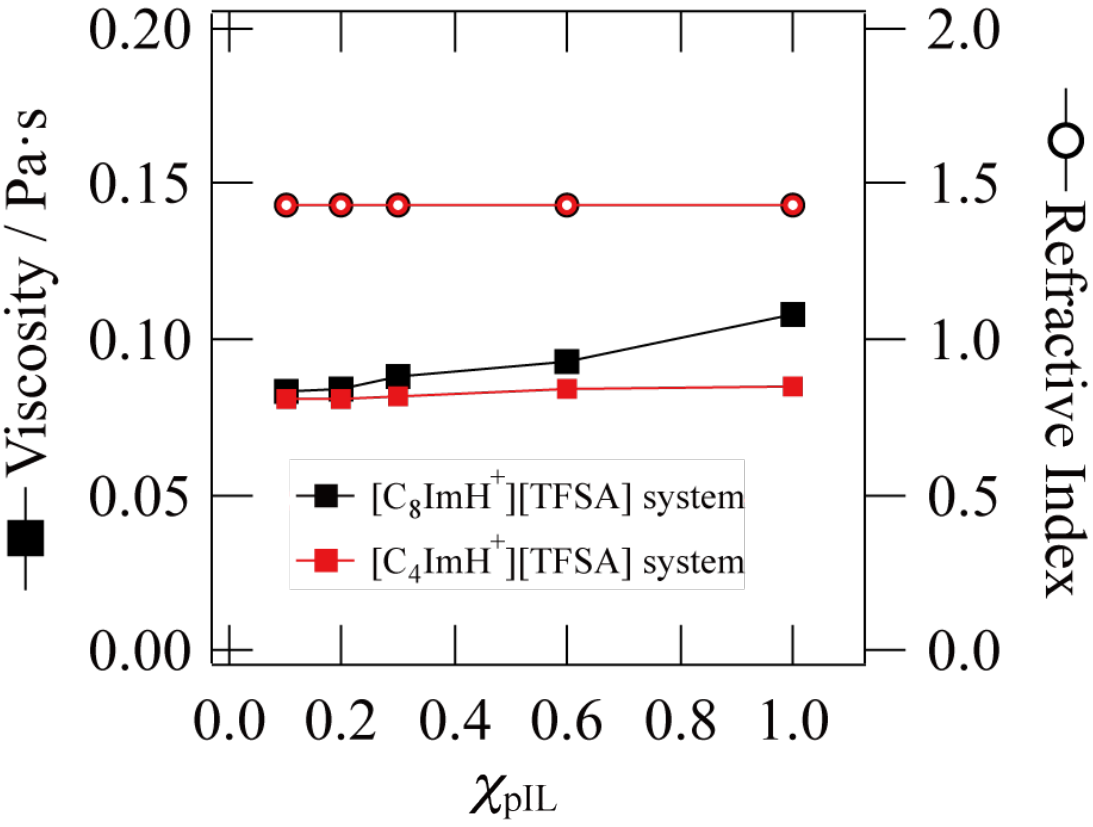

Figure 4-2. Experimental refractive indices and viscosities of solvent mixtures of aprotic and protic ionic liquids at 25 °C. [30]

4-2-4. Small-angle neutron scattering (SANS)

SANS experiments were performed using the JRR–3 reactor at JAEA, Japan for aqueous systems and using the high-flux advanced neutron application reactor (HANARO) at the Korea Atomic Energy Research Institute (KAERI), Korea for IL systems.

At JRR–3, a monochromated cold neutron beam with an average neutron wavelength of 7.00 Å was used. Two sample-to-detector distances of 1 and 4 m were employed to cover the momentum transfer q range from 0.01 to 0.2 Å. The transmission was measured using a ^{3}He detector at the beam-stopper position. Obtained SANS data corrected for background using an empty cell were normalized with respect to the scattering of polyethylene as a secondary standard material.

At HANARO, a monochromated cold neutron beam with an average neutron wavelength 6.00 Å was used to irradiate the samples and the scattered neutrons were counted using a 2D area detector. Two SDDs, i.e., 2 and 17.5 m, were employed to cover the q-range from 0.003 to 0.4 Å^{-1}. All measurements were performed at room temperature. After necessary corrections for open beam scattering, transmission, and detector inhomogeneities were performed, the corrected scattering intensity functions were normalized to the absolute intensity scale. The incoherent scattering intensity subtraction was conducted according to the procedure reported in the literature.[31]

4-3. Results and discussion

4-3-1. Reverse micelle formation in aIL/pIL mixtures

Figure 4-3 shows photographs of mixtures of water, [$C_{8\ m}Im^+$][$TFSA^-$] (aIL), and [C_8ImH^+][$TFSA^-$] (pIL) (a) with and (b) without AOT after rigorous stirring. The mixture shown in fig. 4-3a contains 0.075 mol·dm^{-3} AOT and C_W = 0.83 mol·dm^{-3} (≈ 1.5 vol%) water, whereas that in fig. 4-3b contains only C_W = 0.83 mol·dm^{-3} water, where C_W is the water concentration. The mole fraction of pIL, χ_{pIL}, in the aIL/pIL mixture was χ_{pIL} = 0.2, and the water-to-AOT molar ratio was W_0 = 11. **Figure 4-3a** clearly shows that the mixed aIL/pIL solvent with AOT can solubilize relatively large amounts of water to give rise to a transparent solution. In contrast, the water/IL mixture without AOT (Fig. 5-3b) formed a turbid dispersion. As mentioned in the introduction, Goto et al. have reported

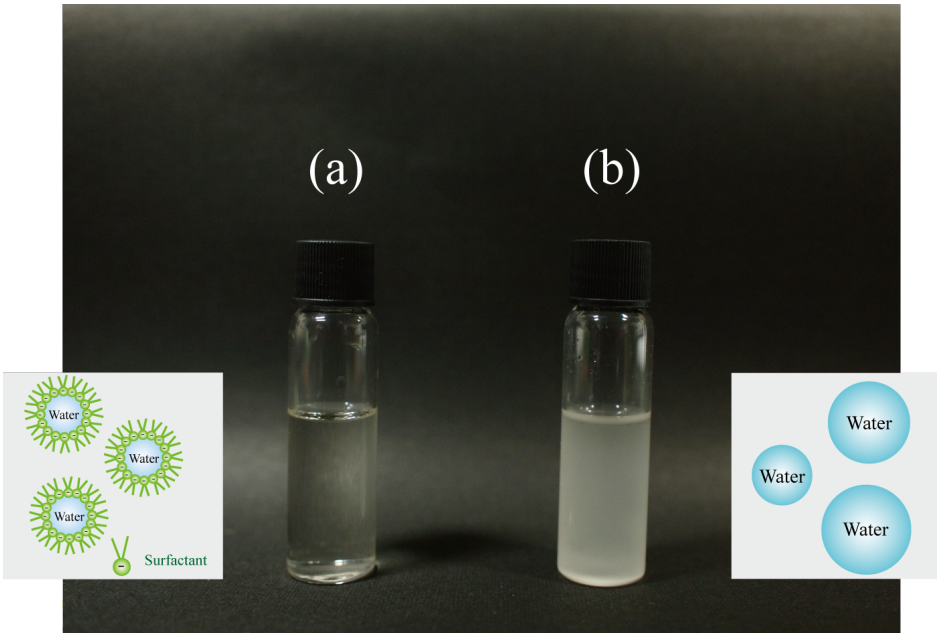

Figure 4-3. Solubilization of water at room temperature in the IL mixtures of (a) [$C_{8\ m}Im^+$][$TFSA^-$] and [C_8ImH^+][$TFSA^-$] with 0.075 mol·dm^{-3} AOT and 0.83 mol·dm^{-3} water and (b) [$C_{8\ m}Im^+$][$TFSA^-$] and [C_8ImH^+][$TFSA^-$] with 0.83 mol·dm^{-3} water.

that water molecules stably exist as droplets in a ternary [$C_{8\ m}Im^+$][$TFSA^-$]/hexanol/AOT system to form water-in-IL RMs, whereas a system without AOT undergoes phase separation. Notably, the typical droplet size of the RMs reported by Goto et al. was ca. 100 nm. In comparison with their study, we deduced that water molecules exist as water droplets also in the aIL/pIL mixture that contains AOT but not an organic solvent (e.g., hexanol) and that the RMs are composed of a water core and an AOT shell.

4-3-2. Water concentration dependence

Figure 4-4 shows the autocorrelation functions, $g^{(2)}(\tau) - 1$, obtained from DLS measurements of the aIL/pIL mixtures with various C_W values ($0.75 \leq C_W \leq 1.0$ mol·dm^{-3}) and fixed concentrations of AOT and pIL ($C_{AOT} = 0.075$ mol·dm^{-3} and $\chi_{pIL} = 0.2$). Note that obtaining meaningful data at lower water concentrations ($C_W \leq 0.6$ mol·dm^{-3}) was not possible because of excessively weak scattering. This weak scattering could be due to a significant amount of water being dissolved in the bulk phase and a failure to form RMs, as will be discussed later. As previously described, the anionic surfactant AOT was required to form RMs in this system. As evident in fig. 4-4, a clear single relaxation

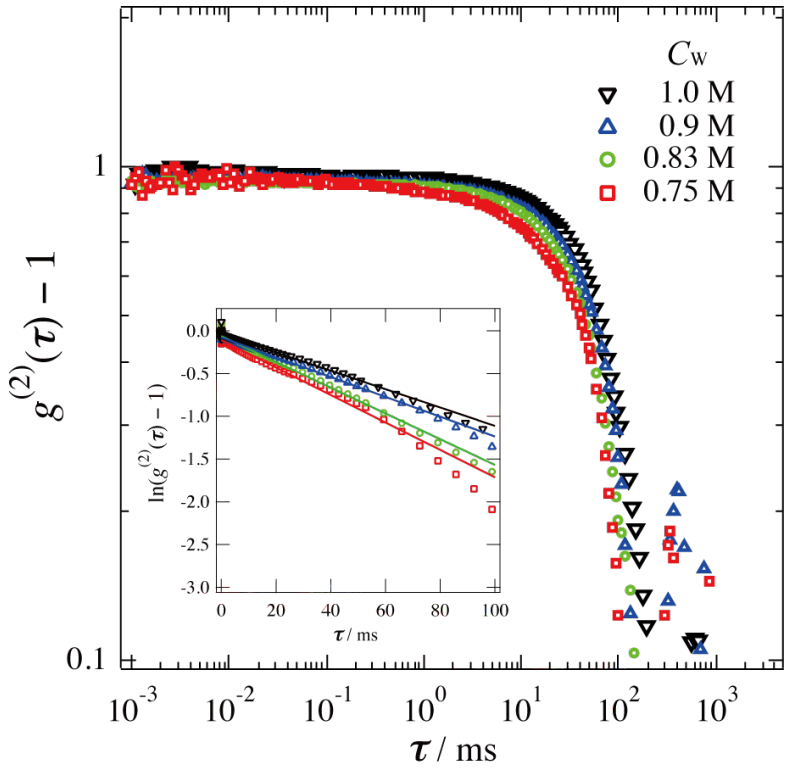

Figure 4-4. Water concentration (C_W) dependence of the correlation functions observed for aIL/pIL mixtures (aIL: $[C_{8\,m}Im^+][TFSA^-]$ and pIL: $[C_8ImH^+][TFSA^-]$) with C_{AOT} = 0.075 mol·dm^{-3} and χ_{pIL} = 0.2 at 25 °C.[30]

was observed in the correlation function of the aIL/pIL mixtures containing AOT for all the C_Ws examined here. With increasing C_W, the characteristic decay time appeared to shift to larger τ values, indicating that the RM size increased with increasing C_W. By applying cumulant analysis to the observed data, i.e., by plotting $\ln[g^{(2)}(\tau) - 1]$ vs. τ, as shown in the inset of fig. 4-4, we estimated the hydrodynamic radius, R_hs, of the RMs. The R_h value was estimated to be 131 nm in the solution with C_W = 0.75 mol·dm^{-3}, and the value increased with increasing C_W to reach 195 nm at C_W = 1.0 mol·dm^{-3}. These results are consistent with previous studies of water-in-IL RM systems.[3] Here, note that $[C_8ImH^+][TFSA^-]$ (pIL) is hydrophilic and is miscible with water, whereas $[C_{8\,m}Im^+][TFSA^-]$ (aIL) is hydrophobic and is immiscible with water. Therefore, this DLS result implies that the RMs formed in the aIL/pIL mixture involve pIL cations (C_8ImH^+) in their shell parts, as well as AOT, and that the RM size strongly depends on χ_{pIL}.

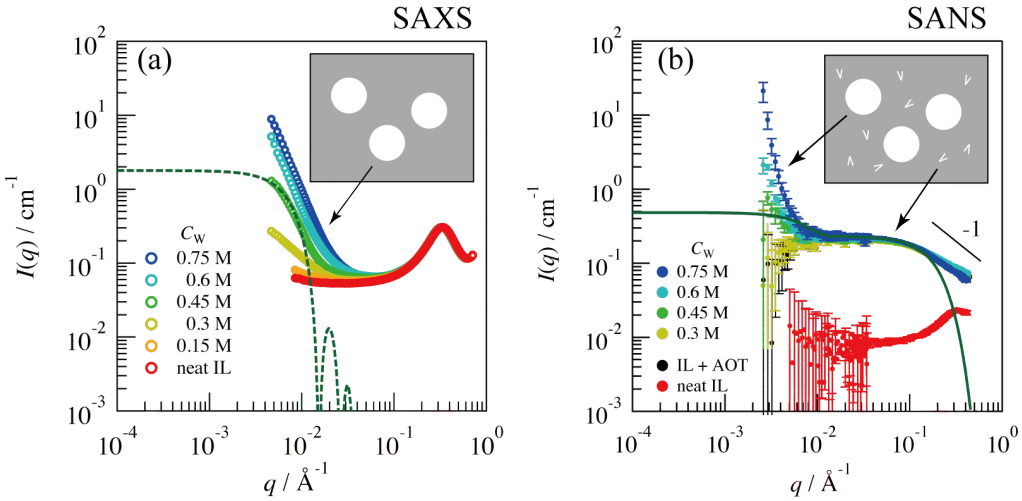

Figure 4-5. SAXS (a) and SANS (b) profiles observed for the aIL/pIL mixtures of deuterated [d_{20}-$C_{8\ m}Im^+$][$TFSA^-$] (aIL) and normal [C_8ImH^+][$TFSA^-$] (pIL) (χ_{pIL} = 0.2) with different water contents, C_Ws, at 25 °C. With the exception of the neat IL, AOT (C_{AOT} = 0.075 mol·dm^{-3}) was also present in the mixtures. The dashed and solid curves represent the fits with eqs. 4.4 and 4.1, respectively. The inset drawing schematically shows the difference in the scattering contrasts between SAXS and SANS. [30]

Figures 4-5a and b show SAXS and SANS profiles, respectively, of mixtures with different C_Ws together with those of neat IL (i.e., C_W = 0). In this study, SANS data was obtained for the mixture of deuterated [$C_{8\ m}Im^+$][$TFSA^-$] (d_{20}-[$C_{8\ m}$Im][TFSA]) and normal [C_8ImH^+][$TFSA^-$] with fixed concentrations of AOT (C_{AOT} = 0.075 mol·dm^{-3}) at various C_Ws. Note that the incoherent scattering arose mainly from pIL, AOT, and water, and this scattering was subtracted by the method reported elsewhere and by numerical estimation based on the chemical structures of the components.[31] The broad peak in the high-q region (q = 0.31 Å^{-1}) of the SAXS profiles is attributed to the liquid structure of the ILs.[19] A SANS curve of neat IL with AOT (neat IL + AOT) is included among the SANS profiles. The results in figs 4-5a and b indicate the following: (1) Neat IL gives similar SAXS and SANS profiles. (2) The addition of water leads to an increase in the scattering intensity in the low-q regions ($q \leq$ 0.02 Å^{-1}) of both the SAXS and SANS profiles. (3) A significant difference exists between the intermediate q regions (0.08 $\leq q \leq$ 0.2 Å^{-1}) of the SAXS and SANS patterns, and the SANS profiles exhibit a plateau. This plateau appears after AOT is added. These results strongly suggest that the systems

exhibit two kinds of scattering: one that originates from RMs and another that originates from AOT molecules dispersed in the IL matrix, as shown in the inset illustration in fig. 4-5b. In the case of the SANS profiles, two scattering contrasts are observed: one between water and the IL and the other between AOT and the IL. In contrast, the SAXS profiles exhibit only single contrast between water and the IL because the electron density difference between AOT and IL is negligible ($\rho_{AOT} = 1.0 \times 10^{-5}$ Å^{-2}, $\rho_{IL} = 1.1 \times 10^{-5}$ Å^{-2}). Hence the SANS scattering intensity from water/AOT/IL systems is given by:

$$I(q) = N_1 v_1^2 (\Delta\rho_1)^2 \Phi^2(q) + N_2 v_2^2 (\Delta\rho_2)^2 F_{AOT}(q) \tag{4.1}$$

where N_1 and v_1 are the number density and volume of the water droplets, respectively, N_2 and v_2 are the number density and volume of the AOT molecules, respectively, $\Delta\rho_1$ is the neutron scattering length density difference between water and the deuterated IL, and $\Delta\rho_2$ is that between AOT and the deuterated IL. $\Phi^2(q)$ and $F(q)$ are the form factors of a spherical object and an AOT molecule, respectively, and are given by:

$$\Phi(q) \equiv \frac{9}{(Rq)^3}\left[\sin Rq - Rq\cos Rq\right] \tag{4.2}$$

$$F(q) = \exp\left[-R_{g,AOT}^2 q^2 / 3\right] \tag{4.3}$$

where R is the radius of the water droplet and $R_{g,AOT}$ is the radius of gyration of AOT. The SAXS scattering intensity from the same system, in contrast, is given by

$$I(q) = N_1 v_1^2 (\Delta\rho_1)^2 \Phi^2(q) \tag{4.4}$$

where $\Delta\rho_1$ is the electron density difference between water droplets and the IL ($\Delta\rho_1 = 2.05 \times 10^{-6}$ Å^{-2}; the X-ray scattering length density difference between water and the IL). Notably, no X-ray scattering contrast was observed between AOT and the IL because their electron densities are very similar. The dashed and solid curve in fig. 4-5a show the fits with eqs. 4.4 and 4.1, respectively. As indicated by the fitting results, the calculated SANS functions will reproduce the observed functions. Hence, the scattering systems are schematically depicted by the illustrations in the insets, where the letter "v" denotes an AOT molecule dispersed in the medium. The R_g value obtained from SANS was evaluated to be 0.85 nm, which is in a good agreement with the van der Waals size of AOT.[32] Furthermore, the N_2 value was 2.55×10^{19} cm^{-3}, which is consistent with

calculated values (1.94×10^{19} cm^{-3}). With regard to the $I(q) \propto q^{-1}$ relationship in the high-q range above 0.1 $Å^{-1}$, Mata et al.[33] have reported similar behavior in a SANS study of RMs formed in aqueous solutions. They pointed out that the $I(q) \propto q^{-1}$ scattering corresponds to a small rodlike component, i.e., monomer surfactant with no micelle formation. In the case of the aIL/pIL mixture system, AOT molecules may exist both at the interface of the RMs and in the IL matrix as a molecular dispersion.

In contrast, the N_1 values obtained from the SAXS measurement ($N_1 = 1.51 \times 10^{11}$ cm^{-3} at $C_W = 0.45$ $mol \cdot dm^{-3}$) were much smaller than the calculated value ($N_1 = 4.53 \times 10^{13}$ cm^{-3}). These smaller N_1 values indicate that a significant amount of water molecules must have been dissolved in the bulk IL. The N_1 values were reexamined to determine the absolute intensities of SANS and SAXS and to determine the critical water concentration below which water is completely dissolved in the bulk phase ($C_W^* = 0.444$ $mol \cdot dm^{-3}$). In the case of $C_W \geq 0.45$ $mol \cdot dm^{-3}$, the excess water molecules, i.e., ($C_W - C_W^*$), form RMs and induce scattering, which indicates that excess of water must be added to the system to ensure the formation of stable RMs in the aIL/pIL mixture.

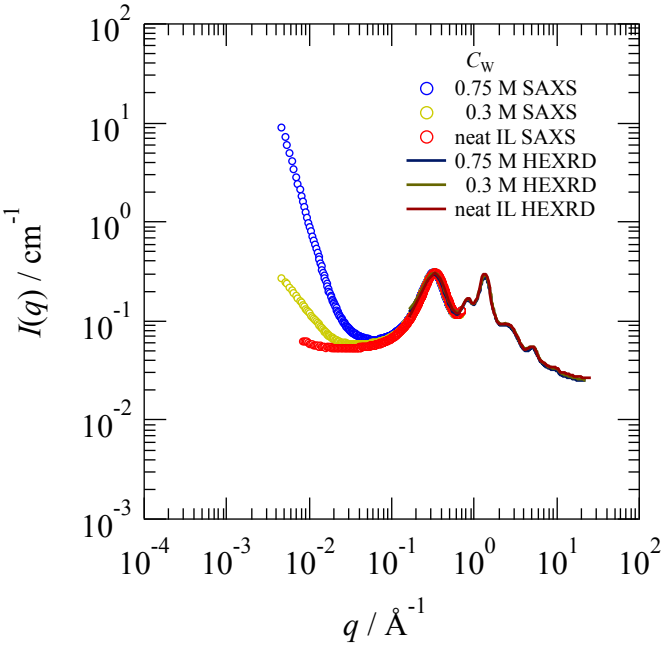

Figure 4-5. SAXS and HEXRD profiles observed for the aIL/pIL mixtures (χ_{pIL} = 0.2) with different water contents, C_Ws, at 25 °C.

Figures 4-5 show SAXS and HEXRD profiles of mixtures with different C_Ws together with those of neat IL (i.e., C_W = 0). The HEXRD profiles in high-q region were independent of water concentration, which indicates the solution structure did not change by adding water. From model fitting results of SAXS profiles, a significant amount of water molecules was dissolved in the bulk IL. However, compared with the bulk IL volume fraction, the amount of dissolved water is too small ($\phi = 0.008$) to affect the solution structure and the solution properties.

Figure 4-6 shows the variation of the radius of water droplets as a function of C_W, as determined by SAXS (R) and DLS (R_h). For comparison of the radii with different physical meanings, the relationship, R_h:$R \approx 1$:1 (for a hard sphere) was used. The RM radius increases rather linearly with C_W. This result is in good agreement with that reported by Goto et al.[3] and indicates that water-in-IL RMs are formed because of the presence of AOT, even in the absence of an organic solvent.

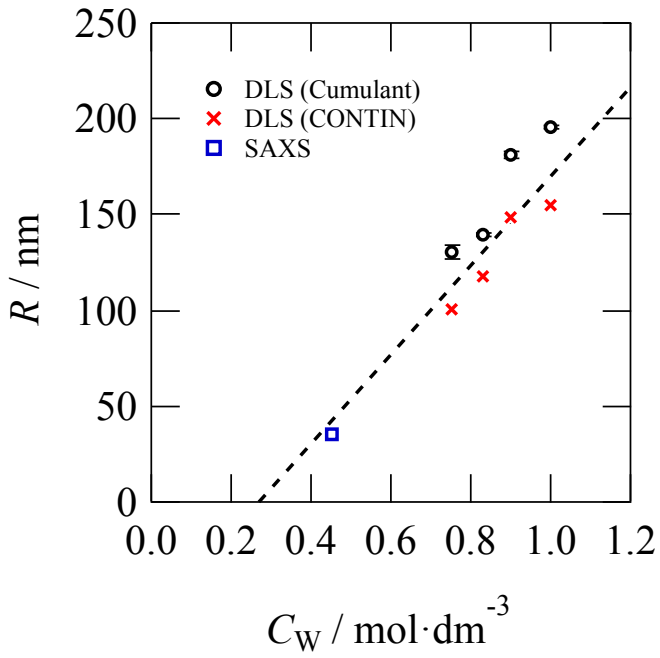

Figure 4-6. C_W dependence of the radius of RMs, R, in the $C_{8\,m}Im^+$(aIL)/C_8ImH^+(pIL) systems with C_{AOT} = 0.075 mol·dm^{-3} and χ_{pIL} = 0.2.[30]

4-3-3. Protic IL concentration dependence

In this section, the role of the pIL in RM formation is discussed. **Figure 4-7** shows a series of DLS correlation functions of water/AOT/IL mixtures, where the molar fraction of pIL, χ_{pIL}, was varied from 0.1 to 1.0. Interestingly, the correlation functions show a single relaxation and the characteristic decay time shifts to longer times with increasing χ_{IL}. The inset shows a semi-logarithmic plot for evaluating the characteristic decay rate via the cumulant method.

Figure 4-8 shows the R_h values observed for the aIL/pIL mixtures in which the piL alkyl chain lengths were n = 4 and 8. The dashed lines are guides for the eye. In the case of the $[C_{8\ m}Im^+][TFSA^-]/[C_8ImH^+][TFSA^-]$ mixture system, i.e., the case where the alkyl-chain lengths are the same for aIL and pIL, the R_h increases with increasing χ_{pIL}. When the pIL with n = 8 was replaced with a pIL with shorter alkyl group (n = 4), the R_h also increased with increasing χ_{pIL}. However, the R_h value was appreciably smaller for the n = 4 system compared to that for the n = 8 system in the high-χ_{pIL} region. Previous

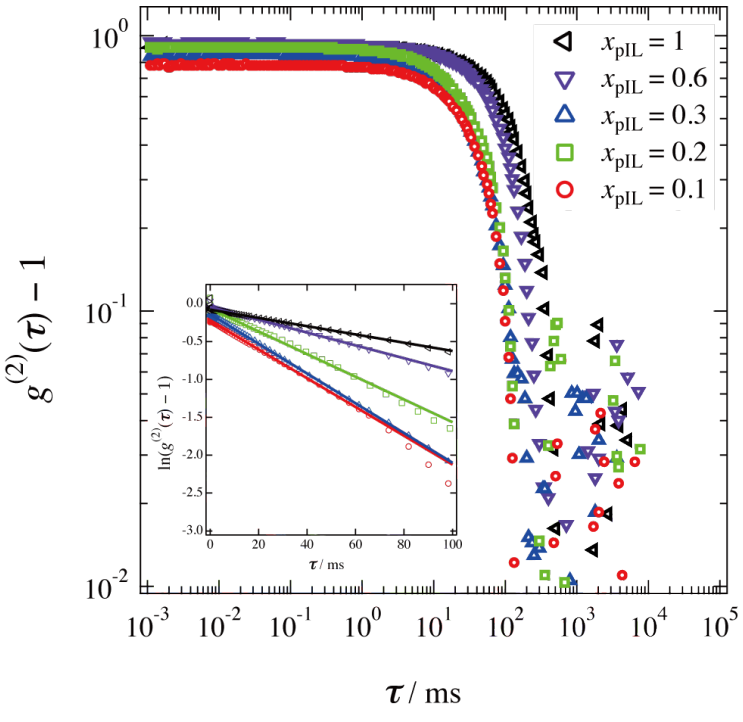

Figure 4-7. Correlation functions observed for water and aIL/pIL mixtures (aIL: $[C_{8\ m}Im^+][TFSA^-]$ and pIL: $[C_8ImH^+][TFSA^-]$) with C_{AOT} = 0.075 mol·dm^{-3} at various χ_{pIL}s from 0.1 to 1.0.[30]

studies[37] have established that the imidazolium-based IL with n = 8 is highly efficient at lowering surface tension because of its long hydrophobic alkyl chain in comparison with that with n = 4. We thus expected that the IL cation (in this case, protic C_nImH^+) acts as a cosurfactant for RM formation, which plays a key role in the formation of RMs. Therefore, we used SANS to investigate the performance of IL cations as surfactants.

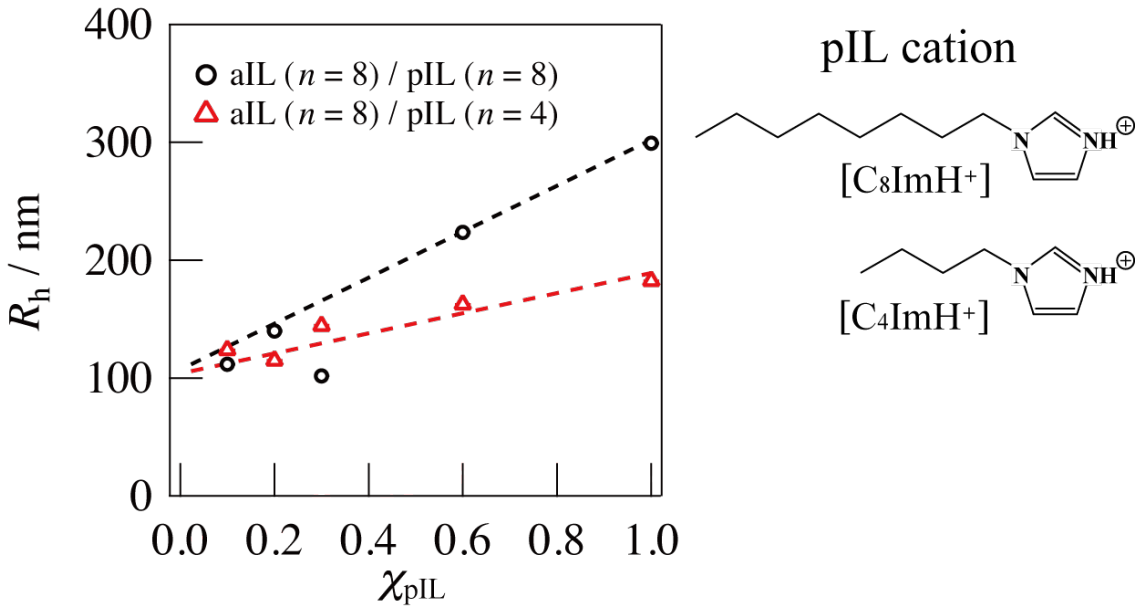

Figure 4-8. pIL mole fraction dependence of the R_h values in the $C_8{}_mIm^+$(aIL)/C_8ImH^+(pIL) and $C_8{}_mIm^+$(aIL)/C_4ImH^+(pIL) systems with C_{AOT} = 0.075 mol·dm^{-3} (ϕ_{AOT} = 0.033) and C_W = 0.83 mol·dm^{-3}.[30]

4-3-4. Aggregation behavior of [C_nmIm$^+$][Br$^-$] in aqueous solutions

In this subsection, the aggregation behavior of IL cations in aqueous solution was investigated. **Figures 4-9a and b** show SANS profiles obtained for aqueous $[C_4{}_mIm^+][Cl^-]$ and $[C_4{}_mIm^+][Br^-]$ solutions, respectively, with various IL concentrations, C_{IL} (mmol·dm^{-3}). As evident in these figures, no noticeable SANS intensity was observed for either system at any IL concentration, which indicates that neither IL forms aggregates with a size scale of 10–1000 Å, resulting in a homogeneous mixing state in the solutions.

Figure 4-10 shows SANS profiles for aqueous $[C_8{}_mIm^+][Br^-]$ solutions at IL concentrations (C_{IL}) of 47.0 to 973 mmol·dm^{-3}. No SANS profile was observed for

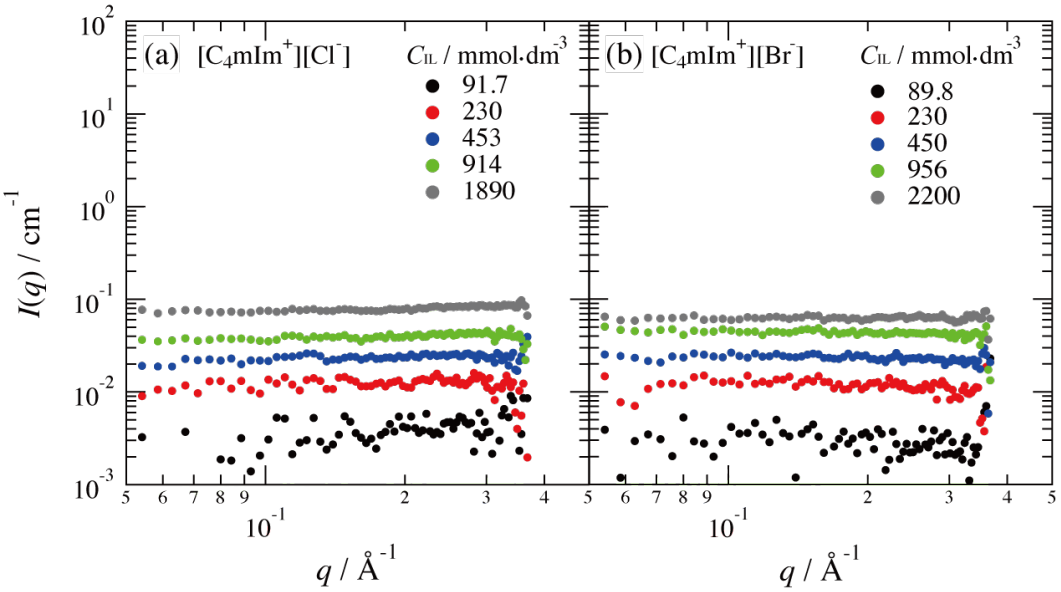

Figure 4-9. SANS profiles for aqueous solutions of (a) $[C_{4\ m}Im^+][Cl^-]$ and (b) $[C_{4\ m}Im^+][Br^-]$ with various IL concentrations (C_{IL}).[34]

solutions with low C_{IL}s (47.0–90.0 mmol·dm^{-3}). However, the SANS profiles gradually appeared with increasing C_{IL}. In previous reports, CMC in the aqueous $[C_{8\ m}Im^+][Br^-]$ solution was estimated to be 150 mmol·dm^{-3}.[35, 36] Therefore, in the C_{IL} region of 455–973 mmol·dm^{-3}, $[C_{8\ m}Im^+][Br^-]$ aggregates to form micelles, resulting in a significant SANS profile. The SANS profiles for C_{IL} = 455 and 972 mmol·dm^{-3} (high concentrations) showed scattering functions with $I(q) \sim q^{-4}$ and exhibited peaks at approximately 0.114 and 0.144 Å^{-1}, which means that $[C_{8\ m}Im^+][Br^-]$ micelles with a smooth surface are formed in the aqueous solution and that the micelles electrostatically repel one another.

As has been well established, the peak position in SANS observed for micelle solution systems corresponds to the distance between particles. The peaks at 0.114 and 0.144 Å^{-1} thus correspond to the particle–particle distance in the charged IL-micelle solution system, which is discussed in detail as follows. In the case of solution with C_{IL} = 230 mmol·dm^{-3} (low concentration), the SANS profile did not exhibit any peak in the low-q region and showed a scattering function with $I(q) \sim q^{-2}$ in the high-q region, which differs substantially from the results obtained for solutions with C_{IL} = 455 and 972 mmol·dm^{-3}. Almasy et al. reported the results of a SANS study of aqueous $[C_{4\ m}Im^+][BF_4^-]$ solutions and noted that the observed SANS profiles were well described by the

Ornstein–Zernike equation with $I(q) \sim q^{-2}$, indicating that the concentrations of [C_4 $_m$Im$^+$][BF_4^-] in the aqueous media fluctuated and that micelles were not present.[37] [C_8 $_m$Im$^+$][Br^-] is concluded to not form micelles having a clear surface at this concentration, although C_{IL} (230 mmol·dm^{-3}) is close to the CMC for this system. [C_8 $_m$Im$^+$][Br^-] heterogeneously mixes with water in the solution at this low C_{IL}, leading to a scattering function with $I(q) \sim q^{-2}$ in the high-q region because of concentration fluctuations. As the C_{IL} is increased further, a structural change occurs and an IL-micelle structure is then formed in the solution. Therefore, an IL cation with n = 8 is concluded to serve as an effective co-surfactant in RM systems.

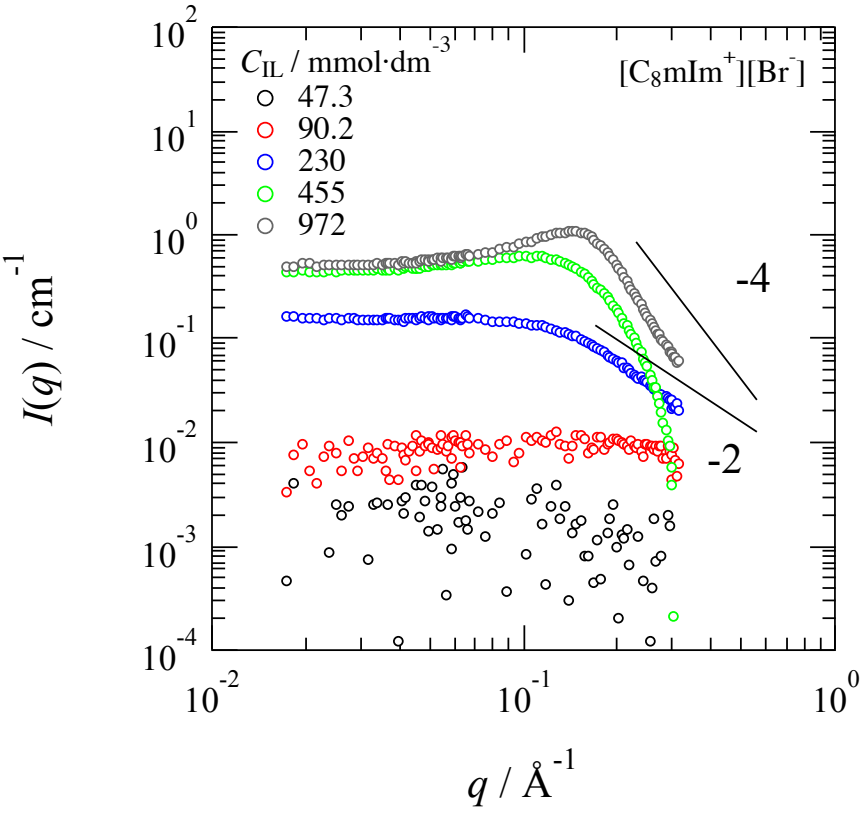

Figure 4-10. SANS profiles for aqueous solutions of [C_8 $_m$Im$^+$][Br^-] with various IL concentrations (C_{IL}s).[34]

4-3-5. Role of protic ionic liquids in reverse micelle formation

On the basis of these results, an RM formation mechanism in the aIL/pIL mixture system was proposed, which is illustrated in **Figure 4-11**. In the [C_8 $_m$Im$^+$][TFSA

$^{-}$]/[C_8ImH^+][$TFSA^-$] mixtures with AOT, water molecules are stably distributed in the mixtures as water-in-IL RMs in addition to being dissolved into the bulk phase. The RM size is determined by the aIL/pIL mixing ratio in the medium, and it increases with increasing χ_{pIL}. [C_8ImH^+][$TFSA^-$] (pIL) is a hydrophilic IL and is thus miscible with water. In contrast, [$C_{8\ m}Im^+$][$TFSA^-$] (aIL) is a typical hydrophobic IL that is immiscible with water and gives rise to phase separation. These behaviors imply that the polar imidazolium head group of a pIL cation (C_8ImH^+) can interact with water molecules at the IL–water droplet interface, whereas the nonpolar head of an aIL cation ($C_{8\ m}Im^+$) cannot. Therefore, the shell parts of RMs are conjectured to be composed of both AOT and C_8ImH^+ cations and to be stabilized by two types of interactions: (1) water–imidazolium-head-group interactions at the core–shell interface and (2) van der Waals interactions between the alkyl chains of C_8ImH^+ and AOT. In contrast, the aIL cations ($C_{8\ m}Im^+$) may not contribute to RM formation in the aIL/pIL mixture system. Indeed, the RM size becomes large, depending on the pIL concentration (see fig. 4-8). The same rule is also applied to the [$C_{8\ m}Im^+$][$TFSA^-$]/[C_4ImH^+][$TFSA^-$] system. However, the RM size in the [C_4ImH^+][$TFSA^-$] system is appreciably smaller than that in the [C_8ImH^+][$TFSA^-$]

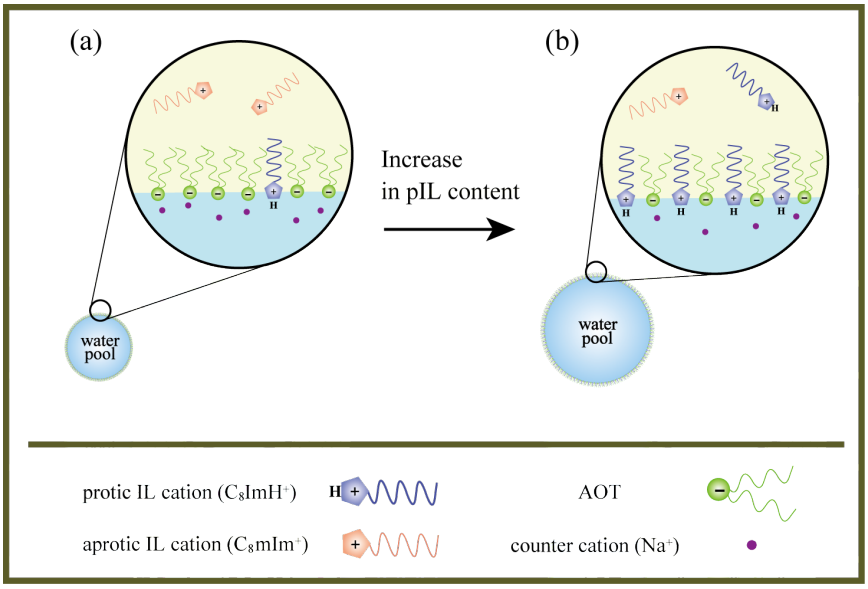

Figure 4-11. Possible microemulsion formation model for an aIL/pIL mixture system at (a) low and (b) high pIL contents.

system at high pIL mole fractions (as shown in fig. 4-8). This trend is explained by the fact that the interaction between C_4ImH^+ and AOT is weaker than that between C_8ImH^+ and AOT because of a weaker van der Waals interaction between the shorter alkyl chain of C_4ImH^+ and the longer chain of AOT. As a result, the number of C_4ImH^+ cations constituting RMs is less than the corresponding number of C_8ImH^+ cations resulting in a smaller RM size in the [C_4ImH^+][$TFSA^-$] system.

Figure 4-12 shows the hydrodynamic radius (R_h) distribution of RMs in aIL/pIL mixtures prepared using AOT and a star-type trimeric surfactant ($3C_{12}$trisQ). $3C_{12}$trisQ shows high hydrophobicity due to its three hydrocarbon chains, which leads to a disadvantage in the application for water systems. On the other hand, $3C_{12}$trisQ cannot be dissolved in non-polar organic solvent, due to its three hydrophilic head groups. Therefore, in this chapter, $3C_{12}$trisQ was used for IL systems, the solubility of which can be controlled by varying the aIL / pIL ratio. The RM systems can also be prepared using $3C_{12}$trisQ, which indicates that the method of preparing RMs by using a pIL can be applied to other surfactant systems. Furthermore, the size of RMs formed by $3C_{12}$trisQ was larger than that of RMs formed by AOT, which is explained by the greater packing

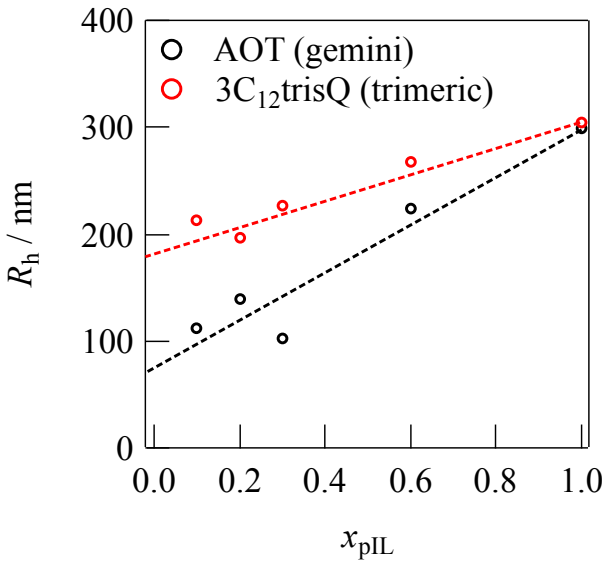

Figure 4-12. Dependence of the R_h values on the pIL mole fraction in the $C_8{}_mIm^+$(aIL)/C_8ImH^+(pIL) systems with $3C_{12}$trisQ (ϕ_D = 0.033) and water (C_W = 0.83 mol·dm^{-3}).

parameter of the star-type trimeric surfactant (**Figure 4-13**). The size of RMs could also be controlled by changing the surfactant species, i.e., the packing parameter. The R_h for $3C_{12}$trisQ systems was independent of χ_{pIL} in comparison with that for AOT systems. This result could be explained by the fact that, in $3C_{12}$trisQ systems, it is difficult for the pIL cation to penetrate the shell part of RMs due to the cation head groups of $3C_{12}$trisQ and the volume exclusion originated from the star-shape structure of $3C_{12}$trisQ. These results indicate that $3C_{12}$trisQ could disperse RMs more stably in the mixture solutions of ILs.

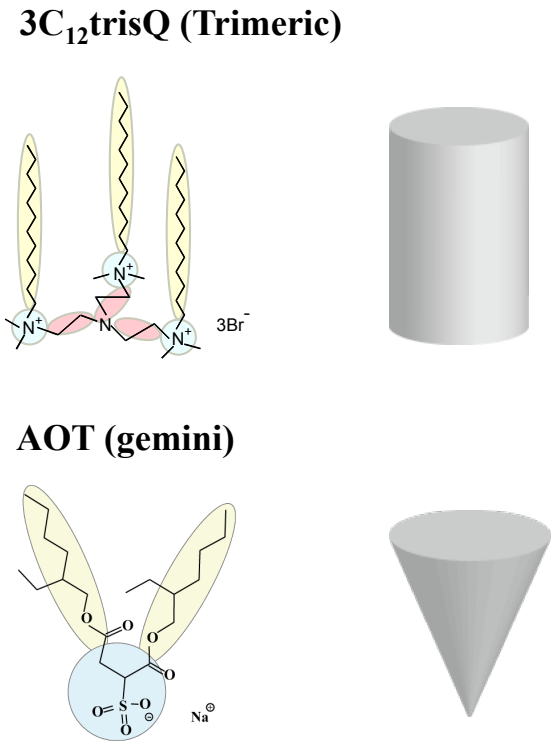

Figure 4-13. Schematic of the packing shapes of $3C_{12}$trisQ and AOT.

4-4. Conclusions

Water-in-IL RMs were successfully prepared in the absence of an organic solvent. The RMs were formed in a mixture of aprotic and protic imidazolium-based ILs containing the anionic surfactant AOT. Structural investigations with DLS, SAXS, and SANS revealed the following facts: (1) The size of RMs increases linearly with increasing water content, i.e., C_W. (2) SANS is capable of distinguishing two types of scattering: one

from RMs and another from AOT molecules dispersed in the aIL/pIL mixtures. (3) The size of RMs increases with increasing χ_{pIL}. (4) The alkyl-chain length of the pIL cation also influences the RM size, especially at high χ_{pIL}s. On the basis of the aforementioned results, the size of RMs formed in this system strongly depends on the pIL content in aIL/pIL mixtures. (5) RM systems were successfully prepared using a different surfactant, star-type trimeric surfactant $3C_{12}$trisQ, indicating that this pIL method can be widely applied to other surfactant systems. Furthermore The size of RMs formed by $3C_{12}$trisQ was independent of χ_{pIL} in comparison with that for AOT systems, which indicates that $3C_{12}$trisQ could disperse RMs more stably in the mixture solutions of ILs. The results obtained herein provide valuable insights into controlling the size of RMs in IL media.

References

(1) Gao, Y.; Han, S.; Han, B.; Li, G.; Shen, D.; Li, Z.; Du, J.; Hou, W.; Zhang, G., TX-100/Water/1-Butyl-3-methylimidazolium Hexafluorophosphate Microemulsions. *Langmuir* **2005,** 21, 5681-5684.

(2) Gao, Y.; Li, N.; Zheng, L.; Zhao, X.; Zhang, S.; Han, B.; Hou, W.; Li, G., A Cyclic Voltammetric Technique for the Detection of Micro-regions of $BmimPF_6$/Tween 20/H_2O Microemulsions and Their Performance Characterization by UV-Vis Spectroscopy. *Green Chem.* **2006,** 8, 43-49.

(3) Moniruzzaman, M.; Kamiya, N.; Nakashima, K.; Goto, M., Formation of Reverse Micelles in a Room-Temperature Ionic Liquid. *ChemPhysChem* **2008,** 9, 689-692.

(4) Moniruzzaman, M.; Kamiya, N.; Nakashima, K.; Goto, M., Water-in-Ionic Liquid Microemulsions as a New Medium for Enzymatic Reactions. *Green Chem.* **2008,** 10, 497-500.

(5) Zhou, G.; Zhang, Y.; Huang, X.; Shi, C.; Liu, W.; Li, Y.; Qu, Y.; Gao, P., Catalytic Activities of Fungal Oxidases in Hydrophobic Ionic Liquid 1-Butyl-3-methylimidazolium Hexafluorophosphate-based Microemulsion. *Colloids Surf. B Biointerfaces.* **2008,** 66, 146-149.

(6) Zhang, Y.; Huang, X.; Li, Y., Negative Effect of [bmim][PF_6] on the Catalytic Activity of Alcohol Dehydrogenase: Mechanism and Prevention. *J. Chem. Technol. Biotechnol.* **2008,** 83, 1230-1235.

(7) Moniruzzaman, M.; Kamiya, N.; Goto, M., Biocatalysis in Water-in-Ionic Liquid Microemulsions: A Case Study with Horseradish Peroxidase. *Langmuir* **2009,** 25, 977-982.

(8) Behera, K.; Malek, N. I.; Pandey, S., Visual Evidence for Formation of Water-in-Ionic Liquid Microemulsions. *ChemPhysChem* **2009,** 10, 3204-3208.

(9) Anjum, N.; Guedeau-Boudeville, M.; Stubenrauch, C.; Mourchid, A., Phase Behavior and Microstructure of Microemulsions Containing the Hydrophobic Ionic Liquid 1-Butyl-3-methylimidazolium Hexafluorophosphate. *J. Phys. Chem. B* **2009,** 113, 239-244.

(10) Xue, L.; Qiu, H.; Li, Y.; Lu, L.; Huang, X.; Qu, Y., A Noval Water-in-Ionic Liquid Microemulsion and Its Interfacial Effect on The Activity of Laccase *Colloids Surf. B Biointerfaces.* **2011,** 82, 432-437.

(11) Porada, J. H.; Mansueto, M.; Laschat, S.; Stubenrauch, C., Microemulsions with Novel Hydrophobic Ionic Liquids. *Soft Matter* **2011,** 7, 6805-6810.

(12) Rai, R.; Pandey, S.; Baker, S. N.; Vora, S.; Behera, K.; Baker, G. A.; Pandey, S., Ethanol-Assisted, Few Nanometer, Water-In-Ionic-Liquid Reverse Micelle Formation by a Zwitterionic Surfactant. *Chem. Eur. J.* **2012,** 18, 12213-12217.

(13) Zhu, W.; Ding, Y.; Li, H.; Qin, J.; Chao, Y.; Xiong, J.; Xu, Y.; Liu, H., Application of a Self-emulfiable Task-specific Ionic Liquid in Oxidative Desulfurization of Fuels. *RSC Adv.* **2013,** 3, 3893-3898.

(14) Rogers, R. D.; Seddon, K. R., Ionic Liquids--Solvents of the Future? *Science* **2003,** 302, 792-793.

(15) Welton, T., Room-Temperature Ionic Liquids. Solvents for Synthesis and Catalysis. *Chem. Rev.* **1999,** 99, 2071-2083.

(16) Fujii, K.; Kanzaki, R.; Takamuku, T.; Fujimori, T.; Umebayashi, Y.; Ishiguro, S., Conformational Equilibrium of Bis(trifluoromethanesulfonyl) Imide Anion of a Room-Temperature Ionic Liquid –Raman Spectroscopic Study and DFT Calculations–. *J. Phys. Chem. B* **2006,** 110, 8179-8183.

(17) Fujii, K.; Soejima, Y.; Kyoshoin, Y.; Fukuda, S.; Kanzaki, R.; Umebayashi, Y.; Yamaguchi, T.; Ishiguro, S.; Takamuku, T., Liquid Structure of Room-Temperature Ionic Liquid, 1-Ethyl-3-methylimidazolium Bis-(trifluoromethanesulfonyl) Imide *J. Phys. Chem. B* **2008,** 112, 4329-4336.

(18) Fujii, K.; Mitsugi, T.; Takamuku, T.; Yamaguchi, T.; Umebayashi, Y.; Ishiguro, S., Effect of Methylation at the C_2 Position on the Liquid Structure of Ionic Liquids Revealed by Large-Angle X-ray Scattering Experiments and MD Simulations. *Chem. Lett.* **2009,** 38, 340-341.

(19) Fujii, K.; Kanzaki, R.; Takamuku, T.; Kameda, Y.; Kohara, S.; Kanakubo, M.; Shibayama, M.; Ishiguro, S.; Umebayashi, Y., Experimental Evidences for Molecular Origin of low-Q peak in Neutron/X-ray Scattering of 1-Alkyl-3-methylimidazolium bis(trifluoromethanesulfonyl)amide Ionic Liquids. *J. Chem. Phys.* **2011,** 135, 244502.

(20) Rantwijk, F.; Sheldon, R. A., Biocatalysis in Ionic Liquids. *Chem. Rev.* **2007,** 107, 2757-2785.

(21) Itoh, T.; Matsushita, Y.; Abe, Y.; Han, S.; Wada, S.; Hayase, S.; Kawatsura, M.; Takai, S.; Morimoto, M.; Hirose, Y., Increased Enantioselectivity and Remarkable Acceleration of Lipase-Catalyzed Transesterification by Using an Imidazolium PEG-Alkyl Sulfate Ionic Liquid. *Chem. Eur. J.* **2006,** 12, 9228-9237.

(22) Greaves, T. L.; Drummond, C. J., Protic Ionic Liquids: Properties and Applications. *Chem. Rev.* **2008,** 108, 206-237.

(23) Hallett, J. P.; Welton, T., Room-Temperature Ionic Liquids: Solvents for Synthesis and Catalysis. 2. *Chem. Rev.* **2011,** 111, 3508-3576.

(24) Plechkova, N. V.; Seddon, K. R., Applications of Ionic Liquids in the Chemical Industry. *Chem. Soc. Rev.* **2008,** 37, 123-150.

(25) Pavlidis, I.; Gournis, D.; Papadopoulos, G.; Stamatics, H., Lipases in Water-in-Ionic Liquid Microemulsions: Structural and Activity Studies. *J. Mol. Catal. B: Enzym.* **2009,** 60, 50-56.

(26) Xue, L.; Li, Y.; Zou, F.; Lu, L.; Zhao, Y.; Huang, X.; Qu, Y., The Catalytic Efficiency of Lipase in a Novel Water-in-[Bmim][PF_6] Microemulsion Stabilized by Both AOT and Triton X-100. *J. Colloid Surf. B: Biointerfaces* **2012,** 92, 360-366.

(27) Moniruzzaman, M.; Kamiya, N.; Nakashima, K.; Goto, M., Recent Advances of Enzymatic Reactions in Ionic Liquids. *Biochem. Eng. J.* **2010,** 48, 295-314.

(28) Huddleston, J. G.; Visser, A. E.; Reichert, W. M.; Willauer, H. D.; Broker, G. A.; Rogers, R. D., Characterization and Comparison of Hydrophilic and Hydrophobic Room Temperature Ionic Liquids Incorporating the Imidazolium Cation. *Green Chemistry* **2001,** 3, 156-164.

(29) Provencher, S. W., A Constrained Regularization Method for Investing Data Represented by Linear Algebraic or Integral Equations. *Comp. Phys. Comm.* **1982,** 27, 213-227.

(30) Kusano, T.; Fujii, K.; Hashimoto, K.; Shibayama, M., Water-in-Ionic Liquid Microemulsion Formation in Solvent Mixture of Aprotic and Protic Imidazolium-Based Ionic Liquids. *Langmuir* **2014,** 30, 11890-11896.

(31) Shibayama, M.; Matsunaga, T.; Nagao, M., Evaluation of Incoherent Scattering Intensity by Transmission and Sample Thickness. *J. Appl. Cryst.* **2009,** 42, 621-628.

(32) Longhi, G.; Fornili, S. L.; Liveri, V. T.; Abbate, S.; Rebeccani, D.; Ceraulo, L.; Gangemi, F., Sodium Bis(2-ethylhexyl)sulfosuccinate Self-Aggregation in Vacuo: Molecular Dynamics Simulation. *Phys. Chem. Chem. Phys.* **2010,** 12, 4694-4703.

(33) Mata, J. P.; Reynolds, P. A.; Gilbert, E. P.; White, J. W., Extended Q-range Small Angle Neutron Scattering from Inverse Micellar Solutions of PIBSA-Micelle and Molecular Scattering. *Colloids and Surfaces A: Physicochem. Eng. Aspects* **2013,** 418, 157-164.

(34) Kusano, T.; Fujii, K.; Tabata, M.; Shibayama, M., Small-Angle Neutron Scattering Study on Aggregation of 1-Alkyl-3-methylimidazolium Based Ionic Liquids in Aqueous Solution. *J. Sol. Chem.* **2013**, 42, 1888-1901.

(35) Wang, J.; Wang, H.; Zhang, S.; Zhang, H.; Zhao, Y., Conductivities, Volumes, Fluorescence, and Aggregation Behavior of Ionic Liquids [C_4mim][BF_4] and [$C_n$mim]Br (n = 4, 6, 8, 10, 12) in Aqueous Solutions. *J. Phys. Chem. B* **2007**, 111, 6181-6188.

(36) Wang, J.; Wang, H.; Zhang, S.; Zhang, H.; Zhao, Y., Conductivities, Volumes, Fluorescence, and Aggregation Behavior of Ionic Liquids [C_4mim][BF_4] and [$C_n$mim]Br (n = 4, 6, 8, 10, 12) in Aqueous Solutions. *J. Phys. Chem. B* **2007**, 111, 6181-6188.

(37) Almasy, L.; Turmine, M.; Perera, A., A. Structure of Aqueous Solutions of Ionic Liquid 1-Butyl-3-methylimidazolium Tetrafluoroborate by Small-Angle Neutron Scattering. *J. Phys. Chem. B* **2008**, 112, 2382-2387.

Chapter 5 Summary

In this thesis, the aggregation structures of trimeric surfactants were investigated using scattering methods and these structures were compared with those of gemini or monomeric surfactants. The trimeric surfactants exhibited unique aggregation behavior because of their dense chemical structure.

In chapter 2, new, star-type trimeric surfactants with three quaternary ammonium surfactants connected by spacer chains were investigated. These surfactants had three hydrocarbon chains composed of 8, 10, 12, or 14 carbon atoms. The aggregation behaviors of these tris(*N*-alkyl-*N*,*N*-dimethyl-2-ammoniumethyl)amine bromides ($3C_n$trisQ, where n is the number of carbon atoms in the alkyl chain) were investigated using rheological, SANS, and cryoTEM techniques. The results indicated that $3C_{10}$trisQ formed ellipsoidal micelles and underwent a sphere-to-rod transition with increasing surfactant concentration. Furthermore, the aggregation structure of $3C_{14}$trisQ was rodlike micelles and was independent of the surfactant concentration because of its high packing parameter and high hydrophobicity. Furthermore, growth mechanisms of wormlike micelles formed in an aqueous solution by the star-type trimeric surfactant $3C_{12}$trisQ with a hydrocarbon chain length of 12 were investigated. The end-cap energies of star-type trimeric, gemini, and monomeric surfactants were evaluated from the φ dependence of the zero-shear viscosity. Wormlike micelles formed by $3C_{12}$trisQ exhibited a higher end-cap energy than those formed by a gemini surfactant.

In chapter 3, the aggregation behavior of star-type trimeric surfactants ($3C_n$trisQ) in the presence of sodium salicylate (NaSal) was investigated. Using small-angle X-ray scattering (SAXS) and rheological measurements, a structural phase diagram of solutions of $3C_n$trisQ with various hydrocarbon chain lengths (n = 10, 12, 14) and various NaSal concentrations (C_S) was constructed. NaSal was observed to induce a structural transition of $3C_n$trisQ that significantly depended on the hydrocarbon chain length. $3C_{10}$trisQ formed ellipsoidal micelles in solution, independent of C_S. In the case

of $3C_{12}$trisQ solutions, the micellar structures changed from ellipsoidal micelles to rodlike micelles with increasing C_S. In addition, at higher C_S levels, $3C_{12}$trisQ appeared to form multilamellar vesicles in solution. $3C_{12}$trisQ solutions exhibited structural transitions from ellipsoidal micelles, though rodlike or wormlike micelles, to vesicles as the C_S was increased. Aggregate structures of $3C_{14}$trisQ were rodlike or wormlike micelles at lower C_S levels and unilamellar vesicles at higher concentrations, respectively. $3C_{14}$trisQ also exhibited a structural transition from rodlike micelles to vesicles with increasing C_S. The surfactant concentration (C_D) dependence of the aggregation behavior of $3C_{12}$trisQ in a solution was also investigated. Even at higher C_D levels, $3C_{12}$trisQ did not form vesicles in the solution. The structural transition of $3C_{12}$trisQ aggregates strongly depended on not only C_S but also C_D in solution.

In chapter 4, the formation of stable water-in-IL RMs in an organic-solvent-free system, i.e., a mixture of aprotic (aIL) and protic (pIL) imidazolium-based ILs containing the gemini surfactant AOT was described. Structural investigations using DLS, SAXS, and SANS were performed for RMs formed in mixtures of aprotic 1-octyl-3-methylimidazolium ($[C_{8\ m}Im^+]$) and protic 1-alkylimidazolium ($[C_nImH^+]$, n = 4 or 8) ILs with a common anion, bis(trifluoromethanesulfonyl)amide ($[TFSA^-]$). The RM structure was observed to strongly depend on the mixing composition of the aIL/pIL in the medium. The RM size appreciably increased with increasing pIL content in both $[C_{8\ m}Im^+][TFSA^-]/[C_8ImH^+][TFSA^-]$ and $[C_{8\ m}Im^+][TFSA^-]/[C_4ImH^+][TFSA^-]$ mixtures. The RM size was larger in the n = 8 system than in the n = 4 system. These results indicated that the shell part of RMs is composed of both AOT and pIL cations and that the RM size can be tuned via the pIL content in the aIL/pIL mixtures. Furthermore, RM systems were successfully prepared using a different surfactant, star-type trimeric surfactant $3C_{12}$trisQ, indicating that this pIL method can be widely applied to other surfactant systems. The results obtained here give valuable insights for controlling the size of RMs in ionic liquid.

In conclusion, oligomeric surfactants are useful in various fields because of their unique aggregation behavior. Furthermore, with increasing number of carbon chains, they exhibit better performance as surfactants. In this thesis, the aggregation behavior of

mainly trimeric surfactants was investigated because they exhibit various aggregation structures as a consequence of their higher packing parameter that stems from their multiple hydrocarbon chains. The applications to which specific surfactant aggregates are best suited depend on the aggregates' structures. Therefore, elucidating the relationship between the aggregation structure and the chemical structure of surfactants is an important research topic. The experimental results indicated that trimeric surfactants form large aggregates at surfactant concentrations lower than those of corresponding gemini and monomeric surfactants because of their unique packing shapes and high hydrophobicities. From an environmental viewpoint, the unique properties of trimeric surfactants are important for reducing the amounts of surfactants used. However, surfactants that possess multiple alkyl carbon chains tend to exhibit greater hydrophobicity. The selection of a surfactant suitable for a given application is important. Trimeric or gemini surfactants are highly promising for use in various applications. The results in this thesis will not only be useful in industrial and consumer applications but will also provide important information for fundamental studies related to oligomeric surfactants.

Acknowledgements

The thesis is a summary of the author's studies carried out in the research group of Professor Mitsuhiro Shibayama at the Institute for Solid State Physics (ISSP), The University of Tokyo from 2010 to 2014. The author would like to express his sincere gratitude to Professor Mitsuhiro Shibayama for his helpful guidance and for giving precious opportunities in laboratory.

The author would like to acknowledge valuable advices and helpful discussions given by Dr. Hiroki Iwase (Comprehensie Research Organization for Science, CROSS). The author also wishes to express his gratitude to Professor. Kenta Fujii (Yamaguchi University) for his helpful advices and useful suggestion.

The author is deeply grateful to Professor Tomokazu Yoshimura (Nara Women's University) for kindly providing samples and helpful discussions. The author wishes to thank Professor Hiroki Kurata and Dr. Tetsuya Ogawa (Kyoto University) for cryo-TEM measurements. The grateful acknowledgement is also due to Dr. Kazuhiro Akutsu (CROSS) for his helps to perform SAXS measurements and Professor Masaaki Tabata (Saga University) for giving valuable advices.

The author would like to thank technical assistance of SANS measurements by Tae-Hwan Kim and Young-Soo Han (Korea Atomic Energy Research Institute). The SAXS and HEXRD experiments were performed at SPring-8 with the approval of the Japan Synchrotron Radiation Research Institute (JASRI) (proposal no. 2011B1506 (BL40B2, SAXS) and 2013B1375 (BL04B2, HEXRD)). The SAXS experiment was also conducted at the second hutch of the Frontier Soft Matter Beamline (FSBL; BL03XU), SPring-8, with the assistance of Atsushi Izumi, Sumitomo Bakelite, Co., Ltd.

The author would like to thank all the member of Neutron Science Laboratory, both the staff and students. The author would also like to thank the staffs and students of Department of Chemistry School of Science, The University of Tokyo. Especially, the author would like to express his gratitude to the members of Shibayama Laboratory.

In addition to his personal acknowledgements, the author cannot forget to recognize the following financial supports: JSPS KAKENHI Grant Numbers 26･1113.

Last but not least, the author is deeply grateful to his family for their supports.

Tokyo, December 2014

List of Publication

[Publications related to this thesis]

1. Yoshimura, T.; Kusano, T.; Iwase, H.; Shibayama, M.; Ogawa, T.; Kurata, H.; Star-Shaped Trimeric Quaternary Ammonium Bromide Surfactants: Adsorption and Aggregation Properties. *Langmuir* **2012** 28, 9322-9331.

2. Kusano, T.; Iwase, H.; Yoshimura, T.; Shibayama, M.; Structural and Rheological Studies on Growth of Salt-Free Wormlike Micelles Formed by Star-Type Trimeric Surfactants. *Langmuir* **2012,** 28, 16798-16806.

3. Kusano, T.; Fujii, K.; Tabata, M.; Shibayama, M.; Small-Angle Neutron Scattering Study on Aggregation of 1-Alkyl-3-methylimidazolium Based Ionic Liquids in Aqueous Solution. *J. Solution Chem.* **2013,** 42, 1888-1901.

4. Kusano, T.; Fujii, K.; Hashimoto, K.; Shibayama, M.; Water-in-Ionic Liquid Microemulsion Formation in Solvent Mixture of Aprotic and Protic Imidazolium-Based Ionic Liquids. *Langmuir* **2014,** 30, 11890-11896.

5. Kusano, T.; Iwase, H.; Akutsu, K.; Yoshimura, T.; Shibayama, M.; Structural Study on the Aggregation Behavior of Star-Type Trimeric Surfactants in the Presence of Organic Salts. *submitted to J. Colloid Interface Sci.*

[Publications not related to this thesis]

1. Shibayama, M.; Matsunaga, T.; Kusano, T.; Amemiya, K.; Kobayashi, N.; Yoshida, T.; SANS Studies on Catalyst Ink of Fuel Cell. *J. Appl. Polym. Sci.*, **2014**, 131, 39842 1-7.

2. Takeda, M.; Kusano, T.; Matsunaga, T.; Endo, H; Shibayama, M.; Shikata., T.; Rheo-SANS Studies on Shear-Thickening/Thinning in Aqueous Rodlike Micellar Solutions. *Langmuir* **2011**, 27, 1731-1738.